İSTANBUL TECHNICAL UNIVERSITY ★ INSTITUTE OF SCIENCE AND TECHNOLOGY

THE INFLUENCE OF DESIGN PARAMETERS ON SOLDER JOINT RELIABILITY IN ELECTRONIC PACKAGES

Ph.D. Thesis by

Aylin YENİLMEZ, M.Sc.

(50394002021)

Date of submission : 18 September 2001

Date of defence examination : 3 December 2001

Supervisor (Chairman): Prof. Dr. Aybars ÇAKIR

Members of the Examining Committee Prof.Dr. Can ÖZSOY (İ.T.Ü.)

Assoc.Prof.Dr. Murat VURAL (İ.T.Ü.)

Prof.Dr. Faris KAYA (Y.T.Ü.)

Prof.Dr. Uğur GÜVEN (Y.T.Ü.)

DECEMBER 2001

İSTANBUL TEKNİK ÜNİVERSİTESİ ★ FEN BİLİMLERİ ENSTİTÜSÜ

TASARIM PARAMETRELERİNİN ELEKTRONİK PAKETLERDE KULLANILAN LEHİM BAĞLANTILARININ GÜVENİLİRLİĞİNE ETKİSİ

DOKTORA TEZİ
Y. Müh. Aylin YENİLMEZ
(50394002021)

Tezin Enstitüye Verildiği Tarih : 18 Eylül 2001
Tezin Savunulduğu Tarih : 3 Aralık 2001

Tez Danışmanı: Prof. Dr. Aybars ÇAKIR

Diğer Jüri Üyeleri Prof.Dr. Can ÖZSOY (İ.T.Ü.)

Doç.Dr. Murat VURAL (İ.T.Ü.)

Prof.Dr. Faris KAYA (Y.T.Ü.)

Prof.Dr. Uğur GÜVEN (Y.T.Ü.)

ARALIK 2001

PREFACE

This study concerns the determination of design parameters with the largest impact on the solder joint life. The design parameters consist of the amount of the solder volume, solder ball upper radius, and mold compounds' material properties. Functional relationships between the average plastic work and these design parameters are established.

I would like thank to my adviser, Professor Aybars ÇAKIR, for his encouragement and guidance of this Ph.D. study. I wish to express my sincere appreciation to Professor Erdoğan MADENCİ from University of Arizona, for his encouragement, guidance, valuable comments and helpful suggestions to this work. Special thanks to each member of ACATC (Alliance for Computational Analysis and Testing of Composites) group at University of Arizona, for their contributions to my study. I would also like to thank to every single person in my life, who supports and encourages me from the beginning of my Ph.D. study to now.

Finally, and the most importantly, thanks to my loving and understanding family, for their support, encouragement, their patience, and being my side throughout the years of my graduate study.

September, 2001 Aylin YENİLMEZ

TABLE OF CONTENTS

ABBREVIATIONS

IC	: Integrated Circuit
PCB	: Printed Circuit Board
BGA	: Ball Grid Array
CSP	: Chip-Scale Packaging
SMT	: Surface Mount Technology
CBGA	: Ceramic Ball Grid Array
TBGA	: Tape-Automated Ball Grid Array
PBGA	: Plastic Ball Grid Array
MBGA	: Metal Ball Grid Array
DBGA	: Dimple Ball Grid Array
RMA	: Rosin, Mildly Activated
CD	: Compact Disc
I/O	: Input/Output
TSOP	: Thin Small Outline Package
PQFP	: Plastic Quad Flat Pack
SMD	: Solder Mask Defined
NSMD	: Non-Solder Mask Defined
PWB	: Printed Wiring Assembly
PWA	: Printed Wiring Assembly
CTE	: Coefficient of Thermal Expansion
ASTM	: American Society for Testing Materials
IPC	: The Institute for Interconnecting, Packaging Electronic Circuits
EIA	: The Electronic Industries Alliance
ANN	: Artificial Neural Network
PCG	: Pre-Conjugate Gradient

LIST OF TABLES

LIST OF FIGURES

LIST OF SYMBOLS

a	: Crack length
a_s	: Secondary crack length
a_p	: Primary crack length
B, B_t	: Transient creep coefficient
C_4, C_{4t}	: Pre factor in hyperbolic sin law steady-state creep equation
C_5, C_{5t}	: Pre factor in hyperbolic sin law steady-state creep equation
C_6, C_{6t}	: Pre factor in time independent plastic flow equation
C_{7t}	: Pre factor in hyperbolic sin law stress-strain rate equation
G	: Shear modulus
G_0	: Shear modulus at 0°C
G_1	: Temperature dependence of shear modulus
k	: Boltzmann's constant
K_1, K_2, K_3, K_4	: Crack growth constants
m	: Exponent in time independent plastic flow equation
n	: Stress exponent in steady-state creep equations
N	: Number of cycles
N_c	: Number of cycles to component failure
N_0	: Number of cycles to crack initiation
N_{0s}	: Number of cycles to secondary crack initiation
N_{0p}	: Number of cycles to primary crack initiation
Q	: True activation energy
Q_a	: Apparent activation energy
s	: Deformation resistance
s^*	: Saturation value of deformation resistance
$s\hat{}$	: Coefficient for deformation resistance saturation value.
V_i	: Volume of the element
t	: Time (sec)
T	: Absolute temperature
ΔW_{ave}	: Average plastic work density
ΔW	: Viscoplastic strain energy density per cycle
α, α_t	: Power law breakdown coefficient in hyperbolic sin law steady-state creep equation
α_1, α_{1t}	: Power law breakdown coefficient in hyperbolic sin law steady-state creep equation
α_{2t}	: Power law breakdown coefficient in hyperbolic sin law stress-strain rate equation
ε	: Tensile strain
γ	: Engineering shear strain
γ_c, ε_c	: Creep component of strain
γ_{in}, ε_{in}	: Total inelastic strain
γ_p, ε_p	: Time independent plastic flow component of strain
γ_s, ε_s	: Steady-state creep strain
γ_T, ε_T	: Transient creep strain
τ	: Shear stress
σ	: Tensile stress

THE INFLUENCE OF DESIGN PARAMETERS ON SOLDER JOINT RELIABILITY IN ELECTRONIC PACKAGES

SUMMARY

A typical electronic package generally consists of a die (Integrated Circuit chip), die attach, substrate and molding compound. The major functions of an electronic package are: to provide a path for the electrical current that powers the circuits on the Integrated Circuit (IC) chip, to distribute the signals onto and off of the IC chip, to remove the heat generated by the circuits and to support and protect the IC chip from environmental hazards. Power distribution involves the distribution and conditioning of the electrical current necessary for the ICs to function. Signal distribution involves creating electrical connections between various components in a module and providing interfaces to the next level of assembly. Thermal management is necessary to remove heat generated by the electronic components so that they stay within an allowable temperature range. Circuit protection involves mechanical support and protection from physical damage as well as protection from environmental hazards such as moisture, contaminants or ionizing radiation.

There are many electronic packaging technologies that have facilitated Printed Circuit Board (PCB) assembly choices that have advanced packaging developments, e.g. solder-bumped flip-chip technology, solder Ball Grid Array (BGA) technology and solder Chip-Scale Packaging (CSP) technology. These are all Surface Mount Technology (SMT) assemblies. There are also many kinds of BGAs depending on their substrates. These are ceramic BGA (CBGA), tape-automated bonding BGA (TBGA), plastic BGA (PBGA), metal BGA (MBGA), and dimple BGA (DBGA), etc.

For these electronic packaging the solder joint is the only mechanical and electrical way of attaching them to the PCB. Because of this, solder joint reliability is one of the most important issues in electronic packaging and interconnect systems.

Solder alloys are used to bond dissimilar materials that have different thermal expansion coefficients. Once the structure is bonded together, the components are subjected to cyclic thermal stresses due temperature changes during operation. These stresses arise from mismatch in thermal expansion coefficients. Because the solder is above half of its melting point at room temperature, it presents a nonlinear creep (viscoplastic) response.

The actual mechanism by which a solder joint fails is due to crack initiation and propagation through a joint. The location and nature of the cracks depend on the joint configuration, intermetallic structure, strain, strain rate and thermal loading.

Based on extensive testing in electronics industry, the number of cycles to solder joint is usually predicted based on the volume weighted average plastic work density in conjunction with empirical constants as part of a life prediction model.

This study concerns the determination of design parameters with the largest impact on the solder joint life. The design parameters consist of the amount of the solder volume, die thickness, die size, pad thickness, pad size, mold compound, mold size and substrate thickness. Functional relationships between the average plastic work and these design parameters are established.

This is achieved by considering three different package types provided by the companies in the electronics industry. The material properties, methodology and boundary conditions are consistent in each package analysis. The analysis is conducted by constructing three dimensional nonlinear finite element models of the package assemblies. The solder material is modeled as a viscoplastic solid, the printed circuit board as orthotropic linear elastic solid and the rest of the materials as linear elastic solids. In each calculation, thermal cycles are simulated in order to establish a stable stress-strain hysteresis loop. These packages are subjected to a specified temperature cycle. In the finite element analysis of each package, a nonlinear global model with a relatively coarse mesh for the substrate, printed circuit board and the solder balls provides the critical joint for the subsequent nonlinear sub modeling of the critical solder joint. The critical joint for sub modeling is identified based on the amount of inelastic (plastic) work density at the end of the last cycle.

The sub modeling permits refinement of the mesh. The displacement boundary conditions are determined from the solution of the global analysis through the use of cut boundary interpolation method. The number of cycles to crack initiation and the crack growth rate per cycle are both correlated with plastic work density. Using the crack initiation, growth constants and characteristic crack length, the number of cycles to solder joint failure is calculated. The empirical constants used in the life prediction model are well accepted in industry.

TASARIM PARAMETRELERİNİN ELEKTRONİK PAKETLERDE KULLANILAN LEHİM BAĞLANTILARININ GÜVENİLİRLİĞİNE ETKİSİ

ÖZET

Klasik bir elektronik paket, genellikle, çip (Entegre devre çipi), yapıştırma bağlantısı, çip taşıyıcı ve kaplama bileşeninden meydana gelir. Elektronik paketlerin esas görevleri: entegre devre (IC) çipi üzerinden devreye güç iletimini sağlayan elektrik akımı için bir yol temin etmek, sinyallerin IC çipine giriş ve çıkış dağıtımını yapmak, devrelerin meydana getirdiği ısıyı ortadan kaldırmak ve IC çipini çevredeki zararlı etkilerden korumak ve desteklemektir. Güç dağıtımı, IC çipinin görevini yerine getirmesi için gerekli olan elektrik akımını dağıtmayı ve istenen duruma getirmeyi temin eder. Sinyal dağıtımı, bir modül içindeki çeşitli bileşenler arasındaki elektriksel bağlantıyı temin eder ve montajın daha sonraki seviyeleri için ara yüzeyler oluşturmayı sağlar. Elektronik bileşenler tarafından meydana getirilen ısının ortadan kaldırılması, bileşenlerin uygun sıcaklık aralığında kalmaları bakımından çok gereklidir. Devrenin korunması, mekanik desteği ve nem, toz, kirlilik gibi çevredeki zararlı etkilerden korunması kadar fiziksel hasarlardan korumayı da temin eder.

Elektronik paketleme teknolojisinde, elektronik paketlerin Baskı Devre Kartına (Printed Circuit Board) montajını kolaylaştıran, lehim bağlantılı flip çip teknolojisi, lehim toplarının belli düzenlerde yerleştirildiği (BGA) teknolojileri ve çipin doğrudan karta takıldığı çip-scale paketleme (CSP) teknolojileri, v.s. gibi çok sayıda ileri paketleme seçenekleri mevcuttur. Bunlar, yüzeye monte tekniğinin kullanıldığı teknolojilerdir (SMT). Ayrıca kullanılan çip taşıyıcılarının malzemelerine bağlı olarak, lehim toplarının belli düzenlerde yerleştirildiği (BGA) çok sayıda teknoloji mevcuttur. Bunlardan bazıları; seramik BGA (CBGA), otomatik bantla birleştirilmiş BGA (TBGA), plastik BGA (PBGA), metal BGA (MBGA) ve gamzeli BGA (DBGA)'dir.

Lehim bağlantıları, elektronik paketleme teknolojilerinde, paketlerin elektriksel ve mekanik olarak baskı devre kartına takılması için tek yoldur. Bu sebeple, lehim bağlantılarının güvenilirliği elektronik paketleme ve parçaların birbirine bağlanmasındaki en önemli konulardan birisidir.

Lehim alaşımları, farklı ısıl genleşme katsayılarına sahip, farklı parçaların birbirine bağlanmasında kullanılırlar. Sistemin bağlantısı tamamlandıktan sonra, parçalar, çalışma sırasında meydana gelen sıcaklık değişimlerinden dolayı periyodik ısıl gerilmelere maruz kalırlar. Bunun sebebi, birleştirilen parçaların malzemelerinin ısıl genleşme katsayılarının birbirine uygun olmamasıdır. Kullanım sıcaklığında, lehim bağlantıları erime noktalarının yarısının üzerinde olduğu için, lineer olmayan (visko plastik) sürünme meydana gelir.

Lehim bağlantısının hasara uğrama mekanizması, çatlak başlangıcı ve çatlağın birleştirme boyunca ilerleyerek kırılmasıdır. Çatlakların konumu ve doğası, birleştirmenin konfigürasyonu, metallerin iç yapısı, birim uzama, birim uzama hızı ve ısıl yüklemeye bağlıdır. Elektronik sanayinde yapılan çok sayıdaki deneysel çalışmalara dayanarak, lehim bağlantısının hasara uğrayacağı periyot sayısı, genellikle, ömür tahmini modelinin bir parçası olan ampirik sabitler yardımıyla, birim hacme düşen ortalama plastik iş yoğunluğu metoduduyla tahmin edilir.

Yapılan çalışma, tasarım parametrelerinin hangisinin lehim bağlantılarının ömrüne etkisinin en fazla olduğunun hesaplanması ile ilgilidir. Tasarım parametreleri, lehim hacmi, çip kalınlığı, çip boyutları, dolgu kalınlığı, dolgu boyutları, kaplama bileşeni, kaplama boyutları ve çip taşıyıcı kalınlığıdır. Ortalama plastik iş ile tasarım parametreleri arasında fonksiyonel bağıntılar oluşturulur.

Elektronik sanayindeki şirketlerden temin edilen üç farklı tip elektronik paket özellikleri kullanılarak çalışmalar yapılmıştır. Malzeme özellikleri, metodoloji ve sınır koşulları her paketin analizinde aynı alınır. Paket bağlantıları için, üç boyutlu lineer olmayan sonlu eleman modelleri oluşturularak analizler yapılır. Lehim malzemesi viskoplastik katı, baskı devre kartı ortotropik lineer elastik katı ve kalan malzemeler de lineer elastik katı olarak modellenir. Her hesaplamada, kararlı bir gerilme-birim uzama histerizis çevrimi elde etmek için ısıl periyotlar simüle edilir. Bu paketler, belli sıcaklık periyotlarına maruz bırakılırlar. Her bir paketin sonlu eleman analizinde, çip taşıyıcı, baskı devre kartı ve lehim topları için daha kaba bir ağ oluşturulan lineer olmayan global model meydana getirilir ve en kritik lehim bağlantısı belirlendikten sonra elektronik paketin o kısmı için lineer olmayan bir alt model oluşturulur. Alt modeldeki kritik lehim bağlantısı, son periyodun sonundaki elastik olmayan (plastik) iş yoğunluğu miktarına dayanarak belirlenir.

Alt modelde daha ince (sık) ağ kullanılır. Alt modeldeki sınır yerdeğiştirme koşulları, sınır interpolasyonu metodu tatbik edilerek doğrudan global modelin analiz sonuçlarından hesaplanır. Çatlağın başlayacağı periyot sayısı ve her periyottaki çatlak ilerleme hızlarının ikisi de plastik iş yoğunluğu ile ilişkilendirilir. Çatlak başlangıcı ve ilerlemesi sabitleri ve karakteristik çatlak uzunluğu kullanılarak, lehim bağlantısının hasara uğrayacağı periyot sayısı hesaplanır. Ömür tahmini metodunda kullanılan ampirik sabitler doğrudan sanayiden alınmıştır.

1. INTRODUCTION

1.1 Background

The development of generations of electronics industry has started the invention of the transistor by Bardeen, Brattain, and Shockley at Bell Laboratories in 1947. The silicon integrated circuit (IC) was invented by Jack Kilby from Texas Instruments in 1958 and developed by Robert Noyce and Gordon Moore from Fairchild Semiconductor in 1959. Progress in electronics has been started by improvements in the silicon IC (or silicon chip). The early 1950s, there wasn't semiconductor industry. After marketing ICs in 1961, they affected the lives of people [1]. The last twenty years have seen major advances in the electronics industry. Electronic systems and machines have also affected the ways people live, work, communicate, and play. Electronic components are used in televisions, camcorders, CD players, toys, games, household appliances such as refrigerators and ovens are being fitted with digital controls, the automobile, passenger or truck, for engine controllers, emission control, anti-lock brakes, air bags, and climate adjustments. The objective of using electronics is to supply more information, intelligence, safety, and communication capabilities into the automobile to meet the needs of costumers. Aircraft operations, navigations, and ground traffic controls are strictly dependent on electronics and computers. Medical instruments and scientific analytical instruments are totally electronic and often microprocessor based. Besides, electronics systems producers made the valuable contributions to the areas of computers and communication. Together these two industries have made many discoveries and innovations and used them efficiently in the machines and equipments they have manufactured and marketed. Computers, servers, workstations, network systems, personal computers, laptops, notebooks, displays, and printers have been well integrated into businesses and linked into networks. New requirements of hand-held and mobile products with wide capabilities of computing, communication, display, and accessing to networks are appearing in the market place, but it is obvious that the people, who work, communicate and play, will be using powerful electronic products as information appliances in this information age. The electronic systems'

industries started to develop by the invention of integrated circuits in 1958. The brains of an electronic product are composed of integrated circuits built into semiconductor chips packaged on modules, mounted onto cards, and boards and interconnected of the others of the electronics system [2].

The IC chip has to communicate with other IC chips in a circuit through an input/output (I/O) system of interconnections. Besides that, the IC chip and its circuitry are sensitive and it requires a package to both carry and protect it. Consequently, the main functions of the electronics packages are to provide a path for the electrical current that powers the circuits on the IC chip, to distribute the signals onto and off of the IC chip, to remove the heat generated by the components of circuits, and to support, and protect the IC chip from environmental effects. There are increasing trend toward higher I/O, higher performance and higher printed circuit board (PCB) manufacturing. In this advanced manufacturing process, ball grid array (BGA), chip-scale package (CSP), and solder-bumped flip chip packages are taking the lead. Many major equipment makers and electronic companies are now gearing up for these emerging technologies. The solder joints are the only mechanical and electrical means of attaching the electronic packages to the PCBs. Solders were thought very poor at resisting thermal fatigue before and recommended not to use as joining materials for interconnections. Since then, after assembling many electronics components on printed circuit boards (PCB), it has been realized that solders are given a remarkable flexibility to interconnect electronics components. Thus, solder joint reliability is one of the most critical issues in the development of electronics industry technologies and it needs to be understood in electronic packaging and interconnect systems [1].

A typical electronic package generally consists of a die (Integrated Circuit chip), die attach, substrate, molding compound, adhesive, solder mask, solder paste, and copper pads. Electronic packages' major tasks are to provide an electrical path, to distribute the I/O signals, to remove the heat generated by the circuits, and to support and protect the chip. Electronic packages have various types of assembly design technology configurations to form mechanical, electrical, and thermal interconnections. Electronic packaging configurations started to develop from through-hole technologies that incorporate, single-sided, double-sided, and plated-through hole types in the 1980s and toward surface-mount technology (SMT) designs, which includes standard, fine, and very fine pitch (≥0.0635 -mm spacing of leads) devices for leaded and unleaded component mounting. Surface Mount

Technology is a packaging method for assembling PCBs or hybrid circuits in which components can be connected electrically and mechanically to the surface of a conductive pattern. New SMT design technology, based on ball and column grid arrays, maximizes the input/output to component size ratio without excessive use of board [3]. Different packaging technologies are required for different semiconductor IC devices and applications as solder-bumped flip chip technologies, ball grid array (BGA) technologies, Chip Scale Package (CSP) technologies [4-6], Thin Small Outline Package (TSOP), and Plastic Quad Flat Packs (PQFPs) technologies. In this study, all analyses were carried out on plastic BGA packages. The demand for higher input/output and higher performance requirements has made Ball Grid Array (BGA) quickly becoming the package of choice. BGA technology has many advantages like reduced placement issues (self-centering), lower profile, better electrical performance, higher I/Os for a given footprint, shorter wire bonds, ease to extend to multichip modules [5].

There are many electronic packaging technologies that have facilitated Printed Circuit Board (PCB) assembly choices that have advanced packaging developments (e.g. solder-bumped flip-chip technology, solder Ball Grid Array (BGA) technology, and solder Chip-Scale Packaging (CSP) technology). These are all Surface Mount Technology (SMT) assemblies. There are also many kinds of BGAs depending on their substrates. These are ceramic BGA (CBGA), tape-automated bonding BGA (TBGA), plastic BGA (PBGA), metal BGA (MBGA), and dimple BGA (DBGA), etc. Tape Automated Bonding is a bonding technology in which precisely etched leads, supported by a flexible tape, are automatically positioned over bonding pads on a chip that is thermo compression bonded.

A typical BGA electronic package generally consists of a die (Integrated Circuit chip), die attach, substrate, and molding compound, and it may generally contain adhesive, solder mask, and solder paste. Electronic packaging parts are briefly described as given below.

Die (Integrated Circuit): The most important part of the electronic package is its integrated circuit or chip for short and it is mainly the nerve center for a computer or computing device. Chips perform requested calculations, manage the internal flow of data and handle the data inputs from and outputs to the user. For years, the chip industry has marched and the number of transistors on integrated circuits would double every 18 months or less. This remarkable rate of advancement has resulted in smaller feature sizes, improved manufacturing techniques, which allow making

larger chips and wafers; and more efficient circuit designs and materials, which allow better circuit performance. Chips are made generally from silicon.

Die-attach: Die-attach layer is in the direct heat flow path between the chips and the substrate, or solder mask, so a high thermal conductivity is needed to maintain a low operating temperature in high power applications. The die-attach material will be subjected to thermal fatigue conditions when it deforms to accommodate expansion mismatch in the structure.

Substrate: The supporting insulating material upon which parts or substances are deposited or attached. Surface mounting technology requires additional printed circuit board substrate preparation prior to component mounting.

Molding Compound: Molding Compound mainly covers the electronic package. There are at least two forms of molding: one side molding and over mold. One side molding is a transfer molding method used for most of the electronic packages that are mass-produced. Over mold for electronic packages is mainly for electronic packages with very high pin counts and for multilayer electronic packages. Molding tasks are to provide flexibility and to protect the chip from hazardous environmental conditions.

Adhesive layer: It takes part between substrate and solder mask to provide the connection.

Solder Mask: A PCB manufacturing technique in which everything is coated with a plastic layer except the contents to be soldered.

Solder paste: Solder paste (cream) is an important part of surface mount substrate preparation prior to solder reflowing. The solder paste acts partially as an adhesive before reflow and its surface tension helps to align skewed parts during soldering. It contains the flux, solvent, and solder that are traditionally supplied by the wave-soldering machine. Therefore, the selection of particular solder paste involves optimizing its rheological characteristics such as viscosity, flow, and spread. The solder paste is generally applied on the lands of the substrate by screening, stenciling, or syringe dispensing.

Copper Pad: The metal portion of a printed circuit board that the leads of a surface mount component are fixed. Sometimes it is called as a footprint or a land. There are two possibilities for definition of the pad surface: Solder Mask Defined (SMD)

and Non Solder Mask Defined (Copper Defined) (NSMD). Each has advantages and disadvantages to its use. While circular shaped pads are most common, alternate shapes are rarely seen in use like ovals and diamonds as well. The input trace to the pad can take a variety of forms as well. It is recommended that the trace would be at least 0.0254 mm when using NSMD pads, to reduce the risk of breaking due to local mechanical stresses [6]. In the solder mask defined pad, the copper for the pad area is made larger than the desired land size. The opening in the solder mask is made smaller than the copper land, thus defining the mounting pad. The solder mask defined pad has two primary advantages. First, as the copper depends on etch control while the solder mask is photo imaged, solder mask size definition is better than copper pad definition. Second, the overlap of the solder mask onto the copper enhances the copper adhesion to the laminate surface. When using resin systems where adhesion is low, this can be an important consideration. The non solder mask (or copper) defined pad has a solder mask opening larger than the copper area. Thus the size of the pad is controlled by the copper etch quality control. This is generally somewhat less accurate than the solder mask photo image control and thus the pad size varies more than with the SMD pad. However, because the edges of the copper do not need to extend under the solder mask, the pad can be either made larger, or provided more line routing space between pads.

Printed Circuit Board: An epoxy glass and metal composite on which circuits are etched and to which components are attached to form a functioning electronic circuit. Sometimes called a printed circuit wiring board (PWB) or printed wiring assembly (PWA). Printed Circuit Board (PCB) term describes a bare board consisting of layers of conductors and insulators and the term printed wiring assembly (PWA) refers to a PCB with components attached to it. PCBs are produced from composite substrate materials and used as laminated and plated copper layer for high-density electrical interconnections. Printed wiring assemblies must withstand significant mechanical and environmental stress in normal operation. The board material is an insulated substrate that provides support for components and electrical insulation between the circuit traces. A glass-fiber and epoxy resin composite (glass-epoxy) is the most common material. The circuits traces, or interconnect, which is made of patterned copper, connects the electronic components on the board. The connections are usually made by traces. Most common board on (SMT) surface mount technologies is always multilayer board that has traces on both sides and interior layers. A multilayer board consists of different layers like polyamide, copper, and FR4 [1]. Copper clad laminates in FR4 are

multifunctional products offering exceptional dimensional stability, dielectric thickness control, and high quality repeatability. End market applications include automotive control boards, industrial and instrumentation controls, and computer motherboards. Polyamide uses special resins that provide improvement in mechanical properties such as X, Y, and Z direction coefficient of thermal expansion (CTE). This material is especially good for performance in high frequencies. There are Military, Federal, and American Society for Testing Materials (ASTM) and The Institute for Interconnecting, Packaging Electronic Circuits (IPC), and The Electronic Industries Alliance (EIA) standards for printed circuit boards. In this study, PCB having nine different layers is used in all finite element analyses. These layers are polyamide, copper, FR4, copper, FR4, copper, FR4, copper, and polyamide from top to bottom.

Solders: Usually an eutectic or near-eutectic alloy of tin and lead used for the electrical and mechanical connection of components. Soft solders are used for a variety of bonding purposes in electronic packaging applications. A solder joint can have an electrical, thermal, and mechanical function at interconnection level in a system. Solder joints can vary considerably in size and shape. In most package configurations, solders are being used to bond dissimilar materials together. Solders mainly contain tin and lead or the other elements in some cases. A primary characteristic of a eutectic alloy is that it has a lower melting point than either of its two constituents. The composition and melting point of solder alloys are shown in Figure 1.1 as a phase diagram. Eutectic tin-lead solder alloy is 63% tin and 37% lead by weight and has a melting point of 183°C (361°F). All other alloys of lead and tin including pure tin and pure lead have higher melting points. Electronic solders are usually composed of tin and lead in ratios close to the eutectic point. When no eutectic mixtures cool, the proeutectic portion solidifies first, leaving a eutectic alloy to cool at the reduced temperatures. This circumstance can result in increasing internal stress and cold solder joints. 63Pb37Sn eutectic tin-lead solder alloy was used in interconnections through all analyses. In this study, eutectic tin-lead solder alloy is used for all electronic packages.

Solder Ball: Small spheres of solder that remain on a PCB after soldering. These spheres affect reliability by moving into positions that cause a short circuit, or cracking that cause fatigue on solder joints. In this study, 63Pb37Sn solder alloy is used as a solder ball material. Since its material properties like elasticity modulus

changes with the temperature, it is defined and modeled as a non-linear material in all finite element analyses.

Pitch: The centerline spacing of the leads on an electronic interconnect. Electronic packaging design includes standard, fine, and very fine pitch (≥0.0635 -mm spacing of leads) devices for leaded and unleaded component mounting depending on the pitch size.

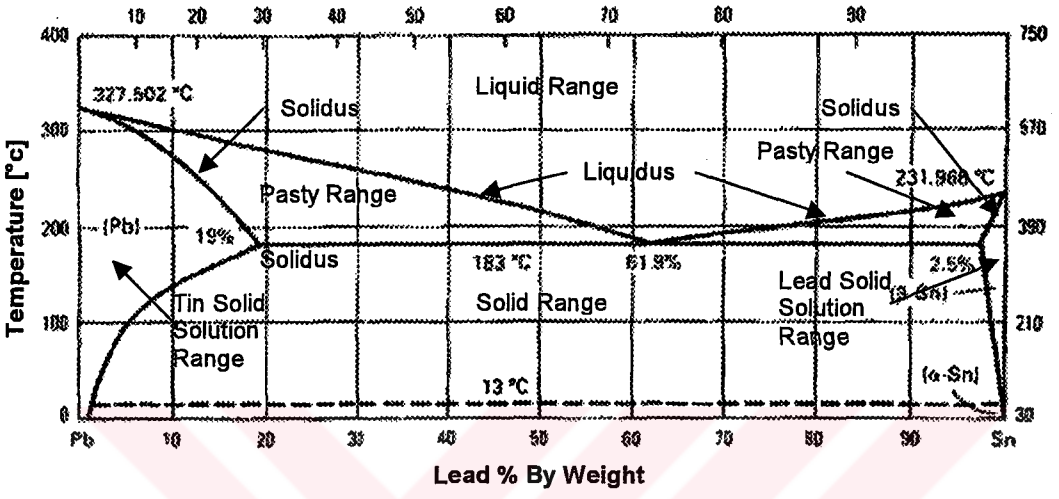

Figure 1.1 The phase diagram [1].

1.2 Literature Survey

The studies on solder joints of electronic packaging have started with experimental tests. Since conducting experiments take much more time than marching in electronics industry, the needs for decreasing the development time urged the researchers to do computational analyses; model the electronic packaging parts by using finite element analyses and examine the reliability of components. Increasing requirements for higher performance and higher I/O caused the researchers to study design parameter effects on fatigue life of solder joints. However, these numerical studies take much time and they are computationally expensive. Recently, many researchers did some studies about automated search techniques.

Darveaux, R. et al. [5] conducted creep tests on actual solder joints to ensure that the exact microstructure in real products was duplicated, and studied on BGA solder joint assemblies under several different conditions to examine crack growth and thermal fatigue. A fatigue life model was established based on the correlations

between the numbers of cycles to crack initiation; crack growth rate per cycle and visco plastic strain energy, and it was applied to a wide range of data from BGA assemblies. Constitutive relations were formulated about steady-state creep, transient creep, total inelastic strain and their tensile forms. Mechanical tests were conducted with thermal aged solder joint samples to characterize BGA solder joints mechanically. As a conclusion, steady state creep behavior and deformation constants of solder alloy were achieved. The crack growth correlations were used to calculate fatigue life of a wide range of test conditions, and a good correlation was obtained for both the failure-free life and the characteristic life. The methodology was then used to form a fatigue life model of solder joint and to predict field reliability. Darveaux, R. has also studied about a generalized solder joint fatigue life model for surface mount packages based on correlation to measured crack data on BGA solder joints during thermal cycle [5,7]. He reestablished crack initiation and growth correlations and constants using measured crack growth data and ANSYS 5.6 simulation results and compared methodologies and constituve models with each other [8].

Anderson, T. et al. [9] have also studied about life prediction analysis of solder joints in electronic packaging and examined the constituve model in finite element analysis program. Special user routines are developed to examine the differences between constituve relations for fatigue life prediction of electronic packages which can incorporate virtually any creep relation and determine the inelastic strain energy density developed in the three dimensional solid elements. Comparisons are performed for the modified creep routines and the viscoplastic formulation of Anand's model in ANSYS by using Ericsson components.

Darveaux, R. et al. [10], Miles, B. et al. [11], Syed, A. et al. [12], and Fjelstad, J. et al. [13] have conducted several tests about board level thermal cycle reliability tests. The packages were *fle*XBGA™ [10], tape array BGA™ [10-11] (die up, wire bonded, tape substrate), chip array BGA™ [11-12], PBGA (die up, wire bonded, laminate substrate), and μBGA [13] (die down, lead bonded, film elastomer, tape substrate).[1],[2] Ejim, T. et al. [14] have also studied about the effects of die size on PBGA assemblies. A similar study was conducted by El-Gore, M.K. et al. using nonlinear finite element analysis on a Micro Star BGA™ package [15].[3] Sato, T. et al. [16] have studied the effects of package size and ball count on solder joints

[1] *fle*XBGA™, TapeArray™, and ChipArray™ are trademarks of Amkor Technology.
[2] μBGA™ is a trademark of Teressa.
[3] Micro Star BGA™ is a trademark of Texas Instruments.

reliability. Schueller, R.D. et al. and Atterwala, A.I. et al. have also studied the effect of substrate/package configuration on different type of BGAs [17-19]. Masumota, K. [20] and Juso, H. et al. [21] optimized tape-based packages considering substrate configurations. Darveaux, R. et al. [22-23] have also studied about thermal and power cycling limits of plastic ball grid array assemblies, optimizing the reliability of thin small outline package (TSOP) solder joints, and test board design. Another study to examine the effects of test board design on PBGA components was carried out by Mawer, A. et al. [24] and it was related to the effect of PBGA solder pad geometry on solder joint reliability. Mawer, A. et al. [25] have also examined the effect of temperature cycle condition. The effect of design and material choices on solder joint fatigue life for fine pitch BGA packages is characterized by Darveaux, R. et al [26].

Gill, P.E. et al. [27], Haug, E.J. and Arora, J.S. [28], and Haftka, R.T. and Gurdal, Z. [29] studied about the automated search techniques of numerical optimization to provide tools that may be applied to design electronic packages in general and solder joints in particular. Since, it is difficult to use these procedures, global approximation, or linear regression models were developed to approximate the fatigue life as a function of solder joint design parameters. Gill, P.E. et al. [30] and Schittkowski, K. [31] determined the direction of search in the space of possible designs by minimizing a simplified sub problem, which is generally built using the first or second order Taylor series approximation to the problem functions. Although, the global approximation methods for optimizing electronic packages are computationally expensive to analyze, the optimization procedure of Sarihan, V. [32] is based on a quadratic approximation to the function that is continuously refined as optimization progresses. In this approach, even though the quadratic approximation is refined at each sub step, the refinement is based on points generated by an optimization algorithm. Therefore, this procedure does not provide a convenient global approximation to the problem function surface. Recently, Subbarayan, G. et al. [33-35] have developed a mathematical model and finite element solution procedures for predicting the shapes of three-dimensional flip-chip/BGA solder joints. Although the determination of fatigue life was automated, the process was taking several hours of CPU time due to the computational expense with the nonlinear finite element analysis. Especially, if gradients are to be computed by forward difference approximation requiring an additional analyses at each iteration considering "n" design parameters. Since, analysis of solder joint is time consuming, approximation techniques that reduce the number of function evaluations are

important. A global approximation concept based on design of experiments and linear regression models, was developed to optimize solder joint shapes for maximum reliability by Deshpande, A.M. et al. [36]. The developed techniques were shown using the PBGA package. Deshpande et al. Compared exact solution method, least squares method and artificial neural network (ANN) method. It is observed that the difference between predicted optimum and exact optimum fatigue lives are less for least squares method. Therefore, least squares method was used as approximation method in this study. Pad size and the amount of solder volume were chosen as the design variables for the optimization process. Only one package was used and meshed consisting of insufficient node and element numbers. A three-dimensional nonlinear finite element model of an over molded chip scale package (CSP) has been used to optimize the package robust design and to determine design rules to keep warpage within acceptable limits by Mertol, A. [37]. An L18 Taguchi matrix has been developed to investigate the effect of die thickness, die size, mold compound material thickness, flex-tape thickness, die attach epoxy thickness, copper trace thickness, and solder ball stand-off height on the reliability of the package. Although, determining the design rules to avoid excessive warpage, simulations have been performed with the package, which is mounted on a multilayer printed circuit board, from certain temperature range to optimize the package design, simulations have been carried out without the PBC. Assuming that the highest plastic strain would correspond to the lowest fatigue life, he didn't compute the fatigue life of solder joints. The mesh of the octant model used in the simulations was also coarse and printed circuit board was not considered in the global model.

1.3 Purpose and Objective of the Study

Costumer demand highly sophisticated and every small device has made semiconductor packaging a vital contributor to system performance. As integrated circuits have become faster and more complex, the cost and performance of interconnection between chip and system board has become both a significant challenge and an enabling technology. Providing the required number of I/Os in the smallest possible design, matching electrical characteristics between chip and printed circuit board, enabling a reliable and economical connection on every pad, delivering functional system integration through system in package solutions, and providing test, design, and reliability services are the goals and the challenges of the leader companies in microelectronics packaging technology. System design and

optimization become paramount to the overall success of developing a system in package.

The ultimate objectives of the study are to increase and predict the fatigue life by using least square method, to find out the influence of design parameters on solder joint's reliability in electronic packages, and related purpose is to extend the useful life, or to lower the cost. The impact of design and material choices on solder joint fatigue life for fine pitch BGA packages are characterized. Package design variables include solder ball size and mold compound material properties. Solder ball upper radius and solder volume are chosen as solder ball design variables for the optimization process. Since the configuration of solder joint is dependent on the solder ball size and the amount of the solder ball volume, these two parameters are taken. As the crack initiates at the neck size of the solder ball, it is important to examine the impact of solder ball upper radius on the reliability and fatigue life of solder joints. The crack initiation and growth is shown in Figure 1.2.

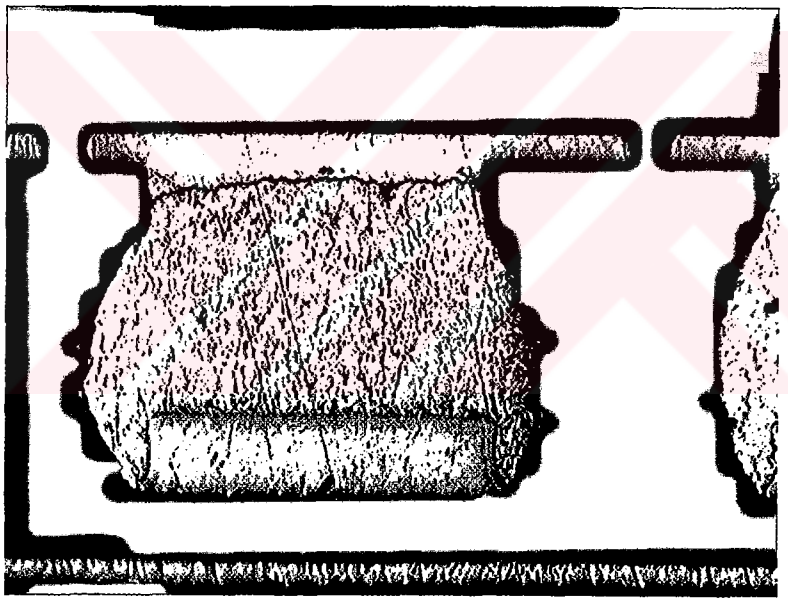

Photo 1.1 – FPBGA 8: VLSI 96, failure after 723 cycles, -40/+100 °C

Figure 1.2 Crack initiation and growth.

As the mass of the package can be determined, the force on each ball due to this weight can be measured. Consequently, the volume of the solder ball is definite and can be considered as a design variable. Molding compound material properties are elasticity modulus and thermal expansion coefficient. Mold material provides the flexibility of the package and protects the integrated circuit chip from the hazardous

environmental conditions. If a mold compound has a higher elasticity modulus and a lower thermal expansion coefficient, it is a higher filler content mold compound. It is expected to result in a lower solder fatigue life. The higher modulus makes the package stiffer; so more stress will be transmitted to the joints. A lower thermal expansion coefficient will increase both the local and global expansion mismatch, which increases the strain and stresses to the solder joints. Since both the solder material and printed circuit board have a higher thermal expansion coefficient than the mold compound, reducing the mold compound thermal expansion coefficient further only may make the situation worse. For these reasons, the impact of mold compound material properties has to be investigated. So, design parameters are solder ball upper radius, solder ball volume, mold compound's elasticity modulus, and mold compound's thermal expansion coefficients. To determine the design parameter values, Mathematica program was used. In this study, three different packages are used and these packages are modeled and analyzed by using ANSYS 5.6, which uses finite element method [37]. The models created in this study have finer mesh than the earlier studies in the literature mentioned above.

Solder connections are one of the remaining packaging challenges. Solder had been known as a weak link with many failures of BGA type of electronic packages to a disruption in the thermal path caused by cracking at the solder interface, but it has been realized that solders are given a remarkable flexibility to interconnect electronics components. For BGA or CSP technologies, solder is the electrical and mechanical glue and, thus, solder joint reliability is one of the most critical issues in the development of these technologies. Typically, solder joints include solder balls and the fatigue life of electronic package depends on the critical solder ball in the package. Although, there are many tests for determining the fatigue life of critical solder joint, qualification testing of electronic packages often involves considerable expense and substantial delays in time to market. Stress-based qualification methodologies require the testing of large numbers of parts in fairly severe conditions and they are time consuming and expensive. Reducing these costs is important, especially in requirements of the expected rapid developments in packaging technologies over the next few years.

After deciding design parameters, range of variable values has also considered. Three values of the solder ball upper neck radius and solder ball volume are selected and assumed that they are uniformly distributed about the nominal value in a range of ±20 percent. Different values of the mold compound's elasticity modulus

and thermal expansion coefficient were selected depending on the package's material properties. Analytical models have several practical uses: rapid design optimization during the development phase of a product, predicting field use limits, and failure analysis of product returned from the field or failed in a qualification tests. In terms of assembly design, it is required to determine design parameters' effects on solder joints reliability, to optimize the design of electronic package assembly, and to predict field reliability based on finite element analyses and optimization methods.

2. MECHANICAL CHARACTERIZATION OF BGA SOLDER JOINTS

2.1 Introduction

Many researchers have conducted several mechanical studies to provide extensive data, analytical techniques, and a generalized methodology for BGA solders joint reliability. These tests were used to characterize the solder behavior and develop constitutive relations, which predict strain as a function of stress, temperature, and time. These researchers used actual solder joints in all creep tests to ensure that the exact microstructure in real products was duplicated. Once the solder joint samples were fabricated, they were subjected to the thermal aging. The aging conditions were either several months at room temperature or certain hours at certain temperatures. The failure modes are generally rupture, interface failure, and thermal fatigue. The data-provided experimental studies are used to predict solder joint failure. The only conflicting requirement is that accelerated tests need to be as rapid as possible to reduce new product development cycle time. Therefore, it is more important to represent the accelerated tests by using computer programs. Finite element method is used to optimize the design of an electronic package assembly and to compute the fatigue life based on accelerated test results. In terms of assembly design of package, it is important to quantify which design parameters have the largest influence on solder joint reliability in electronic packages (e.g., solder ball upper radius, solder volume, molding compound's elasticity modulus, and molding compound's thermal expansion coefficient). Once the model is developed and quadratic functions are formed, it is faster and less expensive to optimize a design analytically than to use a number of experiments. Actually, experimental work is still necessary and fewer experiments need to be conducted, resulting in reduced product development cycle time. As technology keeps changing more rapidly from one generation to the next, computer simulations are much more important to understand the solder behaviors in electronic packaging [5].

2.2 Describe Creep Behavior

Solder alloys are used to bond dissimilar materials that have different thermal expansion coefficients. Once the structure is bonded together, the components are subjected to cyclic thermal stresses due to temperature changes during operation. These stresses arise from mismatch in thermal expansion coefficients. Coefficient of thermal expansion is defined as the ratio of the increase in length, area, or volume of a body per degree rise in temperature compared to its original length, area, or volume, respectively at some specified temperatures. Because the solder is above half of its melting point at a room temperature, it presents a non-linear creep (visco-plastic) response. Steady-state creep strain is generally expressed by a relationship below [38,40-41]

$$\frac{d\gamma_s}{dt} = C_4 \frac{G}{T}\left[\sinh\left(\alpha\frac{\tau}{G}\right)\right]^n e^{\left(\frac{-Q}{kT}\right)} \tag{2.1}$$

Where $d\gamma_s/dt$ is the steady-state creep strain rate, G is the shear modulus, k is the Boltzmann's constant, T is the absolute temperature, τ is the applied stress, Q is the activation energy for the deformation process, n is the stress component, α prescribes the stress level at the which the power law dependence breaks down and C_4 is a constant characteristic of the underlying micro mechanism. The stress component, n, is dependent on the rate-controlling mechanism. For low stresses, n=1 for diffusional creep and n=2 for grain boundary sliding (super plasticity). For intermediate stresses, n=3 to 4 are used for dislocation glide-controlled kinetics while n=5 to 7 are used for dislocation climb processes. The temperature dependence of the shear modulus must be incorporated for obtaining the true activation energy.

$$G = G_0 - G_1(T - 273) \tag{2.2}$$

Where G_0 is the modulus at 0°C (273K) and G_1 gives the temperature dependence. A simplified form of Eq. (2.1) is generally used to define steady-state creep as

$$\frac{d\gamma_s}{dt} = C_5[\sinh(\alpha_1\tau)]^n e^{\left(\frac{-Q_a}{kT}\right)} \tag{2.3}$$

where Q_a is the apparent activation energy

When stress is applied, steady-state creep is not generally achieved immediately. A certain amount of transient (or primary) creep occurs before obtaining steady-state creep. For normal decelerating transient creep, the strain rate starts at a high value and decreases to its steady state value as the material work hardens. Transient creep at constant stress and temperature can be defined by [42]

$$\gamma_c = \frac{d\gamma_s}{dt}t + \gamma_T\left(1 - e^{\left(-B\frac{d\gamma_s}{dt}t\right)}\right) \tag{2.4}$$

where γ_c is the creep strain, $d\gamma_s/dt$ is the steady-state creep rate, γ_T is the transient creep strain, and B is the transient creep coefficient. Taking the time derivative of both sides yields

$$\frac{d\gamma_c}{dt} = \frac{d\gamma_s}{dt}\left(1 + \gamma_T B e^{\left(-B\frac{d\gamma_s}{dt}t\right)}\right) \tag{2.5}$$

where $d\gamma_c/dt$ is the instantaneous creep rate and the $d\gamma_s/dt$ is the steady-state creep rate. Hence, at t=0, the instantaneous creep rate is $(1+\gamma_T B)$ times greater than the steady-state creep rate, once the instantaneous creep rate becomes the steady-state rate. At high stresses, $\tau/G>10^{-3}$, there is also a time-independent plastic strain component in the deformation. The following strain-hardening law can be used to describe high-stress deformation

$$\gamma_p = C_6\left(\frac{\tau}{G}\right)^m \tag{2.6}$$

where γ_p is the time-independent plastic strain, C_6 and m are constants. The total inelastic strain is given by the sum of the creep strain and plastic strain in the form

$$\gamma_{in} = \gamma_c + \gamma_p \tag{2.7}$$

In which γ_{in} is the total inelastic strain, γ_c represents the creep strain, and γ_p is the time-dependent plastic strain. Equations (2.1) and (2.3) to (2.7) can also be written in their tensile forms as

$$\frac{d\varepsilon_s}{dt} = C_{4t}\frac{G}{T}\left[\sinh\left(\alpha_t \frac{\sigma}{G}\right)\right]^n e^{\left(\frac{-Q}{kT}\right)} \tag{2.8}$$

Eq. (2.8) simplified in order to define steady-state creep

$$\frac{d\varepsilon_s}{dt} = C_{5t}[\sinh(\alpha_{1t}\sigma)]^n e^{\left(\frac{-Q_a}{kT}\right)} \tag{2.9}$$

Transient creep at constant stress and temperature can also be defined by the equation as

$$\varepsilon_c = \frac{d\varepsilon_s}{dt}t + \varepsilon_T\left(1 - e^{\left(-B_t\frac{d\varepsilon_s}{dt}t\right)}\right) \tag{2.10}$$

where ε_c represents the creep strain, $d\varepsilon_s/dt$ is the steady-state creep rate, ε_T is the transient creep strain, and B is the transient creep coefficient. Taking the time-derivative of both sides leads to

$$\frac{d\varepsilon_c}{dt} = \frac{d\varepsilon_s}{dt}\left(1 + \varepsilon_T B_t e^{\left(-B_t\frac{d\varepsilon_s}{dt}t\right)}\right) \tag{2.11}$$

$$\varepsilon_p = C_{6t}\left(\frac{\sigma}{G}\right)^m \tag{2.12}$$

$$\varepsilon_{in} = \varepsilon_c + \varepsilon_p \tag{2.13}$$

The following constants can be derived based on application of von Mises yield criteria for effective strain and effective stress as [43]

$$\sigma = \tau\sqrt{3} \tag{2.14}$$

$$\varepsilon = \frac{1}{\sqrt{3}}\gamma \tag{2.15}$$

Based on Eqs. (2.14), and (2.15) the conversion factors between shear and tensile deformation constants are derived as

$$C_{4t} = \frac{1}{\sqrt{3}} C_4 \tag{2.16}$$

$$\alpha_t = \frac{1}{\sqrt{3}} \alpha \tag{2.17}$$

$$C_{5t} = \frac{1}{\sqrt{3}} C_5 \tag{2.18}$$

$$\alpha_{1t} = \frac{1}{\sqrt{3}} \alpha_1 \tag{2.19}$$

$$\varepsilon_T = \frac{1}{\sqrt{3}} \gamma_T \tag{2.20}$$

$$B_t = \sqrt{3} B \tag{2.21}$$

$$C_{6t} = \left(\frac{1}{\sqrt{3}} \right)^{m+1} C_6 \tag{2.22}$$

2.2.1 Creep Deformation Models

There have been defined several different constituve relations for describing the creep behavior of solder joint to predict the fatigue life of a solder joint. There are certain differences between these constituve relations for fatigue life prediction of electronic packages and they cannot be understood exactly, because analysts use finite element programs that are generally limited to specific built-in material models. Once a suitable of failure has been determined, several available models can be employed to predict the lifetime of a solder joint. Although each model has some theoretical basis, all of them rely on empirically determined constants. The formulations are based on some fashion on the damage accumulated in a material per operating cycle. Fatigue is usually correlated in terms of stress and strain. The

most important assumption in such a methodology is that the failure mechanisms are the same under accelerated test and field of use conditions. This assumption can only be verified for highly mature packaging technologies, so that great care must be exercised in the estimation of lifetime predictions [44].

2.2.1.1 Coffin-Manson's Model

Manson, S.S. has developed a model and the following equation describes the fatigue of most metals under cycling load [45].

$$\varepsilon = \varepsilon_e + \varepsilon_p = AN_f^{-c} + BN_f^{-m} \tag{2.23}$$

where ε is the total strain amplitude, which is composed of an elastic component ε_c and a plastic component ε_p. N_f is the lifetime in cycles and A, B, c, and m are the constants dependent on material properties. For large strains, plastic strain is much greater than elastic strain and Eq. 2.23 can therefore rewritten as

$$N_f = \left(\frac{B}{\varepsilon_p}\right)^{1/m} \tag{2.24}$$

This equation is referred to as the Coffin-Manson equation and used for low cycle fatigue formula. It was originally used to describe fatigue due to time independent plastic deformation having results in transgranular cracking along slip planes in a metal. Solder materials typically operate at temperatures greater than half of their melting points. Thus, time dependent creep deformation is generated.

Empirical modifications to the Coffin-Manson equation have been formulated to account for the time and the temperature dependent effects during thermal cycling tests. There are several possible effects such as varying time and temperature in a thermal cycle. Longer dwell time and higher temperatures result in less elastic strain and more plastic creep strain per cycle. Oxidation and corrosion effects are most probably increased. A fundamental problem with this approach is that empirical corrections are only valid for one specific joint and assembly configuration. Extrapolation much beyond the test conditions is difficult. For instance, the effect of increasing dwell time will depend on the assembly stiffness and properties of the solder. Dwell time at the high temperature end of a thermal cycle was more damaging than that at the low temperature end. This would not be predicted from

neither of the empirical relations. The impact of a given dwell time will also depend on the assembly stiffness, because much more rapid stress relaxation occurs in a stiff assembly.

2.2.1.2 Integrated Matrix Creep Model

Ianuzelli, R.J. [45] has developed a model to predict the total creep in solder joints by using integrated matrix creep model. The creep rate equation is defined as

$$\frac{d\varepsilon_{total}}{dt} = Ae^{\left(\frac{-B}{T}\right)}\sigma^{C} + De^{\left(\frac{-E}{T}\right)}\sigma^{F} \tag{2.25}$$

The creep equation can be rewritten in a different form to provide the analyst using finite element method in order to define the constants in terms of user routine variables

$$\frac{d\varepsilon_{total}}{dt} = C_7 e^{\left(\frac{-C_8}{T}\right)}\sigma^{C_9} + C_{10} e^{\left(\frac{-C_{11}}{T}\right)}\sigma^{C_{12}} \tag{2.26}$$

In order to access this creep relation in the user implemented creep routines, the following lines are required,

TB,CREEP,MATNUM

TBDATA,1,3,,,,,100

TBDATA,7,C_7,C_8, C_9, C_{10}, C_{11}, C_{12}

2.2.1.3 Dorn's Model

Dorn has a different model to predict the total creep in solder joints [46] and the creep rate equation is defined as

$$\frac{d\varepsilon_s}{dt} = \frac{AGb}{kT}\left(\frac{b}{d}\right)^{p}\left(\frac{\sigma}{G}\right)^{n} D_0 e^{\left(\frac{-Q}{RT}\right)} \tag{2.27}$$

The creep equation can be rewritten in a more suitable form to provide the analyst to use finite element method and define the constants in terms of user routine variables.

$$\frac{d\varepsilon_s}{dt} = \frac{C_7 G C_{10}}{C_{11} T}\left(\frac{C_{10}}{C_{12}}\right)^{C_{13}}\left(\frac{\sigma}{G}\right)^{C_{14}} C_{15} e^{\left(\frac{-C_{16}}{C_{17}T}\right)} \tag{2.28}$$

$$G = C_8 - C_9 T \tag{2.29}$$

To access this creep relation in the user implemented creep routines, the following lines could be sufficient

TB,CREEP,MATNUM

TBDATA,1,2,,,,,100

TBDATA,7,C_7,C_8, C_9, C_{10}, C_{11}, C_{12}

TBDATA,13,C_{13},C_{14}, C_{15}, C_{16}, C_{17}

2.2.1.4 Anand's Model

Anand, L. [5] developed a creep rate constituve model to predict the total creep in solder joints and the creep rate equation is defined as

$$\frac{d\varepsilon}{dt} = C_{7t}[\sinh(\alpha_{2t}\sigma)]^n e^{\left(\frac{-Q_a}{kT}\right)} \tag{2.30}$$

where $d\varepsilon/dt$ is the total inelastic strain rate combining both time dependent and time dependent plasticity in the form of a curve fit in terms of the constants C_7, α_{2t}, n, Q_a, and k. Values for these constants are generally defined by Darveaux. The creep equation can be written in a different form in order for the analyst to use finite element method and define the constants in terms of user routine variables

$$\frac{d\varepsilon}{dt} = C_7[\sinh(C_8\sigma)]^{C_9} e^{\left(\frac{-C_{10}}{C_{11}T}\right)} \tag{2.31}$$

The equation allows the user to define the constants in terms of the variables. The following lines are required in order to access this creep relation in the user implemented creep routines,

TB,CREEP,MATNUM

TBDATA,1,1,,,,,100

TBDATA,7,C_7,C_8, C_9, C_{10}, C_{11}

2.2.2 Using Creep Deformation Models

To be able to use the creep deformation model, a creep data table must be generated using TB and TBDATA commands. In order to operate the user creep routines, creep data for a particular material has to be entered in the form of data tables. ANSYS provides a method to enter the data using the TBDATA command,

TB,LAB,MAT

and

TBDATA,STLOC,C_1, C_2, C_3, C_4, C_5, C_6

TB command activates a data table. LAB label specifies the type of data table. For the present problem, CREEP is used as the label. MAT specifies the material reference number. TBDATA command provides the data for the data table. STLOC expresses the starting location in the table for entering data. The variables used in the models are given in Table 2.1.

Table 2.1 Value of variables in ANSYS

C_1=1	ANSYS will use the Anand's Model in usercr.F
C_1=2	ANSYS will use the Dorn's Model in usercr.F
C_1=3	ANSYS will use the IMC Model in usercr.F
C_2-C_5=blank	Unused fields
C_6=100	Required for ANSYS to use the user implemented creep
C_7-C_{17}	Fields for material properties in the models

2.2 Mechanical Characterization of BGA Solder Joints

Solder joint samples subjected to thermal aging were used in accelerated experiments [5]. Although there are some experimental errors, an average shear stress and shear strain can be extracted from the following Figure 2.1 [5].

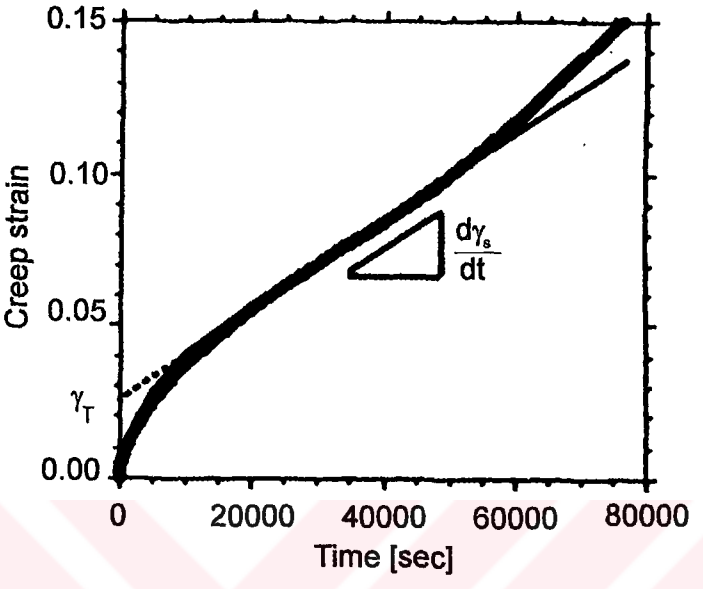

Figure 2.1 Typical creep-strain plot for constant load test [5].

while conducting all experiments, a trial-and-error curve-fitting procedure was used to determine the steady-state constants Q, Q_a, C_4, C_5, α, and α_1. The stress exponent, n, is prescribed by the lowest stress data. The steady-state creep rate, γ_s, and the transient creep rate, γ_T, were determined from the slope and intercept of the linear part of a creep-strain plot, as shown in Figure 2.1. The transient creep coefficient, B, was determined via trial-and-error from the creep strain-time plot. The time-independent plastic strain constants, C_6 and m were determined from the low strain portion of the highest strain rate, lowest temperature test [5].

In general, the alloys with a higher stress exponent, n=5 to 7, also has high transient creep (higher γ_T), which is consistent with conventional creep theory. Alloys with a lower stress exponent, n=3 to 5, exhibit much less transient creep, especially at low stress levels. Time-dependent plastic flow was observed in all of the alloys at high stresses [5]. Derived tensile constants based on a von Mises flow criteria on using the equations described in creep behavior. Solder alloy deformation constants for elastic, steady-state creep, transient creep, and time-dependent plastic flow

behavior are available in literature and they can be used in the creep behavior equations to characterize the solder behavior.

Test conditions can be modeled by using finite element method. Finite element codes have the capability to model both time-independent and time-dependent non-linear deformation and they offer a sinh steady-state creep relation such as Eq. (2.9) for time-dependent deformation and stress-strain input tables for time-independent deformation. In general, the input data is required in terms of unaxial tensile deformation. A von Mises relation is, therefore, used to calculate the effective stress and strain in the material. Transient creep behavior can also be incorporated into most of the available finite element codes.

ANSYS has viscoplastic elements that offer sinh steady-state creep equation simultaneously with time-independent stress-strain input as a standard input. VISCO107 is designed to solve both rate-independent and rate-dependent large strain plasticity problems. Iterative solution procedures must be used along with VISCO107, which is used to represent highly nonlinear behavior. Large deflections [NLGEOM] must be active in order to update the geometry at each sub step. The element input data includes eight nodes with linear and nonlinear material properties. The element can be used to compute stresses, principal stresses, stress intensity, equivalent stress, elastic strains, principal elastic strains, plastic strains, plastic state variable, plastic work/volume, and total strain (excluding thermal strain).

2.3 Thermal Fatigue

To understand the failure on solder joints, the crack initiation and propagation through a joint can be examined. The location and nature of cracks depend on the joint configuration, intermetallic structure, strain rate, and temperature changing on the package. Cracks usually start at high stress concentration points and the direction whereas propagation depends on the shape of the joint and the relative degree of tensile versus shear loading. Higher joint stresses due to higher strain rates or creep-resistant solders result in more fractures near solder/component interfaces. Interfacial fracture is more likely to happen due to poor intermetallic/solder adhesion, brittle intermetallics, or deplection of a solder constituent near the intermetallic layer. Higher strain rates or lower temperatures result in transgranular cracking. Lower strain rates, longer hold times, and higher temperature lead to intergranular cracking. Oxidation also leads to more

intergranular fracture. A higher strain range results in more transgranular fracture and a lower strain range results in more intergranular fracture. For near eutectic Pb/Sn solders, localized coarsening in high stress areas precedes cracking.

Crack initiation and growth depends on the configuration of solder joints. Peripheral leadless joints generally initiate a major crack at the corner of the chip carrier or underneath the carrier [48]. Because of the high stresses and strains in this region, propagation under the carrier is quite fast. Gull-wing leaded joints generally start in the heal fillet and the possibly toe fillet as well [54-55]. These two cracks meet in the center by propagating inward. Ball grid array joints initiate a primary crack on the outer edge of the joint and a secondary crack initiates on the inner edge later. These cracks generally take place near the substrate interface side. On the contrary flip chip joints initiate crack on opposite corners near the interfaces and a single crack will propagate across the joint [54]. Crack initiation and growth in surface mount solder joints are illustrated in Figure 2.2.

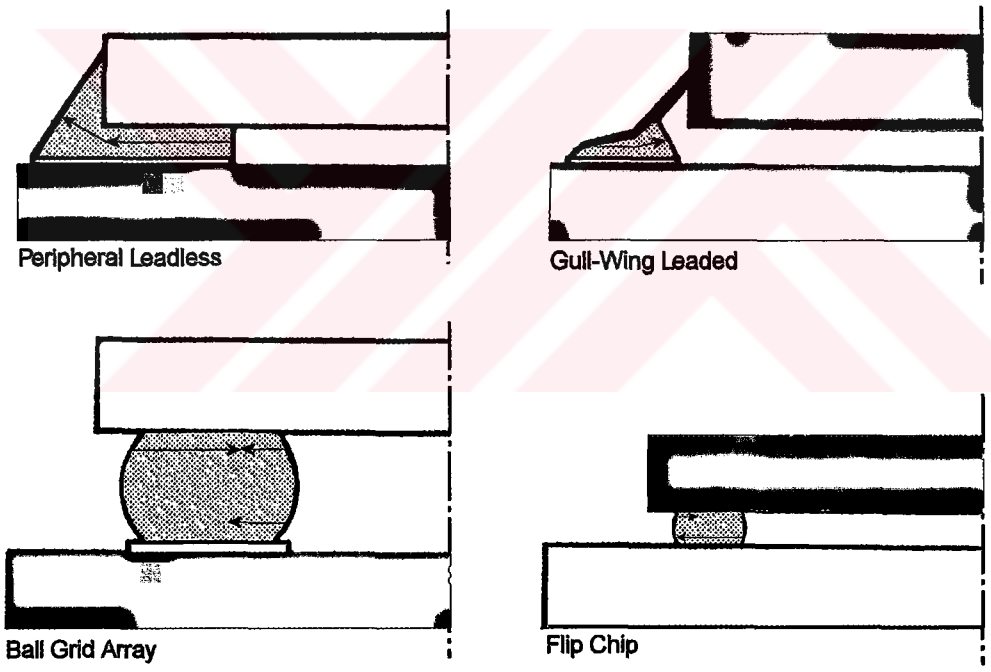

Figure 2.2 Crack initiation and growth in surface mount solder joints [5].

Many researchers have studied crack growth in solder joints. They achieved equations to determine the crack length. First, Solomon, H.D. [58] measured cracked area in scaled-up joints under isothermal shear loading using ultrasonic microscopy and approximately correlated the cracked area with load drop. Afterwards, Solomon, H.D. [59] used the load drop data to predict failure in leadless

surface mount joints under isothermal shear loading. Furthermore, Subrahmanyan, R. [60] derived crack growth rates from load drop data and he incorporated the data into a damage integral function for fatigue life prediction. While applying the approach to thermal fatigue data, he only considered damage integral to correlate different thermal cycle profiles instead of calculating the cycles to failure directly. Satoh, R. et al. [54] and Attarwala, A.I. et al. [61] predicted crack growth rates in solder joints after thermal cycling by measuring striations using high resolution scanning electronic microscopy. Satoh, R. et al. [54] developed fatigue life expressions that accounted crack length, but they didn't derive explicit equations to estimate crack growth rate as a function of calculated stress or strain in the solder joints. Cletch, J.P. et al. [53] developed a methodology to predict the fatigue life based on the average viscoplastic strain energy density in the solder joint. They normalized data from different joint configurations using the crack area.

To determine the crack growth and length, many experiments were conducted for eutectic BGA joints using thermal cycle conditions. Measuring crack growth in solder joints, a technique was developed [5]. Dye penetrant was applied under the chip carriers from the sample population at regular intervals. The chip carriers were pried off the boards showing the fracture surfaces of the solder joints. As all cracked areas are covered by the dye, the initiation locations, size, and shape of the cracks can be easily seen. It is also seen that primary crack grows from outside of the edge while secondary crack grows from inside edge. Besides, primary and secondary crack lengths were measured along lines extending from the package neutral point to the outermost joints. Cletch, J.P. [62] and Nicewarner, E. [62] analyzed the crack length data using 3P Weibull distribution. In their analysis, they determined characteristic length of crack, maximum crack length and shape parameter. Darveaux, R. [64] also determined the mean crack length in his analysis.

If the maximum crack length and the characteristic crack length are compared to each other, it is seen that there is a large variation for populations of short cracks, but much less variation for long cracks. Therefore, as the cracks get longer, their length distribution gets tighter. Agarwala, B.N. [57] also observed this situation before. Figure 2.3 shows a plot for reciprocal crack length and cumulative distribution. The ratio of maximum to characteristic crack length plot is also shown in Figure 2.4. Considering that the fatigue life will be inversely proportional to the crack growth rate, it may be expected that the minimum fatigue life will be about half as long as the characteristic fatigue life. Actually, Cletch, J.P. et al. [62] found that the

ratio of failure free life to characteristic life was about 0.46 based on his analysis on a large database.

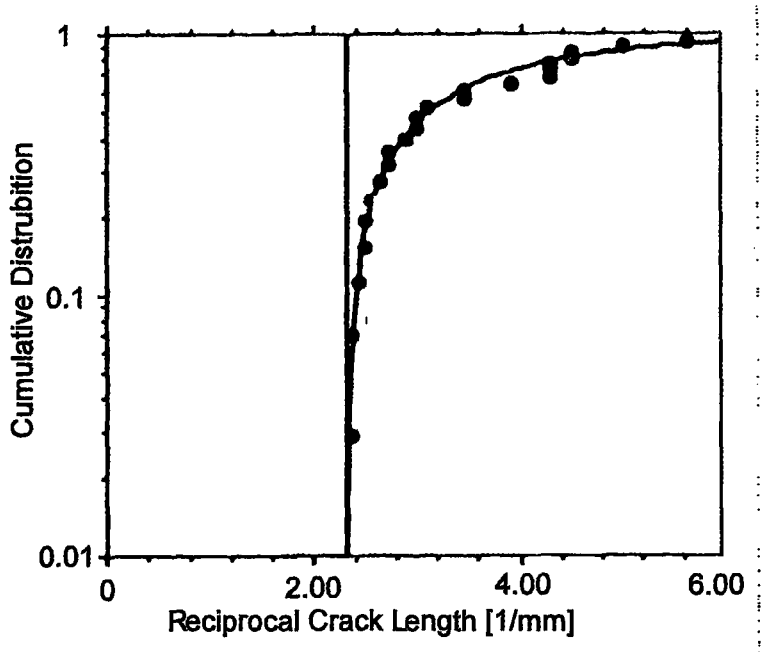

Figure 2.3 3P Weibull plot of reciprocal crack length [5].

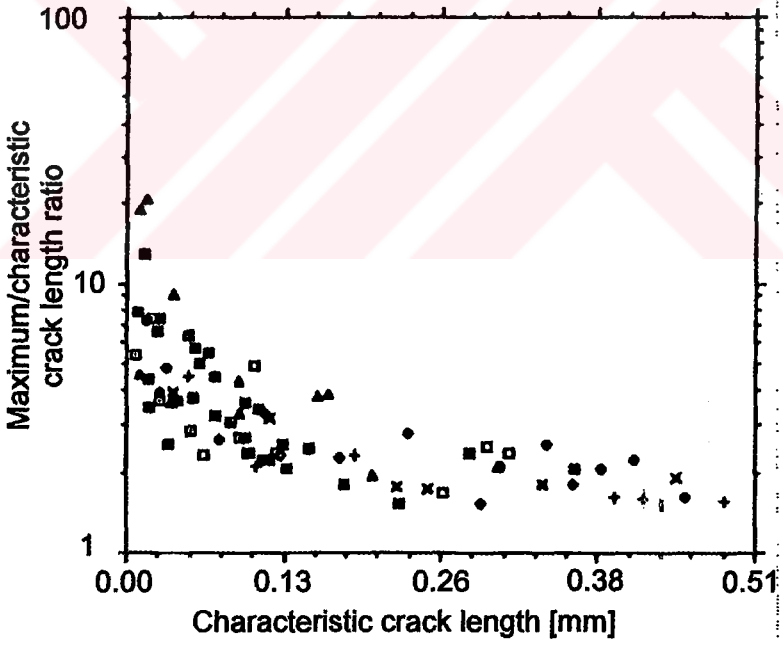

Figure 2.4 Crack length variations [5].

2.4.1 Thermal Failure Prediction Model

It has been found that crack initiation and crack growth has correlation with stresses and strains in the solder joints. Many researchers studied several indicators for

fatigue life, such as total strain range [54], inelastic strain range [67-69], matrix creep strain range [70], viscoplastic strain energy increment (plastic work per unit volume) [62], J Integral and stress intensity factor [75], and the damage integral [60]. Considering all these work, Darveaux, R. [64] used the inelastic strain range and the viscoplastic strain energy density. There are number of thermal fatigue models each having its own merits. Normally, these models employ finite element analysis to calculate key parameter of the package. One of the widely accepted failure criteria for thermal fatigue life correlation is based on the volume-weighted average plastic work density increment, (ΔW_{ave}) [76]. As strain energy density was found to give the best correlation to the crack growth data in most cases, both the inelastic strain range ($\Delta\varepsilon_i$) and the viscoplastic strain energy density (ΔW_{ave}) was used in Darveaux's study. A finite element analysis was used with failure models for fatigue life prediction of electronic packages. The widely accepted model for predicting the fatigue life of a solder joint is based on the volume weighted average plastic work density. This model, introduced by Darveaux, R. [64], contains experimental measurements at the package level and uses specific values of certain parameters. These parameters were determined through curve fitting against measurements in conjunction with the finite element simulation using ANSYS. This failure prediction model provides a relationship between the quantity ΔW_{ave}, the number of cycles to crack initiation (N_0), and the crack propagation rate (da/dN),

$$N_0 = K_1 \Delta W_{ave}^{K_2} \tag{2.32}$$

$$\frac{da}{dN} = K_3 \Delta W_{ave}^{K_4} \tag{2.33}$$

where K_1, K_2, K_3, and K_4 are crack growth constants, and "a" is the characteristic crack length. "a" is generally taken as a pad diameter. However, if the pad diameter and neck size of solder ball are different from each other, it is taken as a solder ball neck size. It can be assumed that crack propagation rate is constant. The characteristic life is then calculated as

$$N_\alpha = N_0 + \frac{a}{da/dN} \tag{2.34}$$

The parameter ΔW_{ave} is defined as

$$\Delta W_{ave} = \left(\sum_{i=1}^{\text{number of elements}} \Delta W_i \cdot V_i \right) / \left(\sum_{i=1}^{\text{number of elements}} V_i \right) \quad (2.35)$$

The equation above represents the volume-weighted average of total plastic work density accumulated per thermal cycle. ΔW_i is the plastic work density in the i^{th} element and V_i is the volume of the element. As the value of ΔW_i is dependent on the thickness of the finite elements, the parameters, K_1, K_2, K_3, and K_4 are dependent on the geometry, loading and finite element analysis method. Gustaffson, G. et al. [77] have found that the type of the finite element analysis method affects the plastic work density calculation significantly. Darveaux, R. [74] stated these parameters using both the nonlinear sub models and linear global models with a nonlinear sub model of the critical solder joint.

3. MODELLING AND OPTIMIZATION PROCEDURE

3.1 Introduction

Three different package types provided by the companies in the electronics industry were used. Three dimensional linear or nonlinear finite element models, describing global and sub models, were created and the material properties, methodology, and boundary conditions were consistent throughout in each package analysis. ANSYS 5.6 was used for all aspects: preprocessing, solution and post processing. The analysis is conducted by constructing three dimensional linear or nonlinear finite element models of the package assemblies.

In order to reduce the computation time, the global model was solved as a linear problem. So, the printed circuit board is modeled as an orthotropic linear elastic solid and the rest of the materials including solder material as linear elastic solids.

Both in analyses of global model and sub model, in order to reduce the computation time, only a part of the assembly were modeled. A quarter of the assembly was modeled in first and second type of packages and an octant of the assembly was modeled in third type of packages.

The solder material is modeled as a visco plastic solid, the printed circuit board as orthotropic linear elastic solid and the rest of the materials as linear elastic solids. In each calculation, thermal cycles are simulated in order to establish a stable stress-strain hysteresis loop. These packages are subjected to a specified temperature cycle. In the finite element analysis of each package, a linear global model with a relatively coarse mesh for the substrate, printed circuit board and the solder balls provides the critical joint for the subsequent nonlinear sub modeling of the critical solder joint. The critical joint for sub modeling is identified based on the amount of inelastic (plastic) work density at the end of the last cycle.

After determining the most critical solder ball, all analyses are conducted by constructing three dimensional nonlinear finite element models of the package assemblies. The solder material is modeled as a visco plastic solid, the printed

circuit board as orthotropic linear elastic solid and the rest of the materials as linear elastic solids.

In order to build the finite element model, the geometry, material properties, coupling, and constraint equations must be defined step by step. The geometry is defined by using the package sizes obtained through the industry. SOLID45, PLANE42, and VISCO107 are used in the global model of the packages.

PLANE42 is used for 2-D modeling of solid structures. The element can be used either as a plane element (plane stress or plane strain) or as an axisymmetric element. Four nodes having two degrees of freedom at each node define the element: translations in the nodal x and y directions. The element has plasticity, creep, swelling, stress stiffening, large deflection, and large strain capabilities. The element input data includes four nodes, a thickness (for the plane stress option only), and the orthotropic material properties. Orthotropic material directions correspond to the element coordinate directions. Pressures may be input as surface loads on the element faces. Temperatures and fluencies may be input as element body loads at the nodes. TUNIF command can be used for this. It is possible, if the element is linear, to obtain stress intensity, equivalent stress, elastic strains, principal elastic strains, stresses, principal stresses. If the element is used in nonlinear analysis, plastic strains, equivalent plastic strain, creep strains can also obtained.

SOLID45 is used for the three-dimensional modeling of solid structures. The element is defined by eight nodes having three degrees of freedom at each node; translations in the nodal x, y, and z directions. The element has plasticity, creep, swelling, stress stiffening, large deflection, and large strain capabilities. The other features are similar to the PLANE42.

VISCO107 is three-dimensional viscoplastic solid and used for three-dimensional modeling of solid structures. It is defined by eight nodes having three degrees of freedom at each node; translations in the nodal x, y, and z directions. The element is designed to solve both isochoric (volume preserving) rate independent and rate dependent large strain plasticity problems. Iterative solutions must be used with VISCO107 since it is used to represent highly nonlinear behavior. Large deflections [NLGEOM] must be active in order to update the geometry each step. The element input data includes eight nodes and linear and nonlinear material properties. Pressures may be input as surface loads on the element faces. Temperatures may

be input element body loads at the nodes. All elements must have eight nodes. A tetrahedron shape is also available. Only the isotropic and Anand material laws (BISO. MISO, ANAND on the TB command) are valid for this element.

Material properties can be assigned certain element types. The main objective to create the model geometry is to generate the finite element model including nodes and elements, which adequately describes the model geometry. In this study, several input files were created to form the model geometry. Solder balls, copper pads, substrate, die attaches, molding compound, silicon die, solder mask and motherboard were created by using several different macro files. After creating the model, meshing process was applied to obtain the nodes. When generating the model, the relationships among different degrees of freedom must be defined by using elements to link the other nodes. Sometimes, it is needed to be able to model distinctive features (rigid regions, pinned structural joints, sliding symmetry boundaries and other special connections), which cannot be adequately described with elements. But, unfortunately all constraint equations are based on small deflection theory. Therefore, their use in large deflection analyses [NLGEOM] is invalid. Constraint equations cannot be used in combination with the Jacobi Conjugate Gradient solver [EQSLV]. Consequently, Pre-Conjugate Gradient (PCG) solver is used in this study.

3.2 Creating Global Model

The package geometry is defined by using the package sizes obtained through the industry. Preprocessor was used to create the global model geometry. Electronic package geometry is shown in Figure 3.1. The package geometry was formed and the materials and their properties were defined. SOLID45 and PLANE42 are used in the global model of the packages. After creating the model, meshing process was applied to obtain the elements and the nodes. Global model's mesh is respectively coarse to the sub model to reduce the computation time. In all global models, appropriate symmetry boundary conditions are utilized to minimize the computations. The center of the package is constrained in all directions at the bottom to prevent free rigid body rotations and translations. In the global modeling of each package, either quarter or octant model is considered, depending on the symmetry conditions. To apply the boundary conditions, a macro file was developed and used. The primary objective of a finite element analysis is to examine the response of a structure or component to certain loading conditions. Therefore, the

proper loading conditions must be applied to express the situation. In global model, one load step is used. 1 °C thermal changing is applied to the model as a body load at the nodes. And all results are saved a file to use for the sub model. TUNIF command is used for this. After doing the finite element analysis of the global model as a linear problem, results were kept to use in sub models.

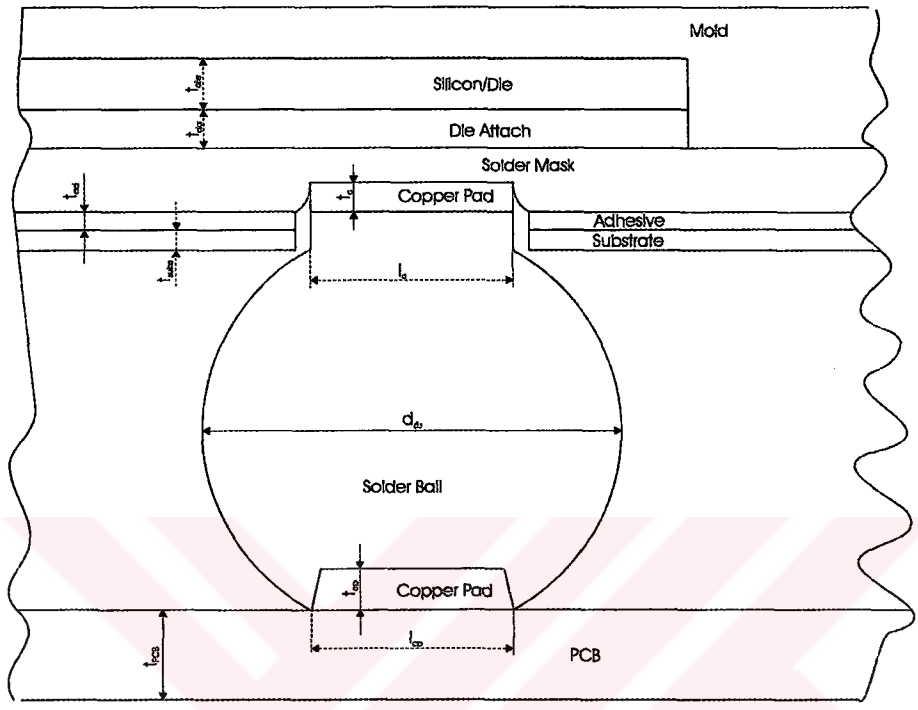

Figure 3.1 An electronic package.

3.3 Finding Out Most Critical Solder Ball by Using SED (Strain Energy Density) Method

To be able to create the sub model, the most critical solder ball of the package must be found. There are several methods to find out the critical ball. One of them is to compare the displacements in certain directions. This method was used to find out the critical solder ball in this study, but it was seen that it was not convenient and sufficient to decide to critical solder joint. So, the strain energy density method was applied to the package and it was realized that most critical solder ball can be found by using strain energy density method. A macro was created and applied to the package. After choosing the neck part of the solder ball, the strain energy density was computed for each ball in each package. Most critical solder ball is the one having highest strain energy density. It is also confirmed by doing the analysis for sub model for many cases. The macro first computes the strain energy and volumes

for the balls separately. Then strain energy density can be determined by using these values.

Most critical solder ball having highest strain energy density is computed for each package used in the study. They are represented with the numbered balls below. The one in the square is the critical solder ball for the package. These numbered balls namely critical solder balls are shown below.

For the first package, the critical solder ball is the one at the corner near the chip end as it is expected. If the balls are represented to show the solder ball's location in the quarter global model, it can be easily seen. 6th solder ball is the critical solder ball. To check the results, more than one sub model was created and solved to compare the results. The critical solder ball has the highest strain energy density and lowest fatigue life.

1	5	9	13
2	6	10	14
3	7	11	15
4	8	12	16

For the second package, the critical solder ball is the one at the corner of the chip end of the quarter global model. If the balls are represented with the same way, 7th solder ball is the critical solder ball. To check the results, more than one sub model was created again and solved to compare the results.

		5		10
		6		11
1	3	7		12
				13
2	4	8	9	14

For the third package, the critical solder ball is at the corner near the chip end of the octant global model. If the balls are represented with the same way, 4th solder ball is the critical solder ball. To check the results, more than one sub model was created

again and solved to compare the results. It is also seen that the critical solder ball has the highest strain energy density and lowest fatigue life.

1 8

2 9

3 10

4 11

5 12

6 13

7 14

3.4 Creating Sub Model

In order to build the finite element model of the sub model, the geometry, material properties, coupling, and boundary conditions must be defined. The geometry is created by using the package geometrical sizes. SOLID45, PLANE42, and VISCO107 are used in the global model of the packages.

The sub modeling permits refinement of the mesh. Sub modeling is a finite element method to get more accurate results in a region of the model. To obtain more accurate results sub modeling technique used. Sub modeling is also known as the cut-boundary method or the specified boundary displacement method. The cut boundary is the boundary of the sub model, which represents a cut through the coarse global model. Displacements on the cut boundary of the coarse model are specified as boundary conditions for the sub model. Sub modeling is based on St. Venant's principle, which states that if an actual distribution of forces is replaced by a statically equivalent system, the distribution of stress and strain is altered only near the regions of load application. This implies that stress concentration effects are localized around the concentration; therefore, if the boundaries of the sub model are far enough away from the stress concentration region, reasonably accurate results can be calculated in the sub model. The displacements from the global model become the boundary conditions for the nonlinear sub model of the critical solder joint. The displacement boundary conditions are determined from the solution

of the global analysis through the use of the cut boundary interpolation method. But, to adapt the value of the displacements to the thermal cycle behavior, each displacement multiplied with the temperature. For these multiplying processes, another macro is developed and used. In the sub modeling of each package, either half or entire solder ball is considered, depending on the location of the critical solder ball.

Nonlinear stress-strain relationships are a common cause of nonlinear structural behavior. Many factors can influence materials' stress-strain properties, including load history (as in elasto-plastic response), environmental conditions (such as temperature), and the amount of time that a load is applied (as in creep response). Nonlinear solutions involve breaking the load into a series of load increments. The load increments can be applied either over several load steps or over several sub steps within a load step. At the completion of each incremental solution, the program adjusts the stiffness matrix to reflect the nonlinear changes in structural stiffness, before proceeding to the next load increment. The ANSYS program uses Newton-Raphson equilibrium iterations, which drive the solution to the equilibrium convergence (within some tolerance limit) at the end of each load increment. If convergence criteria are not satisfied, the out-of-balance load vector is re-evaluated, the stiffness matrix updated, and a new solution is obtained.

Creep is a rate dependent material non-linearity in which the material continues to deform under a constant load. The creep strain may be a function of stress, strain, and temperature. For highly nonlinear creep strain, a small time step must be used. A creep time step optimization procedure is available ([AUTOTS], [CRPLIM]) for automatically adjusting the time is appropriate. Viscoplasticity is a time-dependent phenomenon, where the development of the plastic strains is dependent on the rate of loading. The plastic strains are typically very large, requiring large strain theory [NLGEOM,ON]. Viscoplasticity is modeled with element types VISCO107 here, using Anand's model for given material properties.

In sub model, 60 load steps are used for four thermal cycles. Finite element model is subjected to a temperature between –40°C and 125°C with dwell times of 24 minutes and 26 minutes, respectively. The time from the minimum temperature to the maximum temperature was 4 minutes and the time from maximum temperature to the minimum temperature was 6 minutes and the stress-free reference temperature was 25°C. These thermal cycles simulate the accelerated tests on solder joints, or another saying, they simulate the thermal changing on the electronic

package during operating the machines using packages. A macro is created and used to give the thermal cycle conditions and the solutions were achieved by using LSSOLVE command. The program has done the analysis for 60 load steps.

The temperature cycling profile and temperature portions are shown in Figure 3.2. First, the temperature was ramp up from room temperature (stress free reference temperature) of 25°C to 125°C in certain increments. The model was then held at the dwell temperature of 125°C for 26 minutes for creep analyses to be performed. After 125°C dwell, the temperature will be ramp down to -40°C with visco plastic analysis performed on the model at every increment. Following this, the model was then held at the -40°C for 24 minutes for creep analysis. Finally, the temperature was ramp back to 25°C for similar visco plastic analysis after the -40°C dwell to complete one temperature cycle. Similarly, this temperature cycling pattern was also executed four times to obtain the complete equivalent stress and strain hysteresis for the solder material. The equivalent plastic strain range and equivalent creep strain range obtained will then be used for fatigue and creep life prediction.

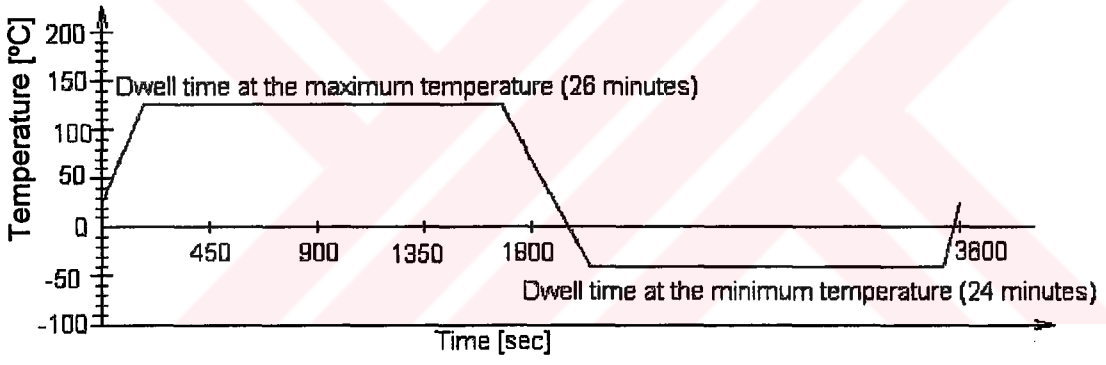

Figure 3.2 Creep analysis in relation to temperature cycling profile.

3.5 Rate Dependent Plasticity (Viscoplasticity) in Finite Element Analysis

Rate-dependent plasticity (or viscoplasticity) is characterized by the irreversible straining that occurs in a material over time. The plastic strains are assumed to develop as a function of the strain rate. The ANSYS program provides two options to characterize different type of rate-dependent material behaviors and they are only available with the large strain solids. These options are Anand's model and user specified behavior.

Rate-dependent plasticity model is proposed by Anand, L. [78] and Brown, S.B. [79] et al. This rate dependent model differs from the rate independent model is that there is no explicit yield condition and no loading/unloading criterion is used. Instead, plastic flow is assumed to take place at all non-zero stress values, at low stresses the rate of plasticity flow may be immeasurably small. Further, the equivalent plastic strain rate, which is determined by the consistency condition in the rate independent model, needs to be prescribed by an appropriate constituve function in the rate dependent model.

3.5.1 Theory of Anand's Model

There are two basic features in Anand's model applicable to isotropic rate dependent constituve model for metals. First, there is no explicit yield surface; rather the instantaneous response of the material is dependent on its current state. Secondly, a single scalar internal variables "s", called the deformation resistance, is used to represent the isotropic resistance to inelastic flow of the material. The specifies of this constituve equation are the flux equation

$$\frac{d\varepsilon_p}{dt} = Ae^{\left(\frac{-Q}{kT}\right)}\left[\sinh\left(\xi\sigma/s\right)\right]^{1/m} \tag{3.1}$$

and the evolution equation

$$\frac{ds}{dt} = \left(h_0\left(|B|\right)^a \frac{B}{|B|}\right)\frac{d\varepsilon_p}{dt} \tag{3.2}$$

Eq. (3.2) allows modeling not only strain hardening, but also strain softening. Where

$$B = 1 - \frac{s}{s^*} \tag{3.3}$$

with

$$s^* = s\hat{}\left[\frac{d\varepsilon_p/dt}{A}e^{\left(\frac{Q}{kT}\right)}\right]^n \tag{3.4}$$

where $d\varepsilon_s/dt$ is affective inelastic strain rate, σ is effective Cauchy stress, s is deformation resistance, s^* is saturation value of deformation resistance, ds/dt is time derivative of deformation resistance and T is absolute temperature. The remaining terms are defined in Table 3.1. The inelastic strain rate in Anand's definition of material is temperature and stress dependent as well as dependent on the rate of loading. Determination of the material parameters is performed by curve-fitting a series of the stress strain data at various temperatures and strain rates as in Anand, L. [78] or Brown, S.B. et al. [79].

Table 3.1 Material parameter units and values for Anand model.

TBDATA Constant	Parameter	Meaning	Units	Value
C_1	S_0	Initial value of deformation resistance	Stress [MPa]	12.41
C_2	Q/k	Activation energy/universal gas constant	1/Temperature [1/°K]	9400
C_3	A	Pre-exponential factor	1/Time [1/sec]	4000000
C_4	ξ	Multiplier of stress		1.5
C_5	m	Strain rate sensitivity of stress		0.303
C_6	h_0	Hardening/softening constant	Stress [MPa]	1379
C_7	s^	Coefficient of deformation resistance saturation value	Stress [MPa]	13.79
C_8	n	Strain rate sensitivity of saturation (deformation resistance) value		0.07
C_9	a	Strain rate sensitivity of hardening or softening		1.3

The deformation resistance s is output quantity [PSV]. The accumulated plastic work is output as output quantity [PLWK].

Creep is defined as material deforming under load over time in such a way as to tend to relieve the stress. Creep may also be a function of temperature. The term relaxation has also been used interchangeably with creep. The material is assumed to be isotropic and the basic solution technique used in the initial stiffness by Newton-Raphson method.

3.6 Optimization Procedure

The numerical optimization automated search techniques provide tools that optimal design of electronic packages in general, and solder joints in particular to maximize solder joint reliability through optimal design. There is also considerable difficulty in using these procedures for solder joints since the estimation time of the fatigue life is computationally very time consuming. In this study linear regression models are developed to approximate the fatigue life as a function of solder joint design parameters. Although these approximate surfaces are easier to evaluate, their use of the numerical optimization techniques leads to a computationally efficient method for optimizing electronic packages. The developed techniques are demonstrated using three different packages. An exact optimization method of the solder joints (without approximations) is also carried out and used for comparing the accuracy and efficiency of the developed models.

Gill, P.E. et al. [27], Haug, E.J. and Arora, J.S. [28], and Haftka, R.T. and Gurdal, Z. [29] have studied about the automated search techniques. The numerical optimization techniques are iterative procedures, usually based on local approximation of the design criteria. In most efficient applications, the direction of search in the space of possible designs is determined by minimizing a simplified sub problem (often quadratic programming), which is generally built using the first or second order Taylor series approximation to the problem functions [30]. Thus, derivatives of problem functions are necessary to build the local approximations and to determine the search direction.

The fatigue life of solder joints depends on the strains and stresses in the solder joints under the user environment. The stresses depend on the shape of solder joints. Since the solder joint design parameters will have to be iteratively improved during design optimization, automatic determination of fatigue life is important for efficiency. Although a system for optimizing solder joint configurations has been investigated in the literature by Nigro, N.J. et al. [80], such a system has been difficult to achieve in practice due to difficulty in automating the procedure for fatigue life determination. However, Subbarayan, G. [33] has also developed a mathematical model and a finite element solution procedure for predicting the shapes of three-dimensional flip-chip BGA/solder joints with arbitrary pad shapes and with possible misalignment between pads. Subbarayan, G. also developed an automated three-dimensional mesh generation procedure that was coupled with a commercial finite element code for nonlinear stress analysis. The result was a CAD

system for flip-chip BGA/solder joints that was capable of automatically determining the fatigue life given inputs on the shapes of pads, solder volume, solder material behavior, and environmental use condition. Although the determination of fatigue life was automated by his system, the process was taking several hours of CPU time on a fast workstation due to the computational expense associated with the nonlinear finite element analysis [33]. Therefore, the iterative optimization process would be highly expensive, especially if gradients were to be computed by forward difference approximation requiring an additional function evaluation for each variable (n additional analyses at each iteration if there are n design parameters). In conclusion, analysis of solder joints is computationally expensive, approximation techniques that will reduce the number of function evaluations are necessary for improved efficiency. One such technique was global approximation method of structural optimization by Haftka, R.T and Gurdal, Z. [29]. These approximations were global in nature unlike the local Taylor series approximation used in optimization codes for search direction determination. Consequently, these methods built an approximate representation of the problem function surfaces over the entire range of design parameter space, rather than in the neighborhood of a design point.

Although the global approximation methods were considerable important for optimizing electronic packages that are computationally expensive to analyze a few years ago, there were a few applications of the method in the literature. The optimization procedure of Sarihan, V. [32] was based on a quadratic approximation to the function which is continuously refined as optimization progresses. In his approach, even though the quadratic approximation was refined at each iteration, the refinement was based on points generated by an optimization algorithm. Therefore, this procedure didn't provide a truly global approximation to the problem function surface.

In general, there are several difficulties in building a global approximation. Mainly, the number and location of points at which is evaluated will critically determine the computational expense and accuracy of the resulting approximation. Furthermore, the accuracy of representation depends on the ability of the approximation procedure to capture surfaces that are geometrically nonlinear for a given set at which the function value is known. In this study, a global approximation concept based on design of finite element analyses, linear regression models, is developed to optimize solder joint shapes and mold compound material properties for

maximum reliability and maximum fatigue life. Three different packages, namely 64 I/O, 56 I/O, and 96 I/O PBGA, were used by applying the techniques.

The life of all the solder joints in a BGA package is only as good as the worst solder joint. The worst solder joint is found by using maximum strain energy density method, which is developed in this study. So the solder joint configuration that gives the maximum fatigue life for this worst-case solder joint was chosen as the goal of the optimization in this study. Since the configuration of the solder joint is dependent on the upper neck radius of the solder ball and the amount of solder volume, these two parameters were chosen as the first design variable group for the optimization process. As Mold Compound material properties were still challenging subject for solder joints reliability, mold compound's elasticity modulus and thermal expansion coefficient were chosen as the second design variable group. In this study, due to the design focus, the solder joint volume includes the solder ball including solder ball neck volume and subtracting solder pad volume. The volume of this solder ball and the diameter of the top radius of solder ball were chosen as the design variables in present study. Solder ball upper radius (neck size) and solder ball volume cannot be increased because of the geometrical restrictions. To reduce the number of variables and to avoid the arbitrariness in the values of the top and bottom diameters, it was assumed that the bottom diameter was constant. At the same time, the bottom diameter depends on the bottom pad's diameter and it can only be changed by the PCB manufacturers.

The determination of the fatigue life for a given combination of solder ball top radius and solder ball volume involves predicting the shape of the solder joint, conducting stress analysis, and estimating the fatigue life from the stress/strain data and plastic work.

Obtaining an approximate representation of the fatigue life as a function of the two design variables, three different values (levels) of the variables were selected. These values were assumed to be distributed about the nominal value in a certain range. This choice of a range was motivated by a belief that even within a reasonably small range around the nominal value, an optimal solution other than the nominal solution must exist. A total of nine analyses were carried out amounting to a three-level full-factorial experiment in two design variables. This method was also used by Montgomery, D.C. [81]. It was also stated that building a global approximation in a problem with a large number of variables, a partial factorial experiment such as an orthogonal array of Taguchi Methods [82] may be more

appropriate for economy of analysis. Once the analyses have been carried out for the designed experiment, a surface approximately representing the data needs to be built. A natural choice for such a surface is linear least squares fit. In the present study, a complete quadratic model of the following form was fitted:

$$f(d_p, d_b) = a_0 + a_1 d_I + a_2 d_{II} + a_3 d_I^2 + a_4 d_{II}^2 + a_5 d_I d_{II} \quad (3.1)$$

where d_I and d_{II} are the first and the second design parameters, respectively.

In general, the ability of linear regression models to fit highly nonlinear data is limited by the assumed regression model. For instance, a quadratic model would provide a poor fit over a wide range of data that has an exponential form. Since it is difficult to know the functional form of the data a priori, several regression models would have to be tried before a suitable can be chosen [36]. This optimization problem is classified as a nonlinear programming problem since the dependence of the fatigue life on the variables is nonlinear.

4. NUMERICAL RESULTS

4.1 Package Descriptions

Three different package types provided by the companies in the electronics industry were used. These packages are 64 I/O Plastic Ball Grid Array package (PBGA), 56 I/O PBGA, and 96 I/O Plastic BGA.

Package I is a ball grid array package with an 8x8 full solder joint array subjected to a temperature between –40°C and 125°C with dwell times of 24 minutes and 26 minutes, respectively. The time from the minimum temperature to the maximum temperature was 4 minutes and the time from maximum temperature to the minimum temperature was 6 minutes. Also the stress-free reference temperature was 25°C. The package has 64 solder balls. The pad configuration is non solder mask defined (NSMD) on the printed circuit board (PCB) surface side, and solder mask defined (SMD) on the chip side of the package. The package has two copper pads on both PCB and chip side, plastic substrate, die attach between die, and copper pad or substrate. It also has molding compound covering silicon die and substrate part. The finite element model was generated based on typical solder joint profile of 64 solder balls, 0.8 mm pitch Plastic Ball Grid Array (PBGA) package using symmetry condition, only one-eight of the PBGA package and PCB was modeled.

Package II is a ball grid array package with a 56 balls peripheral solder joint array subjected to a temperature between –40°C and 125°C with dwell times of 24 minutes and 26 minutes, respectively. The time from the minimum temperature to the maximum temperature was 4 minutes and the time from maximum temperature to the minimum temperature was 6 minutes; the stress-free reference temperature was 25°C. The pad configuration is non solder mask defined (NSMD) on the printed circuit board (PCB) surface side and non solder mask defined (NSMD) on the chip side of the package. The package has two copper pads on both PCB and chip side, plastic substrate, solder mask on the copper pad or substrate part and die attach between die and solder mask. It also contains compound covering silicon die, die attach, and solder mask part.

Package III is a ball grid array package with a 96 balls peripheral solder joint array subjected to a temperature between –40°C and 125°C with dwell times of 24 minutes and 26 minutes, respectively. The time from the minimum temperature to the maximum temperature was 4 minutes and the time from maximum temperature to the minimum temperature was 6 minutes while the stress-free reference temperature was 25°C. The pad configuration is non solder mask defined (NSMD) on the printed circuit board (PCB) surface side and solder mask defined (SMD) on the chip side of the package. The package has two copper pads on PCB and chip side, plastic substrate, adhesive on the substrate, solder mask on the copper pad or adhesive part and die attach between die or solder mask. It also includes molding compound covering silicon die, die attach, and solder mask part.

The geometrical properties of each package and printed circuit board are given in Tables 4.1 and 4.2.

Table 4.1 Package details.

		Package I	**Package II**	**Package III**
Solder Ball	Ball Array Type	Full (8x8)	Peripheral	Peripheral
	Pitch Distance [mm]	0.8	0.5	0.5
	Diameter [mm]	0.510	0.352	0.38
	Standoff Height [mm]	0.3963	0.2127	0.2382
Copper Pad	Thickness [mm]	0.028	0.03	0.021
	Diameter [mm]	0.50	0.43	0.47
Substrate	x length [mm]	8	6	8
	y length [mm]	8	6	8
	Thickness [μ]	85	54	75
Adhesive	x length [mm]			8
	y length [mm]			8
	Thickness [μ]			12
Solder Mask	x length [mm]		6	8
	y length [mm]		6	8
	Thickness [μ]		45	48

Solder Mask	Thickness [μ] (on component)		15	15
Die Attach	Thickness [μ]	100	70	70
Silicon Die	x length [mm]	3.7	3.2	5.2
	y length [mm]	3.9	3.2	5.2
	Thickness [mm]	0.3	0.3	0.3
Molding Compound	x length [mm]	7.9	6	8
	y length [mm]	7.9	6	8
	Thickness [mm] (Die Attach+Die+ Mold Compound on the top of Die)	0.77	0.67	0.73

Table 4.2 Printed circuit board details.

		Package I	**Package II**	**Package III**
Printed Circuit Board	Thickness [mm]	0.692	0.692	0.692
Copper Pad	Thickness [mm]	0.066	0.060	0.067
	Diameter [mm]	0.30	0.290	0.292

Material properties of the package components and printed circuit board layers are shown in Tables 4.3 and 4.4. In order to use in the analyses of linear global models and nonlinear sub models, both temperature dependent and temperature independent material properties are given in the tables. The material properties are given for global modeling was evaluated at 1°C.

In order to reduce the computation time, the global model was created such that solder ball was modeled as a linear elastic solid. In the sub model, however, solder ball is modeled as a visco-plastic solid. If the solder ball is linear elastic solid, linear material properties are used. On the other hand, if the solder ball is visco-plastic solid, nonlinear material properties must be used.

Table 4.3 Temperature independent material properties.

		Solder Ball	Copper	Copper	FR4	Polyamide	Adhesive
E_x (MPa)	Package I	34254	0.12893E+06	0.12893E+06	20000	5170	
	Package II	34254	0.12893E+06	0.12893E+06	20000	5170	
	Package III	34254	0.12893E+06	0.12893E+06	20000	5170	4800
E_y (MPa)	Package I				10000		
	Package II				10000		
	Package III				10000		
E_z (MPa)	Package I				20000		
	Package II				20000		
	Package III				20000		
ν_{xy}	Package I	0.35	0.344	0.344	0.38	0.33	
ν_{yz}	Package II	0.35	0.344	0.344	0.38	0.33	
ν_{xz}	Package III	0.35	0.344	0.344	0.38	0.33	0.3
G_{xy}	Package I				7246.4		
G_{yz}	Package II				7246.4		
G_{xz}	Package III				7246.4		
α_x (/°C)	Package I	0.245E-04	0.16066E-04	0.16066E-04	0.18E-4	0.16E-3	
	Package II	0.245E-04	0.16388E-04	0.16388E-04	0.18E-4	0.16E-3	
	Package III	0.245E-04	0.16388E-04	0.16388E-04	0.18E-4	0.16E-3	0.1E-3
α_y (/°C)	Package I				0.5E-04		
	Package II				0.5E-04		
	Package III				0.5E-04		
α_z (/°C)	Package I				0.18E-4		
	Package II				0.18E-4		
	Package III				0.18E-04		

		Substrate	Solder Mask	Die Attach	Silicon Die	Molding Compound
E_x (MPa)	Package I	5170		10000	0.1627E+06	26000
	Package II	5170	4900	265	0.1627E+06	13800
	Package III	5170	4900	265	0.1627E+06	13800
ν_{xy}	Package I	0.33		0.35	0.278	0.35
	Package II	0.33	0.3	0.33	0.278	0.22
	Package III	0.33	0.3	0.33	0.278	0.22
α_x (/°C)	Package I	0.16E-03		0.6E-04	0.23598E-05	0.105E-04
	Package II	0.16E-03	0.95E-04	0.16E-03	0.23598E-05	0.17E-04
	Package III	0.16E-03	0.95E-04	0.16E-03	0.23598E-05	0.17E-04

Table 4.4 Temperature dependent material properties.

Temperature			240°K	280°K	320°K	360°K	400°K	440°K
Solder Ball	E_x (MPa)	Package I	39435	33367	27299	21231	15163	9095
		Package II	39435	33367	27299	21231	15163	9095
		Package III	39435	33367	27299	21231	15163	9095
Copper	α_x (/°C)	Package I	0.16066E-4	0.16443E-4	0.16821E-4	0.17198E-4	0.17576E-4	0.17954E-4
		Package II	0.16066E-4	0.16443E-4	0.16821E-4	0.17198E-4	0.17576E-4	0.17954E-4
		Package III	0.16066E-4	0.16443E-4	0.16821E-4	0.17198E-4	0.17576E-4	0.17954E-4
Copper	α_x (/°C)	Package I	0.16066E-4	0.16443E-4	0.16821E-4	0.17198E-4	0.17576E-4	0.17954E-4
		Package II	0.16066E-4	0.16443E-4	0.16821E-4	0.17198E-4	0.17576E-4	0.17954E-4
		Package III	0.16066E-4	0.16443E-4	0.16821E-4	0.17198E-4	0.17576E-4	0.17954E-4
Silicon Die	α_x (/°C)	Package I	0.20154E-5	0.24188E-5	0.2716E-5	0.29651E-5	0.3224E-5	0.35508E-5
		Package II	0.20154E-5	0.24188E-5	0.2716E-5	0.29651E-5	0.3224E-5	0.35508E-5
		Package III	0.20154E-5	0.24188E-5	0.2716E-5	0.29651E-5	0.3224E-5	0.35508E-5

4.2 Finite Element Modeling

In the finite element analysis of each package, a linear global model with a relatively coarse mesh for the substrate, printed circuit board, and the solder balls provides the critical joint for the subsequent nonlinear modeling of the critical solder ball. The critical solder ball for sub modeling is identified based on the amount of strain energy density. To compute the strain energy density, a macro model was created. In all global models, appropriate symmetry boundary conditions are utilized to minimize the computation time. The center of the package is constrained in all directions at the bottom in order to prevent free rigid-body rotations and translations. In the global modeling of each package, either quarter or octant model is considered, depending on the symmetry conditions.

Package I is created as a quarter global model and contains 53299 elements, 55418 nodes, and 1291 specified constraints. **Package II** is created as a quarter global model and contains 52676 elements, 54689 nodes, and 1029 specified constraints. **Package III** is created as a quarter global model and contains 47272 elements, 50543 nodes, and 2464 specified constraints.

The sub modeling permits refinement of the mesh. The displacements from the global model become the boundary conditions for the nonlinear sub model of the critical solder joint. The displacement boundary conditions are determined from the solution of the global analysis through the use of the cut boundary interpolation method. But, to adapt the value of the displacements to the thermal cycle behavior, each displacement multiplied with the temperature. For these multiplying processes, another macro is developed and used. In the sub modeling of each package, either half or entire solder ball is considered, depending on the location of the critical solder ball. However, a macro file, which creates the sub model of the solder ball on the right location, is used.

Package I sub model contains 3376 elements, 3676 nodes, and 1059 specified constraints. **Package II** sub model contains 4896 elements, 5232 nodes, and 1587 specified constraints. **Package III** sub model contains 5088 elements, 5441 nodes, and 2070 specified constraints.

To create the finite element models of the packages, input files are used. In the global analyses, the temperature is changed as 1°C at the reference temperature. In

sub model analyses, the thermal cycle is simulated. The reference temperature (stress-free) for each package is 25°C. In the simulations, six load steps for the ramps and one load step for dwells are used with an automatic time-stepping option. Four complete thermal cycles are simulated in order to establish the stable stress-strain hysteresis loop.

The nonlinear sub model analyses include temperature dependent and visco-plastic material behavior through visco-plastic solid finite elements (VISCO107) with Anand's nonlinear material response (it is available in Ansys software). The large deformation effects option is enabled when these elements are used. The package substrate, printed circuit board, mold compound, silicon die, and die attach are modeled as a linear elastic solid elements (SOLID45) which is appropriate for linear material behavior.

4.2.1 Global Model of PBGA Packages

The quarter models of 64 PBGA and 56 PBGA packages' global models and cross sections are shown in Figures 4.1-4.

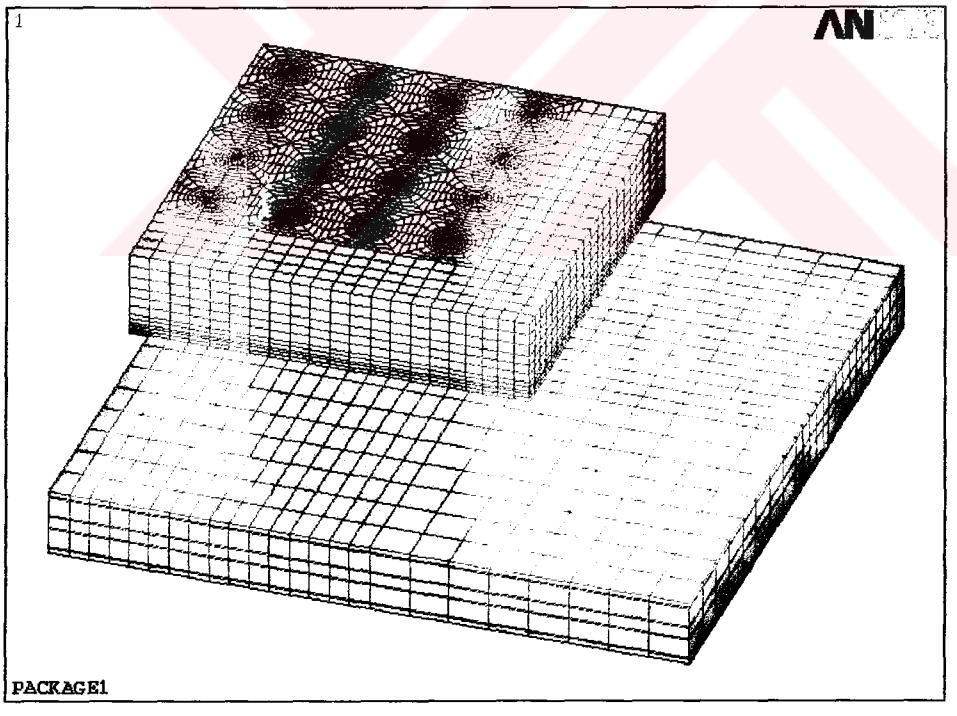

Figure 4.1 The isometric view of the quarter global model of 64 I/O PBGA Package (Package I).

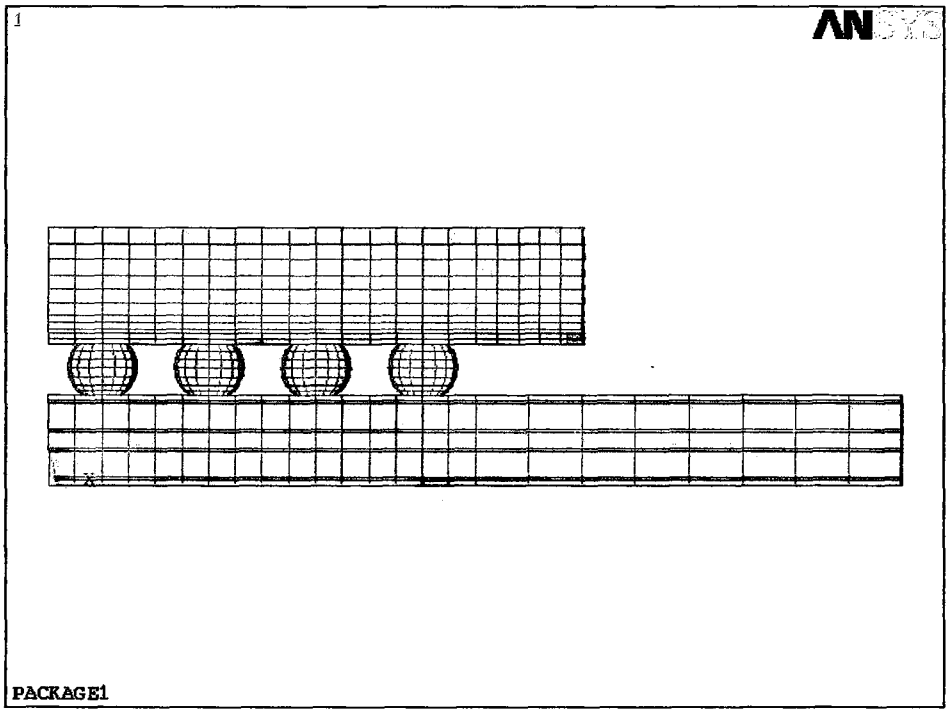

Figure 4.2 The cross section view of the quarter global model of 64 I/O PBGA Package (Package I).

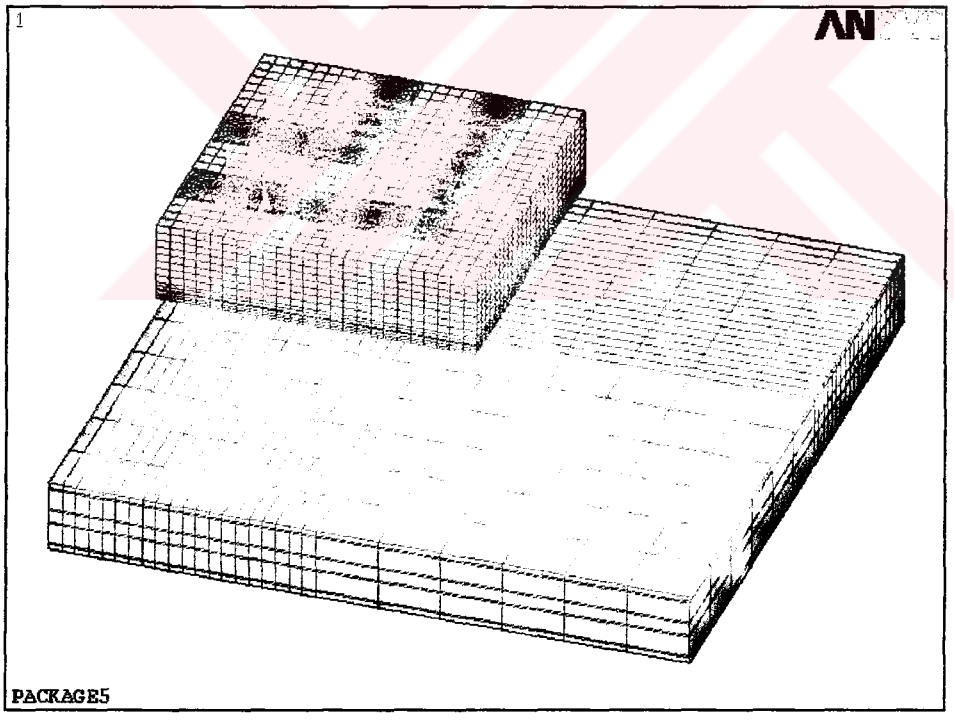

Figure 4.3 The isometric view of the quarter global model of 56 I/O PBGA Package (Package II).

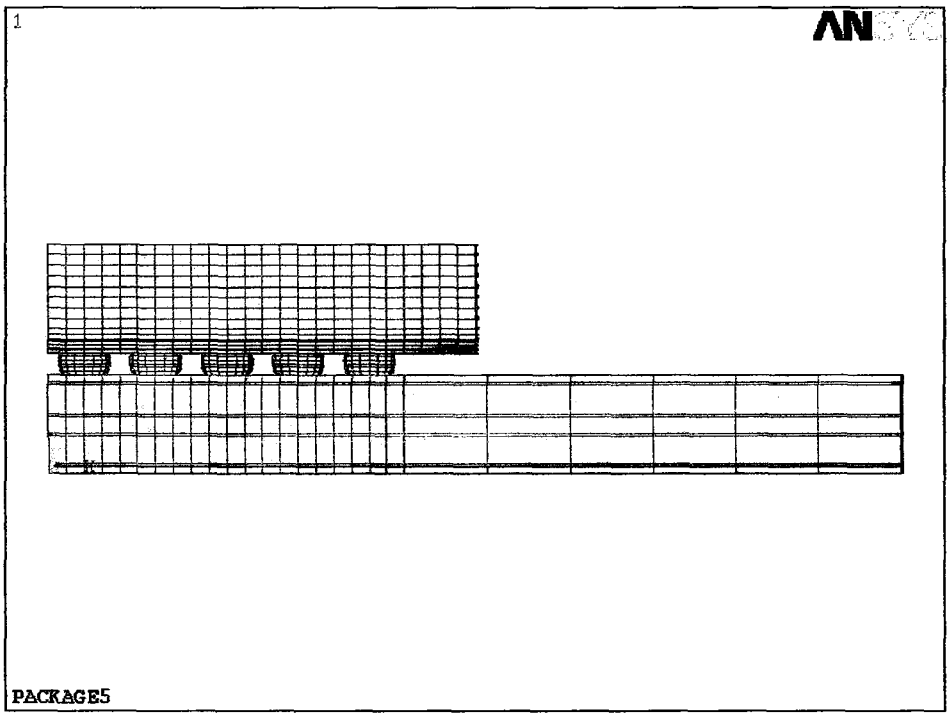

Figure 4.4 The cross section view of the quarter global model of 56 I/O PBGA Package (Package II).

The octant model of 96 PBGA package global model and cross section are shown in Figures 4.5-6.

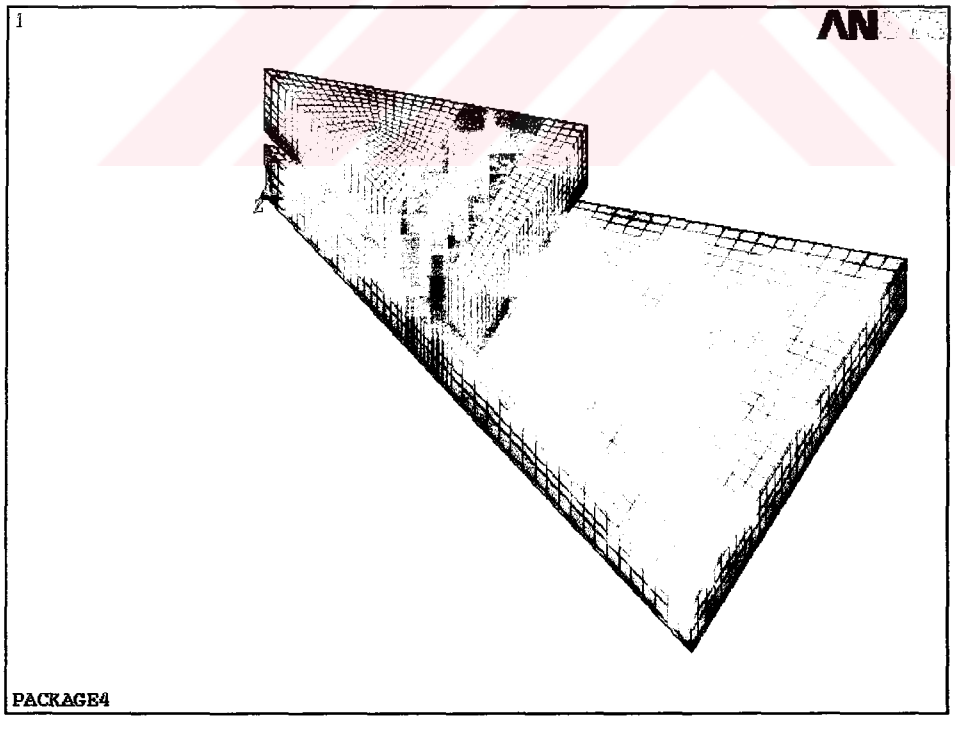

Figure 4.5 The isometric view of the octant global model of 96 I/O PBGA Package (Package III).

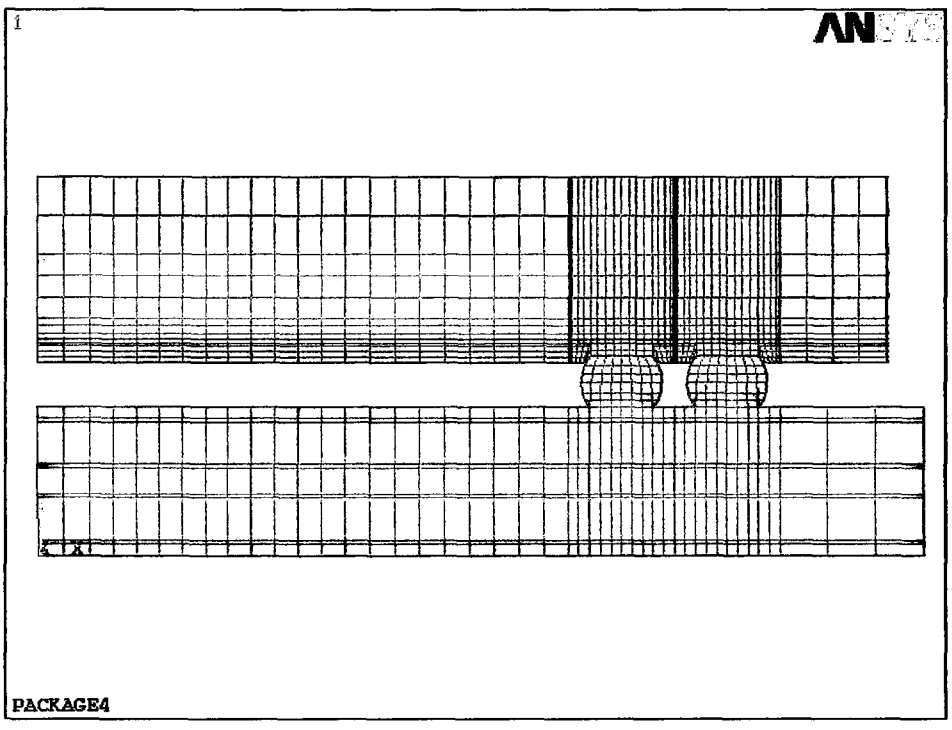

Figure 4.6 The cross section view of the octant global model of 96 I/O PBGA Package (Package III).

Magnified views of the packages are also given in Figures 4.7-9 to show the package components in details.

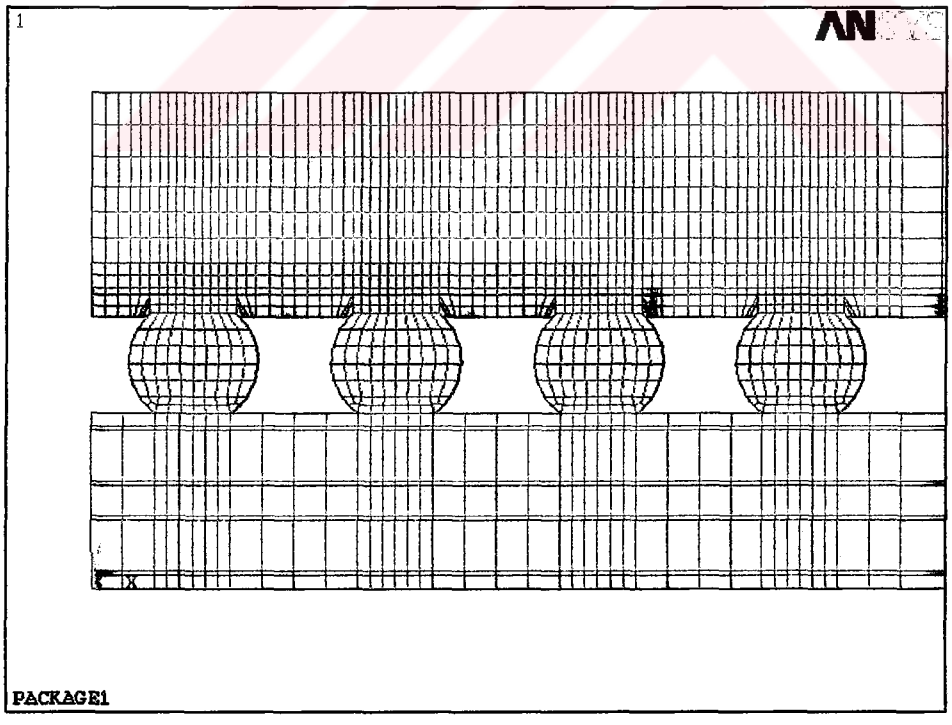

Figure 4.7 Magnified view of 64 I/O PBGA Package (Package I).

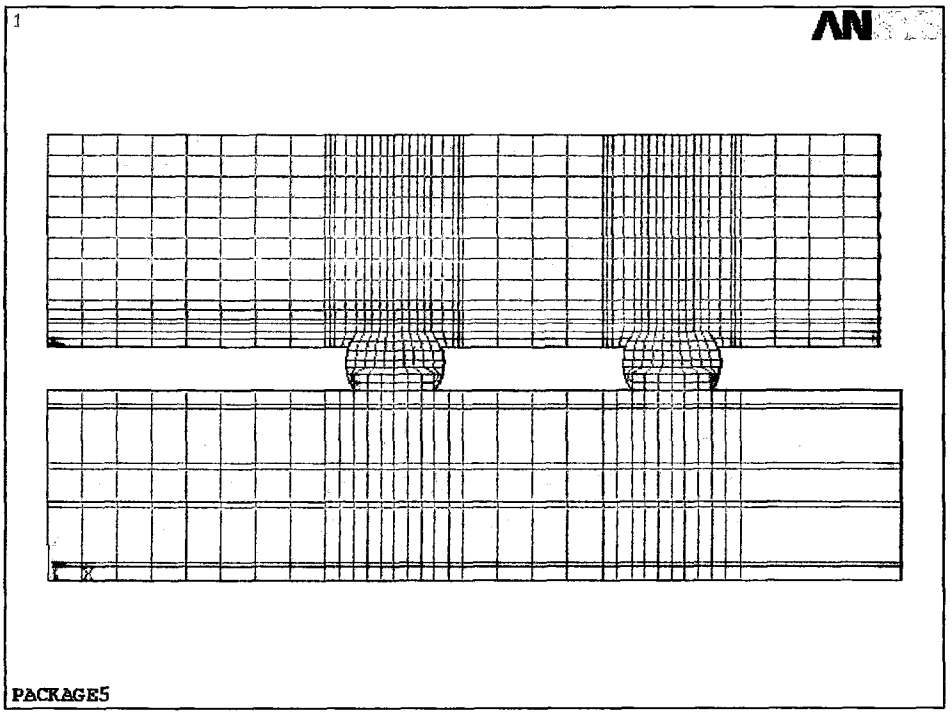

Figure 4.8 Magnified view of 56 I/O PBGA Package (Package II).

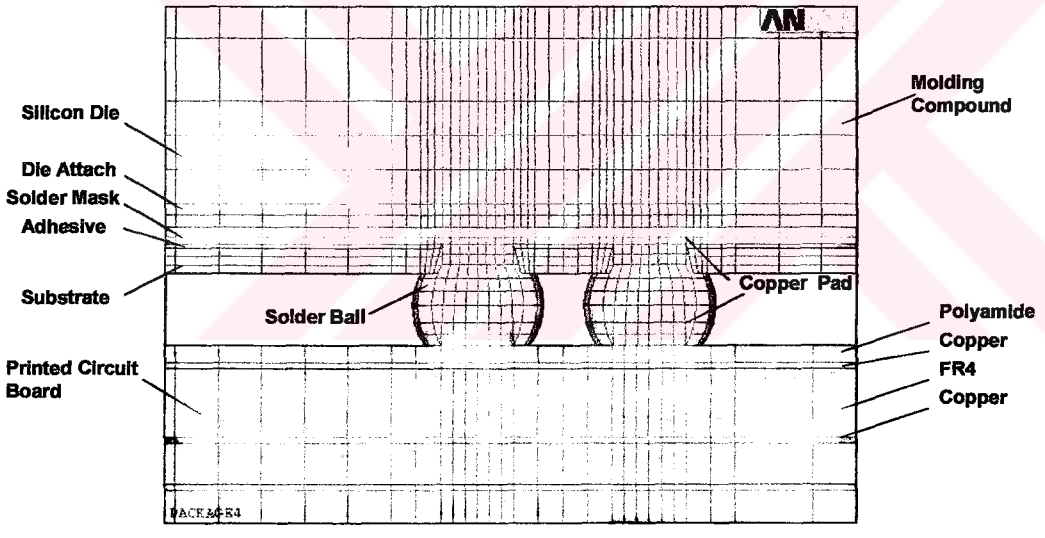

Figure 4.9 Magnified view of 96 I/O PBGA Package (Package III).

In the finite element analysis of this package, a linear global model was used and a macro was written to grab strain energy density of top necks of solder joints in the models to figure out which joint is the most critical one. The solder ball, which has the highest strain energy density, is considered the most critical one. It is shown in the Table 4.5 that if the strain energy density increases, fatigue life decreases and the plastic work increases.

Table 4.5 Plastic work

Solder Ball #	Solder Ball Volume	Strain Energy	Strain Energy Density	Fatigue Life	Plastic Work
1	0.619335E-02	0.355527E-07	0.574046E-05		
2	0.619335E-02	0.364298E-07	0.588208E-05		
3	0.619335E-02	0.343801E-07	0.555113E-05	1490.99894	32.7898806
4	0.619335E-02	0.161298E-07	0.260437E-05	2843.7736	18.7803836
5	0.619335E-02	0.364312E-07	0.588231E-05		
6	**0.619335E-02**	**0.378681E-07**	**0.611432 E-05**	**1038.85492**	**45.0409374**
7	0.619335E-02	0.359084E-07	0. 579790 E-05		
8	0.619335E-02	0.153412E-07	0. 247704 E-05		
9	0.619335E-02	0.343552E-07	0. 554711 E-05	1492.10381	32.7686764
10	0.619335E-02	0.358670E-07	0. 579121 E-05		
11	0.619335E-02	0.274131E-07	0. 442622 E-05	1780.5022	28.0962257
12	0.619335E-02	0.138890E-07	0. 224257 E-05		
13	0.619335E-02	0.161271E-07	0. 260394 E-05		
14	0.619335E-02	0.153365E-07	0. 247629 E-05		
15	0.619335E-02	0.138831E-07	0. 224161 E-05		
16	0.619335E-02	0.204947E-07	0. 330915 E-05	4290.45298	13.2651473

4.2.2 Sub Model of PBGA Packages

The sub models of 64 PBGA and 56 PBGA packages' global models and cross sections are shown in Figures 4.10-13.

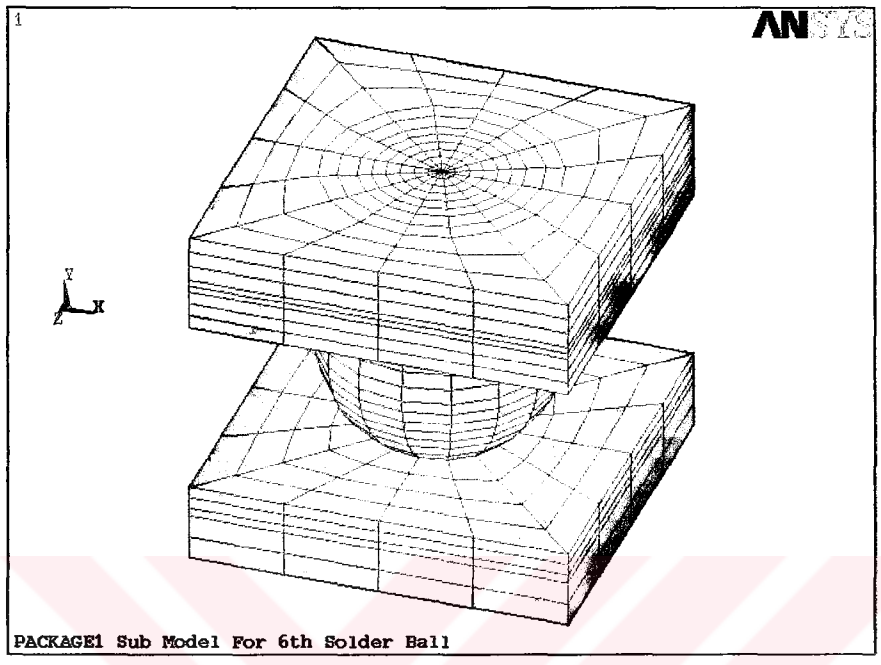

Figure 4.10 The isometric view of the sub model of 64 I/O PBGA Package (Package I).

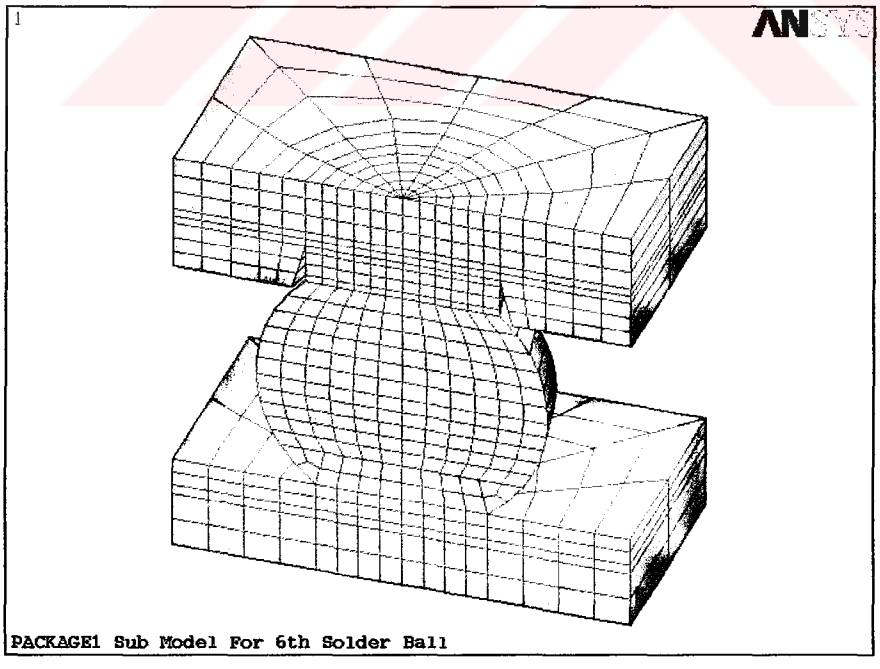

Figure 4.11 The cross section view of the sub model of 64 I/O PBGA Package (Package I).

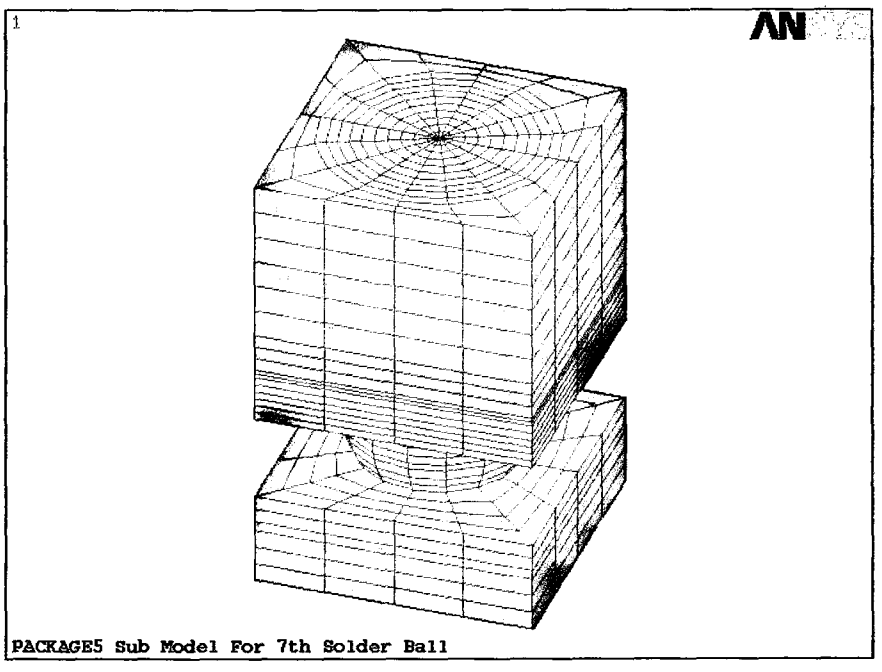

Figure 4.12 The isometric view of the sub model of 56 I/O PBGA Package (Package II).

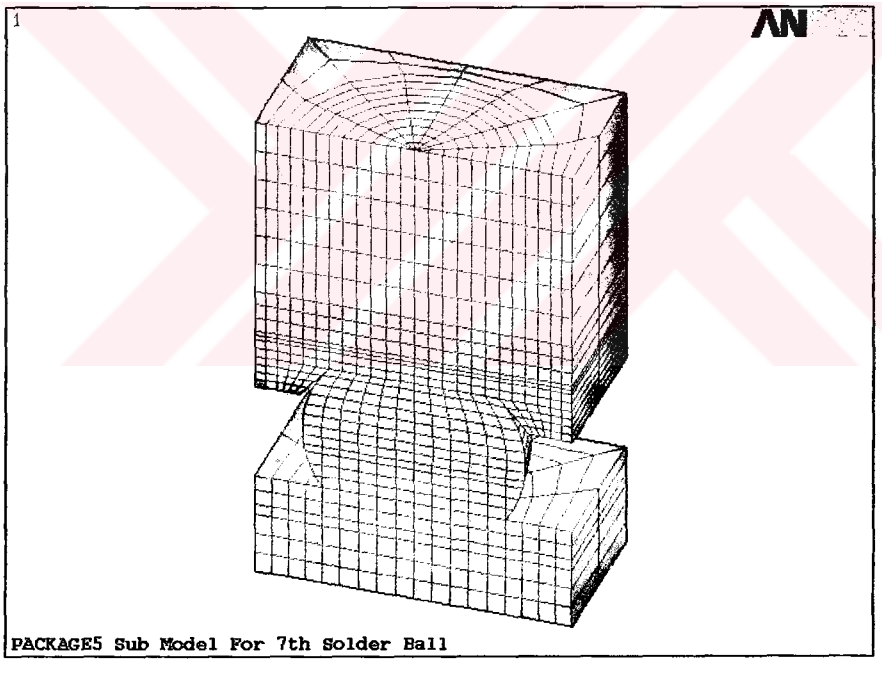

Figure 4.13 The cross section view of the sub model of 56 I/O PBGA Package (Package II).

96 PBGA package global and cross section model are shown in Figures 4.14-15.

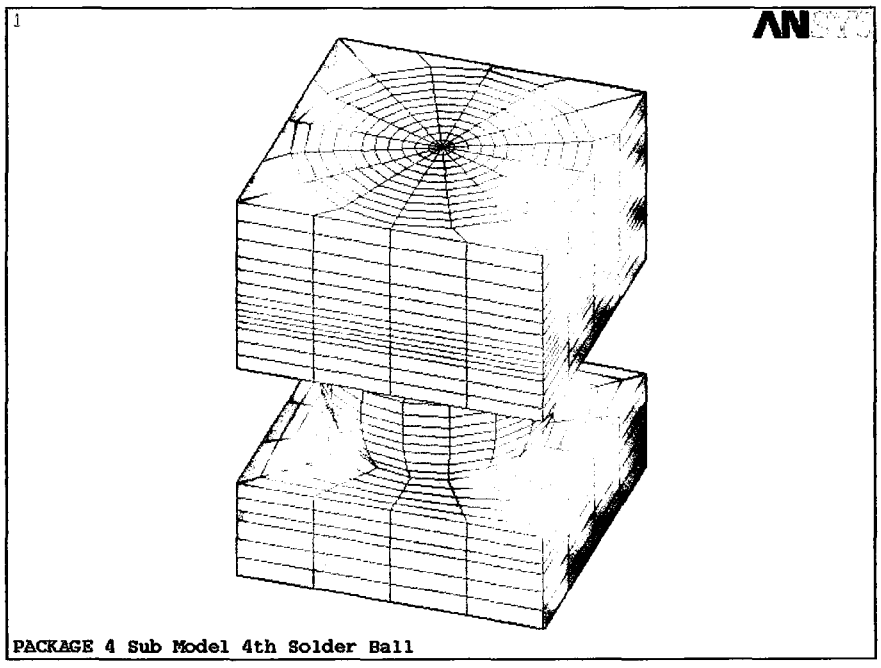

Figure 4.14 The isometric view of the sub model of 96 I/O PBGA Package (Package III).

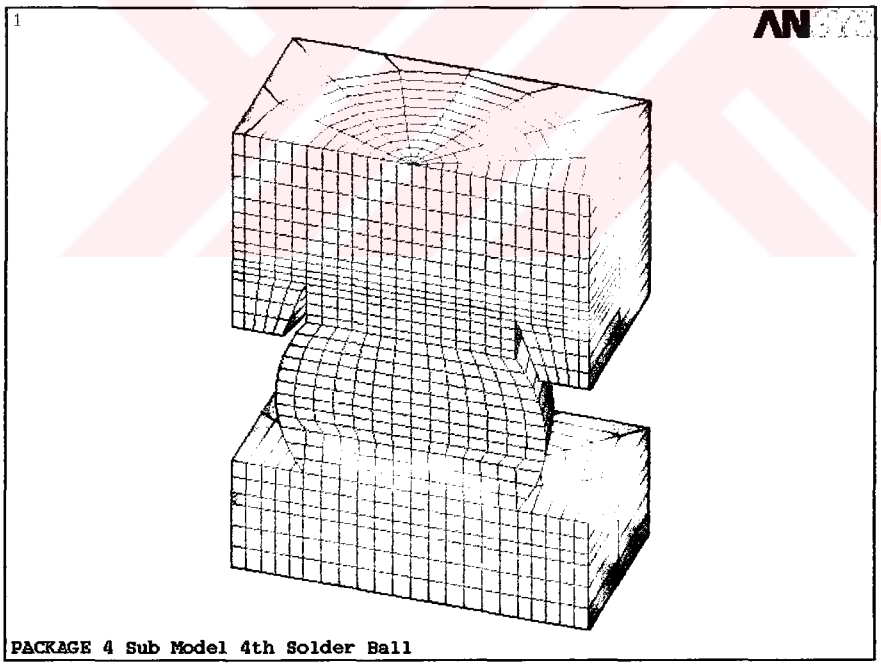

Figure 4.15 The cross section view of the sub model of 96 I/O PBGA Package (Package III).

The nonlinear sub model analyses include temperature dependent and visco-plastic material behavior through 3D visco-plastic solid finite elements (VISCO107) and it also permits refinement of the mesh. The large deformation effects option

(NLGEO,ON) is enabled when these elements are used. The package substrate, printed circuit board, mold compound, silicon die, and die attach are modeled by 3D linear elastic solid elements (SOLID45) appropriate for linear material behavior. It was found that elemental values were more dependent on the mesh size than the nodal values. Therefore the nodal values were used in all correlations and predictions [1]. To apply the symmetry boundary conditions to the sub model, the displacements are used from the global model. The displacement boundary conditions are determined from the solution of the global analysis through the use of the cut boundary interpolation method. However, adapting the value of the displacements to the thermal cycle behavior, each displacement multiplied with the temperature. For these multiplying processes, another macro file was created. In the sub modeling of each package, either half or entire solder ball is considered depending on the location of the critical solder ball.

The main objective of the simulations was to calculate the maximum plastic work per unit volume in the solder. In each calculation, four thermal cycles are simulated in order to ensure the stability of hysteresis loop. The temperature ramps were divided into six sub steps and in each sub step and the convergence is reacted iteratively. During the dwell periods, however, one sub step was used.

Using the results of the analyses, plastic work was computed and volume-weighted average plastic work density method introduced by Darveaux [1], was used to compute thermal fatigue life. It uses volume-weighted average plastic work density increment, ΔW_{ave} and the number of cycles to crack initiation, N_0 and the crack propagation rate. Assuming a constant crack propagation rate, the characteristic life is

$$\text{Package Life} = N_0 + \frac{a}{da/dN} \tag{4.1}$$

$$N_0 = K_1 \Delta W_{ave}^{K_2} \tag{4.2}$$

$$\frac{da}{dN} = K_3 \Delta W_{ave}^{K_4} \tag{4.3}$$

Volume-weighted average of total plastic work density accumulated per thermal cycle is shown below and it is dependent on the thickness of the finite elements and

the parameters, K_1, K_2, K_3 and K_4 are dependent on geometry, loading and finite element analysis and they were also determined by Darveaux. Using these empirical parameters, fatigue life was computed. In order to compute the fatigue life in finite element analyses, another original macro was created.

$$\Delta W_{ave} = \frac{\left(\sum_{i=1}^{n} \Delta W_i . V_i\right)}{\sum_{i=1}^{n} V_i} \tag{4.4}$$

The plastic work for a critical solder ball for a package is shown in Figures 4.16 as an example.

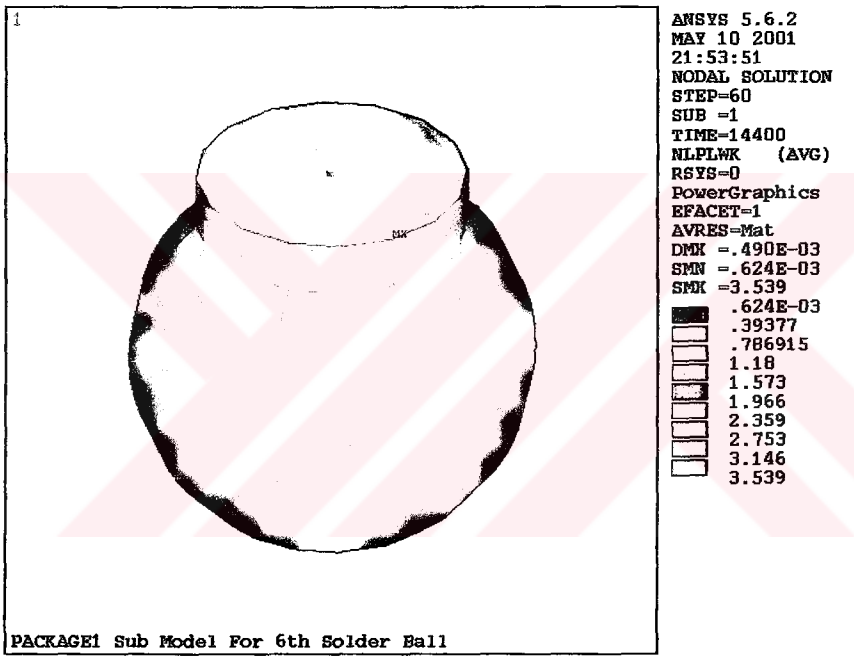

Figure 4.16 Plastic work for the critical solder ball (Package I).

4.3 Optimization Procedure

4.3.1 The Influence of Solder Ball's Geometrical Properties

The fatigue life of solder joints depends on the stress and strain. The stresses depend on the shape of solder joints. Since the configuration of the solder joint is dependent on solder ball upper radius and the amount of volume of the solder ball, these two parameters were chosen as the design variables for the optimization

process. The first parameter was the volume of the solder ball. As the top pad diameter and the top (upper) diameter of the solder ball vary, the top diameter of the solder ball was taken as a second design parameter.

To obtain an approximate representation of the fatigue life as a function of these two design variables, namely solder ball upper radius and solder volume, three different values of the variables were selected. These values were assumed to be uniformly distributed about the nominal value in a range of ±20 percent. Building the global approximation, nine different cases were carried out amounting to a three level full-factorial experiment in two design variables.

Analyses were carried out for the three different PBGA package designs. The results that were obtained from finite element analyses of packages are shown in Tables A.1-3 in Appendix A. Nine different global models and nine different sub models were created using finite element modeling for each package. After doing all analyses, tables were formed for each package and fatigue life diagram, related to solder ball volume and solder ball upper radius, was drawn using these nine points' values. Results for all packages are shown in Figures 4.17-19. The solder volume and upper radius were computed through least square minimization technique, which can be found in any textbook on numerical methods.

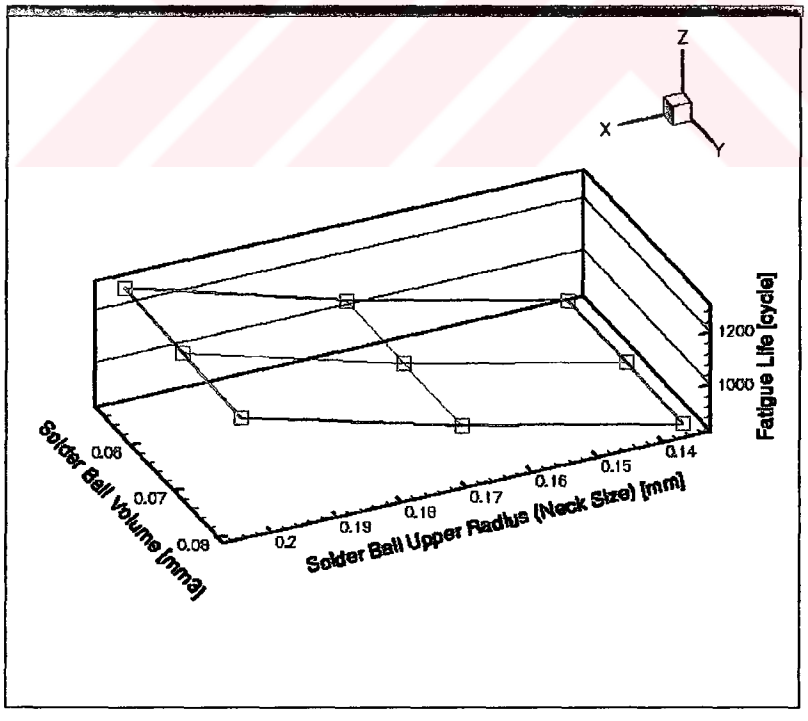

Figure 4.17 Fatigue life diagram related to solder ball volume and solder ball upper radius for Package I.

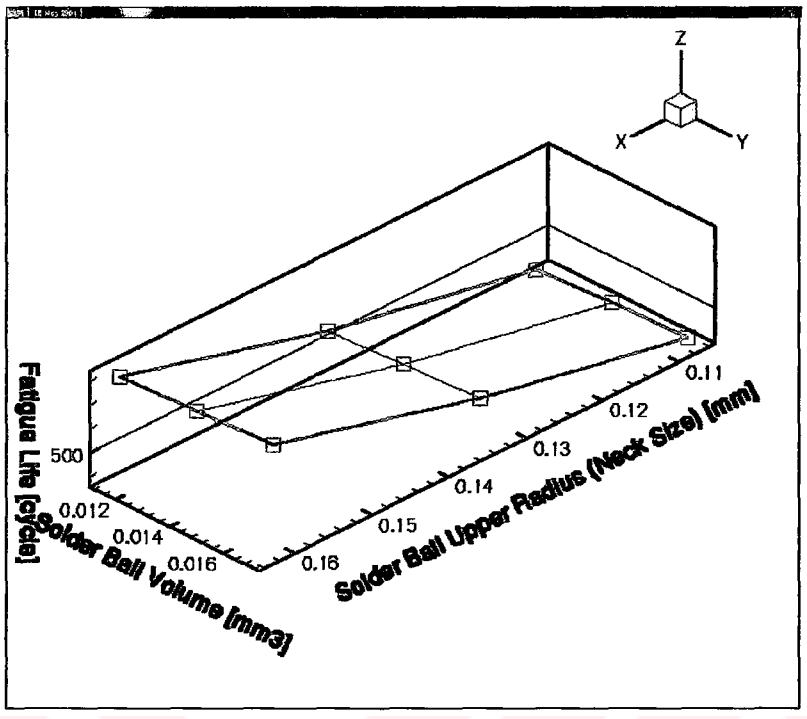

Figure 4.18 Fatigue life diagram related to solder ball volume and solder ball upper radius for Package II.

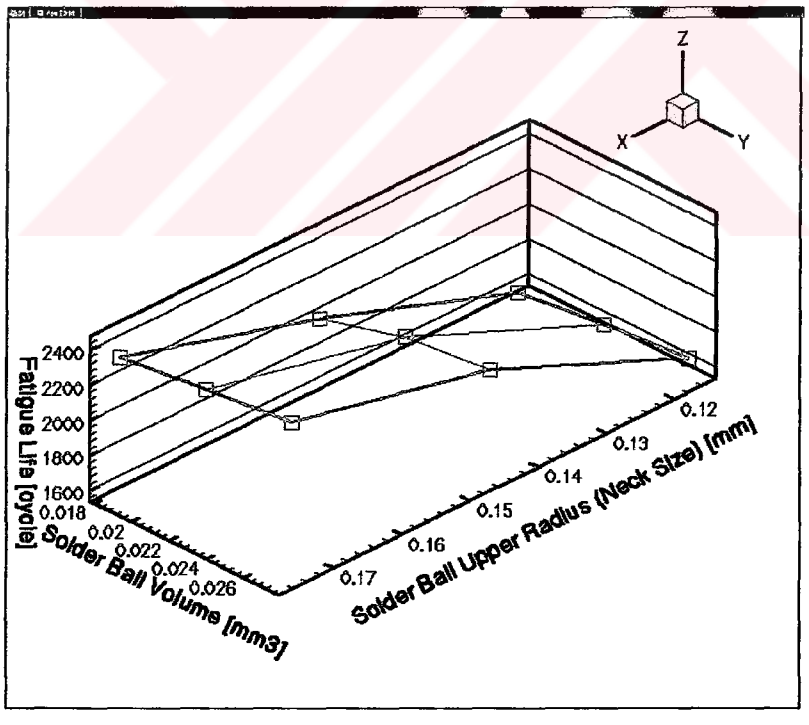

Figure 4.19 Fatigue life diagram related to solder ball volume and, solder ball upper radius for Package III.

After analyses have been carried out for the design parameters, a surface that represents the data point's needs to be built and this surface is a linear least square fit. A complete quadratic model of the following form was fitted:

$$f(d_p, d_v) = a_0 + a_1 d_p + a_2 d_v + a_3 d_p^2 + a_4 d_v^2 + a_5 d_p d_v \quad (4.5)$$

where d_p and d_v are the size (radius) and the volume of the solder ball, respectively. The quadratic functions were established by using Mathematica program. The unknown coefficients of the quadratic function for each package are obtained as follows:

Package I:

$$f(d_p, d_h) = 460.07 + 639.79 d_p + 347.78 d_v + 18340.74 d_p^2 + 6976.29 d_v^2 - 10087.01 d_p d_v \quad (4.6)$$

Package II:

$$f(d_p, d_h) = 194.41 - 3647.78 d_p + 8848.49 d_v + 42224.52 d_p^2 - 82742.43 d_v^2 - 6547.8 d_p d_v \quad (4.7)$$

Package III:

$$f(d_p, d_h) = -2687.49 + 42343.64 d_p + 51964.84 d_v - 102425.05 d_p^2 - 869305.38 d_v^2 + 18016.18 d_p d_v \quad (4.8)$$

Using the quadratic equation, 400 data points are used to form the quadratic surface with Excel. The quadratic least squares surfaces are shown in Figures 4.20-22. Relative errors were also investigated for the quadratic functions obtained by using least square method. The relative errors for Package I, Package II, and Package III are %0.054, %0.16, and %0.77, respectively.

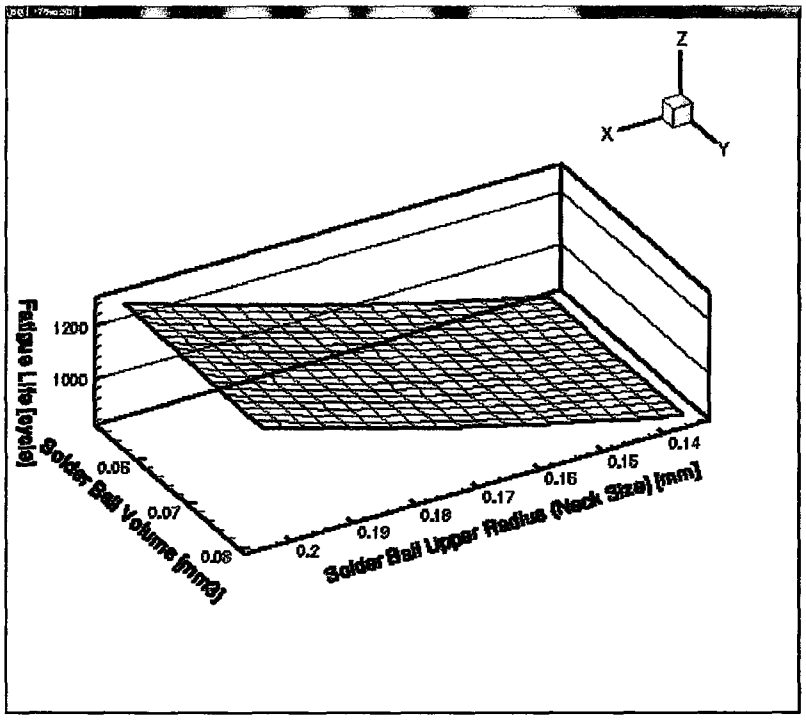

Figure 4.20 The quadratic least squares surface for Package I.

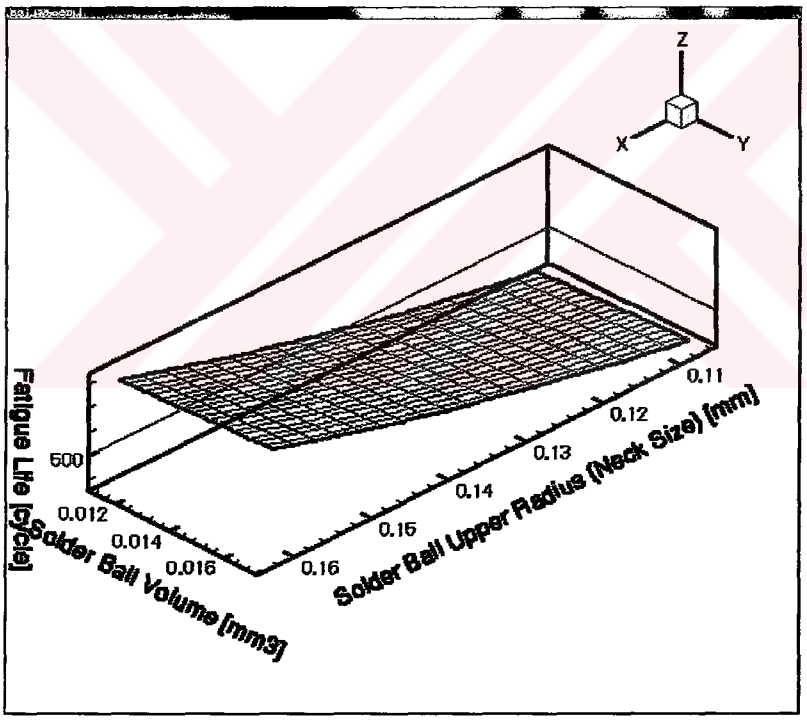

Figure 4.21 The quadratic least squares surface for Package II.

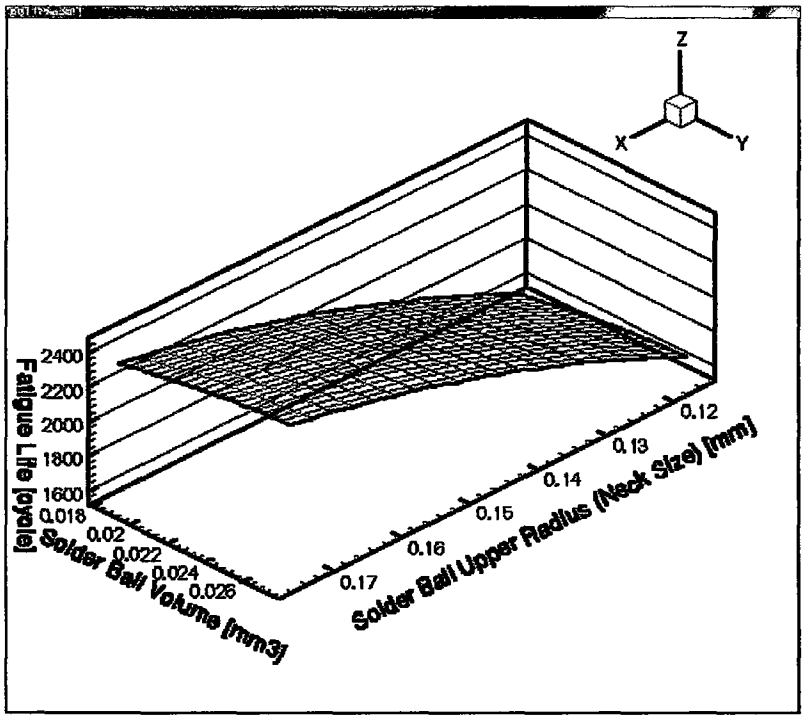

Figure 4.22 The quadratic least squares surface for Package III.

Fatigue life diagram related to solder ball volume and solder ball upper radius and the quadratic least squares surfaces are given in Figures 4.23-25, to show the quadratic functions fit to the real curves.

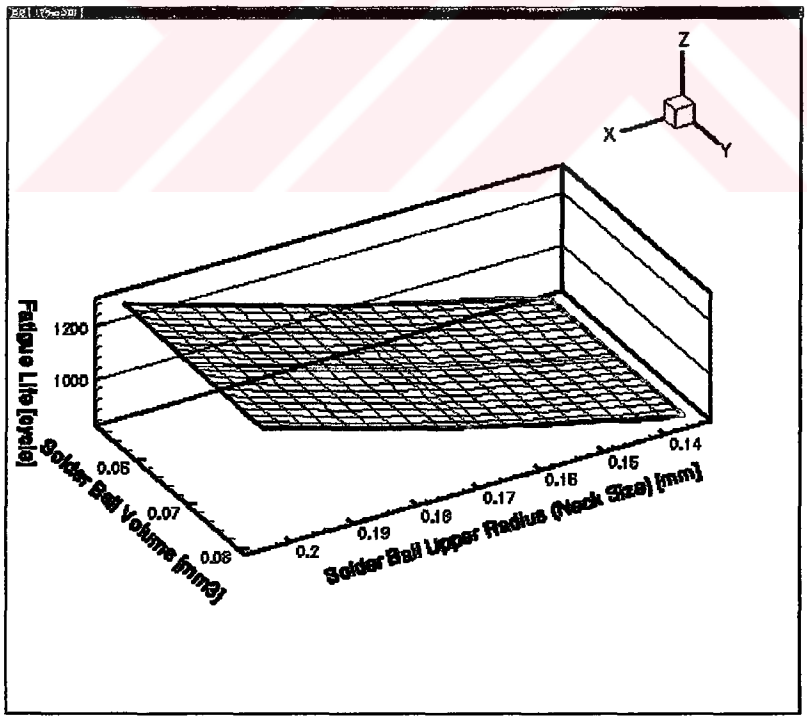

Figure 4.23 Fatigue life diagram related to solder ball volume and solder ball upper radius and the quadratic least squares surface for Package I.

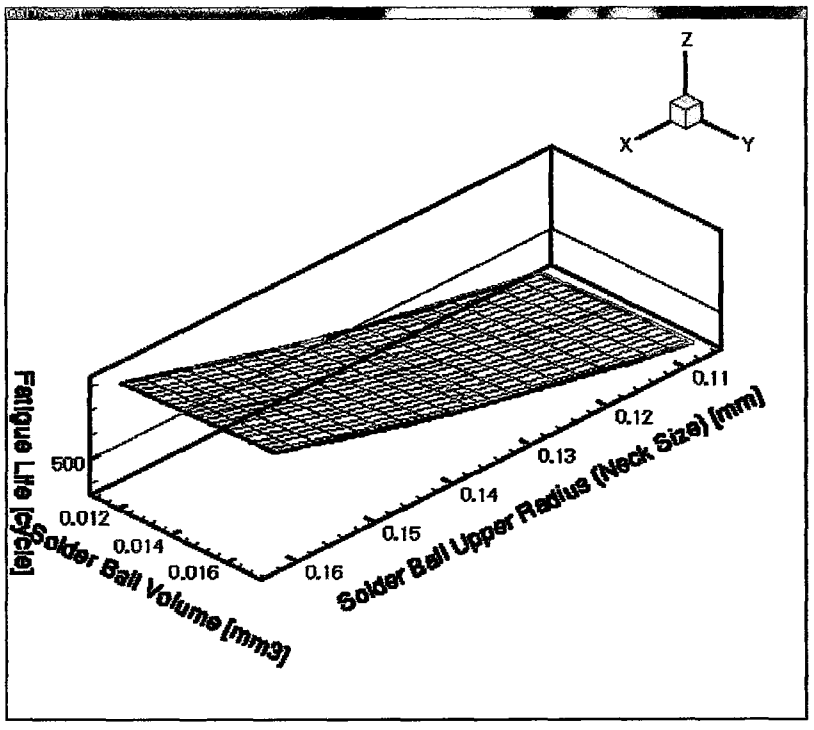

Figure 4.24 Fatigue life diagram related to solder ball volume and solder ball upper radius and the quadratic least squares surface for Package II.

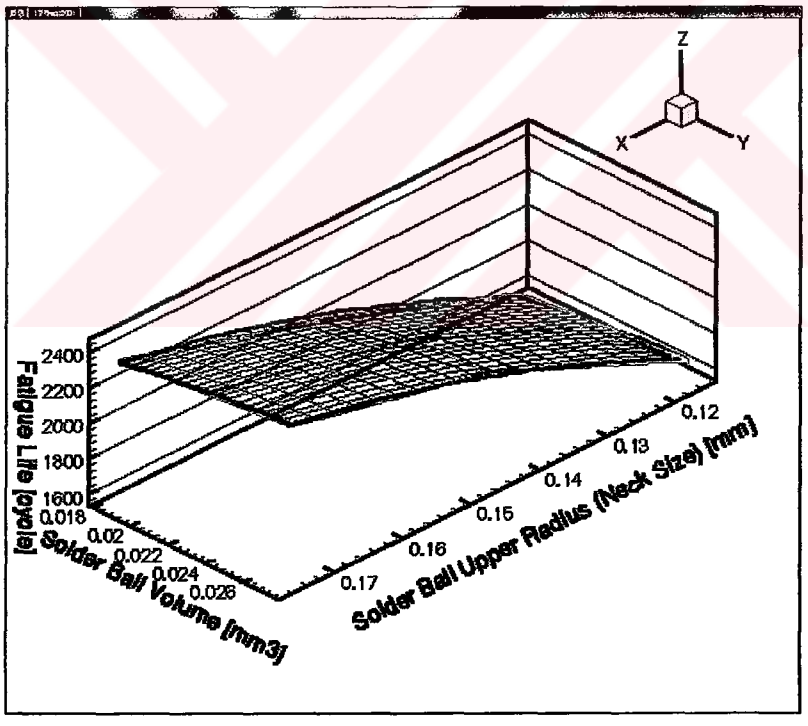

Figure 4.25 Fatigue life diagram related to solder ball volume and solder ball upper radius and the quadratic least squares surface for Package III.

4.3.2 The Influence of Molding Compounds' Properties

The fatigue life on solder joints depend on the strains and stresses. During the process, thermal stresses occur in packages because of the materials' different thermal expansion coefficients. Different parts have different amount of expansions. Changing the properties of molding compound materials, that cover the packages, the influence on the fatigue life of solder joints was determined.

To obtain an approximate representation of the fatigue life as a function of these two design variables, namely the elasticity modulus and thermal expansion coefficient, three different values of the variables were selected.

Package I: Elasticity modulus was assumed to be distributed about in a range of 20000-30000 MPa and thermal expansion coefficient was assumed to be distributed about in a range of $5x10^{-6}$-$15x10^{-6}$.

Package II: Elasticity modulus was assumed to be distributed about in a range of 5000-20000 MPa and thermal expansion coefficient was assumed to be distributed about in a range of $10x10^{-6}$-$25x10^{-6}$.

Package III: Elasticity modulus was assumed to be distributed about in a range of 5000-25000 MPa and thermal expansion coefficient was assumed to be distributed about in a range of $10x10^{-6}$-$30x10^{-6}$.

Nine different cases were carried out amounting to a three level full-factorial experiment in two design variables for each package by building the global approximation.

Analyses were carried out for the three different PBGA package designs. The results that are obtained from finite element analyses of packages are shown in Tables B.1-3 for each package. Nine different global models and nine different sub models were created using finite element modeling for each package. After doing all analyses, tables were formed for each package. Also, fatigue life diagram, related to the elasticity modulus and thermal expansion coefficient was drawn using these nine data points. Results for these three packages are illustrated in Figures 4.26-28.

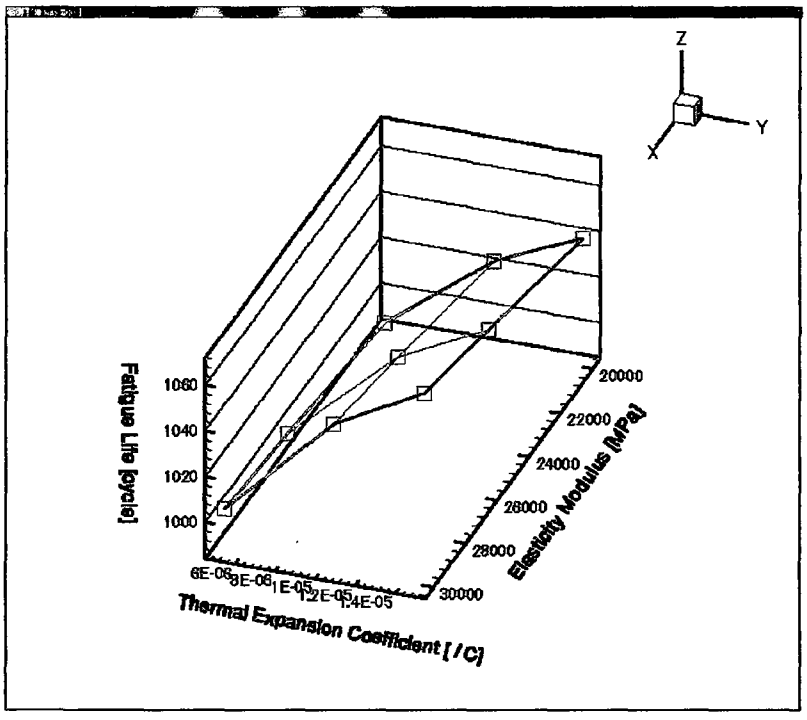

Figure 4.26 Fatigue life diagram related to the elasticity modulus and thermal expansion coefficient for Package I.

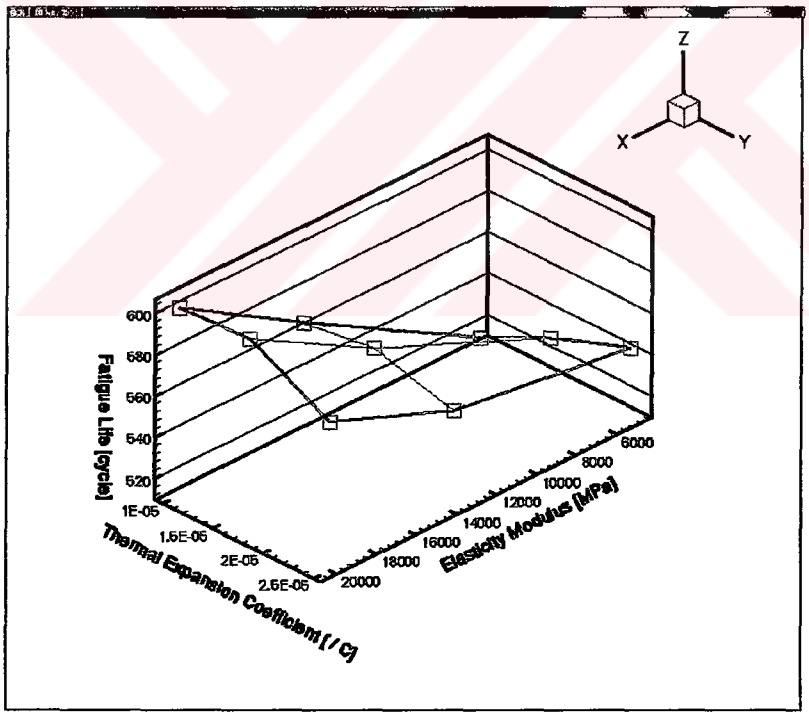

Figure 4.27 Fatigue life diagram related to the elasticity modulus and thermal expansion coefficient for Package II.

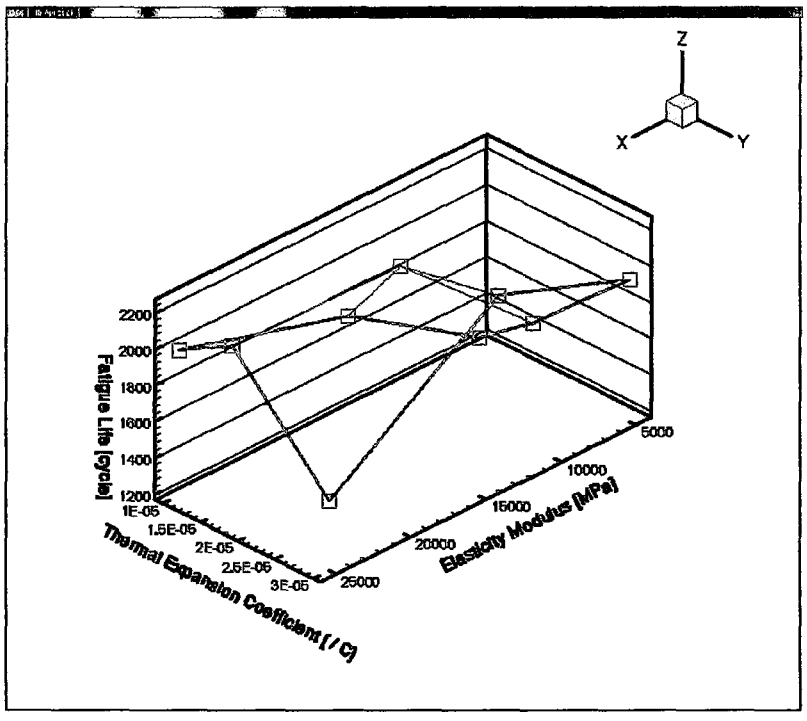

Figure 4.28 Fatigue life diagram related to the elasticity modulus and thermal expansion coefficient for Package III.

After analyses have been carried out for the design parameters, a surface representing the data points' needs are generated using the linear least square minimization technique. A complete quadratic model of the following form was assumed:

$$f(d_E, d_A) = a_0 + a_1 d_E + a_2 d_A + a_3 d_E^2 + a_4 d_A^2 + a_5 d_E d_A \quad (4.9)$$

where d_E and d_A are the elasticity modulus and the thermal expansion coefficient, respectively. The quadratic coefficients functions were determined by using Mathematica program are given as follows:

Package I:

$$f(d_E, d_A) = 861.37 + 0.007 d_E + 5.605.10^6 d_A - 1.22.10^{-7} d_E^2 - 8.28.10^{10} d_A^2 + 99.01 d_E d_A \quad (4.10)$$

Package II:

$$f(d_E, d_A) = 431.94 + 0.006 d_E + 7.2810^6 d_A + 9.3.10^{-7} d_E^2 - 11.95.10^{10} d_A^2 - 229.57 d_E d_A \quad (4.11)$$

Package III:

$$f(d_E, d_A) = -72867 + 0.1759 d_E + 13615.10^6 d_A - 33.10^{-7} d_E^2 - 191.51.10^{10} d_A^2 - 312344 d_E d_A \quad (4.12)$$

Using the quadratic equation, 400 data points obtained to form the quadratic surface by using Excel and the quadratic least squares surfaces are shown in Figures 4.29-31. Relative errors were also investigated for the quadratic functions obtained by using least square method. The relative errors for Package I, Package II, and Package III are %0.299, %0.36, and %4.73, respectively.

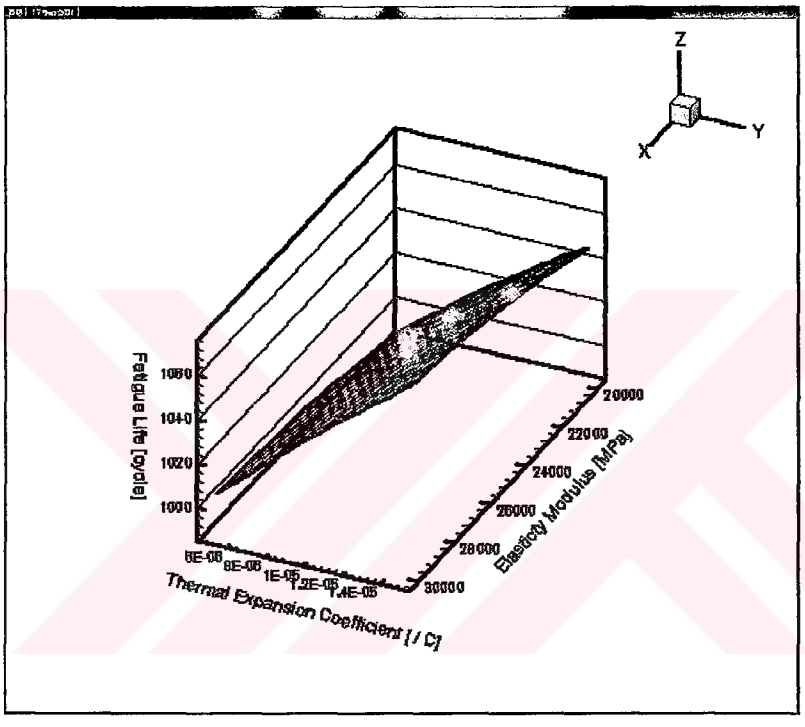

Figure 4.29 The quadratic least squares surface for Package I.

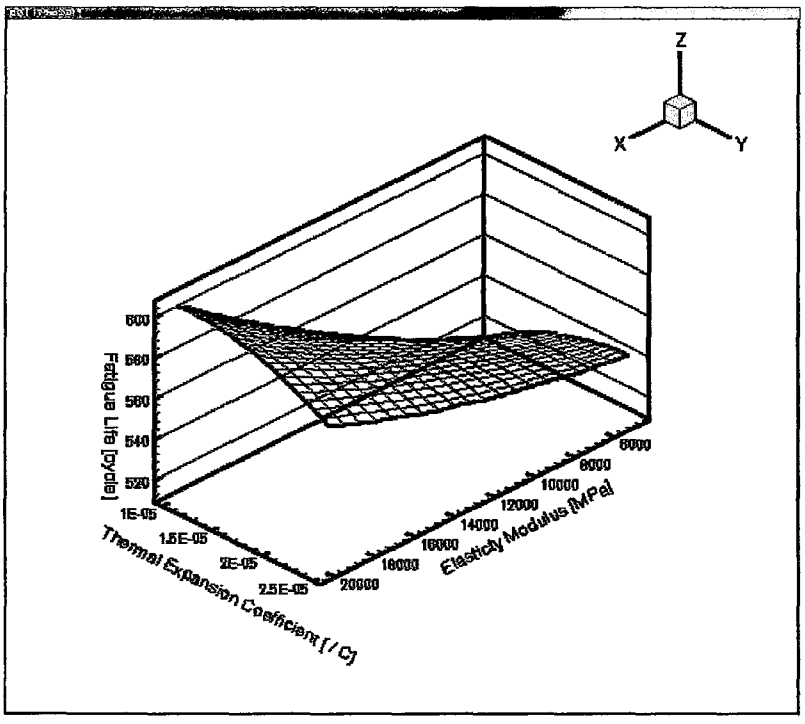

Figure 4.30 The quadratic least squares surface for Package II.

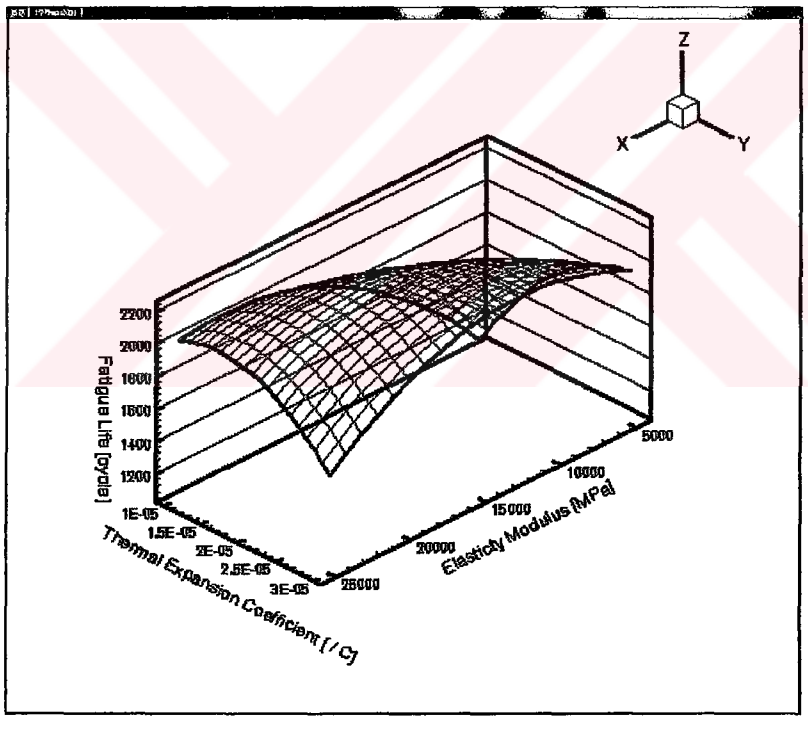

Figure 4.31 The quadratic least squares surface for Package III.

Fatigue life diagram related to solder ball volume and solder ball upper radius and the quadratic least squares surfaces are given in Figures 4.32-34, to show quadratic functions fit to the real curves.

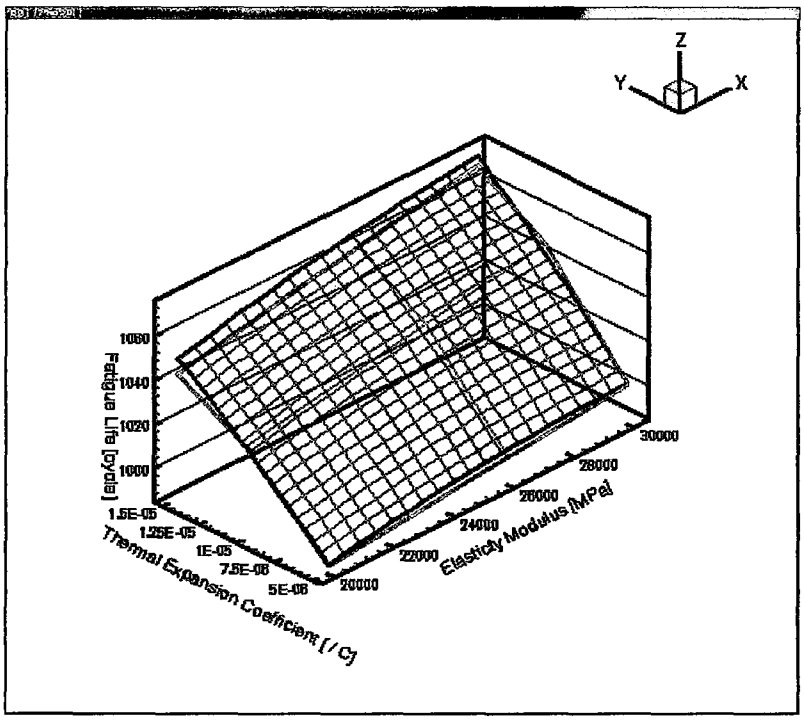

Figure 4.32 Fatigue life diagram related to the elasticity modulus and thermal expansion coefficient, and the quadratic least squares surface for Package I.

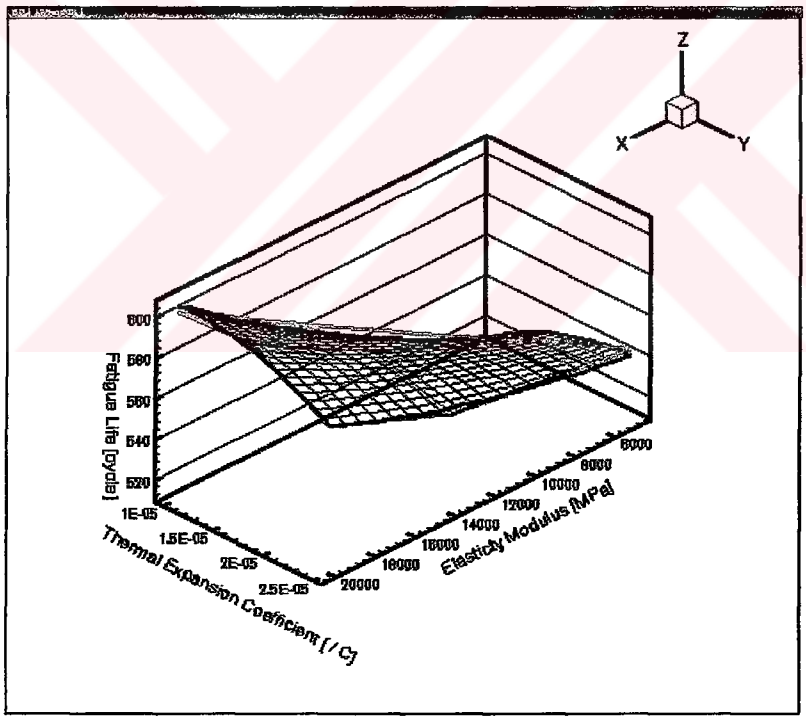

Figure 4.33 Fatigue life diagram related to the elasticity modulus and thermal expansion coefficient, and the quadratic least squares surface for Package II.

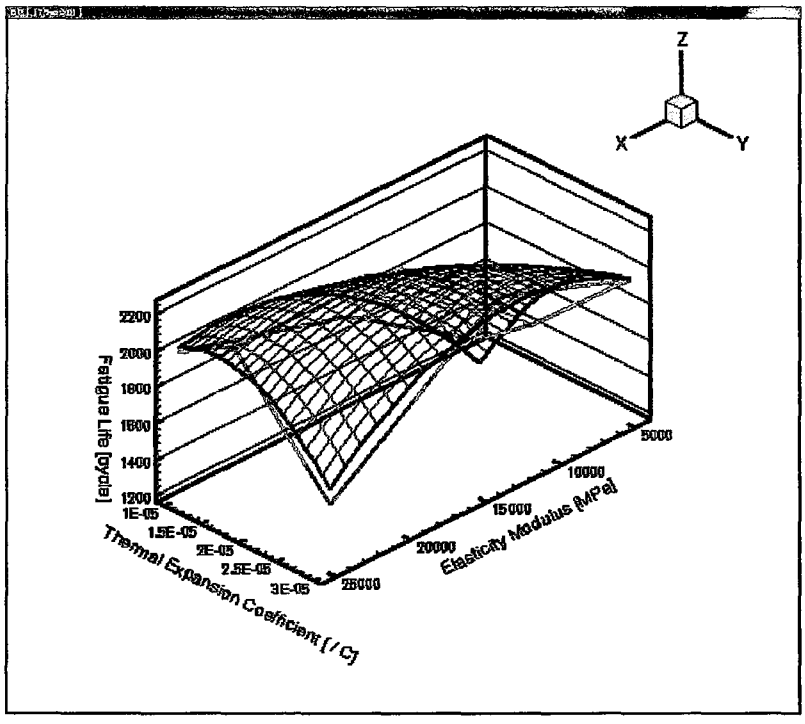

Figure 4.34 Fatigue life diagram related to the elasticity modulus and thermal expansion coefficient, and the quadratic least squares surface for Package III.

5. CONCLUSIONS AND FUTURE WORK

The influence of design parameters on solder joint reliability in electronic packages has been investigated and optimum design parameters were found to maximize the fatigue life of solder joint interconnections. Optimum design variables have been achieved for chosen design parameters. The results have obtained for two different design parameters' sets at each time.

First two design parameters were geometrical properties, namely solder ball upper radius and solder ball volume. Nine different cases have been analyzed using three level full factorial finite element analyses in these two design variables. These results and the quadratic function surfaces were graphically shown in Figure 4.17-25. The fitted surfaces represent very good approximations to the underlying data points since R^2 correlation coefficient values of between 0.998 and 0.999 were obtained for the fit. The optimal solder ball top radius and solder ball volume were achieved for each package by optimizing least squares surfaces and shown in Table 5.1. This table also represents the relative errors and correlation coefficients comparing with the fatigue life obtained from finite element analyses to the ones achieved from optimization technique. As shown in Table 5.1, these relative errors are 0.00054 for Package I, 0.00163 for Package II, and 0.00773 for Package III. While this high degree of accuracy may be indication of the simplicity of the exact surface, the number of finite element analyses required for least squares and exact solutions clearly demonstrates that a use of exact optimization procedures may be computationally very inefficient. Even in a problem with more complex surfaces, it will be disadvantageous to examine the nature of the problem surfaces through designed finite element analyses before attempting optimization. In this present study, quadratic function surfaces fit the data to a very high accuracy by using least squares models. Consequently, the optimum solutions that were predicted based on these approximate surfaces are very accurate. These global approximation schemes also proved to be far more efficient than exact optimization. These quadratic functions that were obtained in this study make easier to compute the fatigue life without doing analysis for the electronic packages, which have various configurations.

Optimum solutions for three different packages are shown in Table 5.1. Because of the geometrical restrictions, solder ball upper radius (neck size) and solder ball volume cannot be increased more than certain values. As the solder balls expand during the operation, excessive expansion will probably cause contact between them and harm to electrical path for I/Os. After investigating the diagrams between the solder ball upper radius, the solder ball volume, and the fatigue life of the electronic package, it can be said that as the solder ball upper radius increases, the fatigue life of the electronic package will increase. Increasing the solder ball volume will also improve and extend the life slightly. Solder ball upper radius has much more influence on the fatigue life than the solder ball volume. Solder ball upper neck radius has the largest effect on the fatigue life for all packages and it should be carefully considered while deciding package configurations. The solder ball volume's effect is not considerable. These results are valid for three different packages investigated in this study. Except for determining the influence of design parameters, optimum electronic package configurations, which increase the fatigue life, are also given in Table 5.1.

Table 5.1 Optimum results.

Nominal Model	**Package I**	**Package II**	**Package III**
Solder Ball Upper Radius	0.17	0.135	0.146
Solder Ball Volume	0.06672	0.014186	0.02288
Fatigue Life	1038.8549	568.1276	2120.7621
Optimum Model			
Solder Ball Upper Radius	0.204	0.162	0.1752
Solder Ball Volume	0.05338	0.01702	0.02745
Fatigue Life	1282.1925	820.2043	2445.2653
Relative Error	0.00054198	0.00162817	0.00772649
Correlation Coefficient	0.99999320	0.99998253	0.99846872

Second set of design parameters were material properties of mold compound, namely the thermal expansion coefficient and the elasticity modulus. Nine different cases have been analyzed by changing the elasticity modulus and the thermal expansion coefficient using three level full factorial finite element analyses. These results and the quadratic function surfaces were also graphically shown in Figure 4.26-34 for second set of design parameters. The fitted surfaces show very

good approximations to the computed data points since R^2 correlation coefficient values of between 0.992 and 0.996 were obtained for the fit. The optimal elasticity modulus and the thermal expansion coefficient were obtained for each package by optimizing least squares surfaces and shown in Table 5.2. This table also shows the relative errors and correlation coefficients comparing with the fatigue life obtained from finite element analyses to the ones achieved from optimization technique. As shown in Table 5.2, these relative errors are 0.00299 for Package I, 0.00360 for Package II, and 0.04728 for Package III. High degree of accuracy also achieved by using least squares method for predicting the fatigue life of the electronic packages. Optimum electronic package values depending on the molding compound material properties, which increase the fatigue life, are also given in Table 5.2. It can be also said that the influence of first design set on the fatigue life of the electronic packages more than second design set, comparing the changing in fatigue lives.

Table 5.2 Optimum results.

Nominal Model	**Package I**	**Package II**	**Package III**
Elasticity Modulus	26000	13800	13800
Thermal Expansion Coefficient	10.5×10^{-6}	17×10^{-6}	17×10^{-6}
Fatigue Life	1038.8549	568.1276	2120.7622
Optimum Model			
Elasticity Modulus	30000	20000	15526.3158
Thermal Expansion Coefficient	15×10^{-6}	11.58×10^{-6}	22.63×10^{-6}
Fatigue Life	1072.0385	603.8394	2210.4123
Relative Error	0.00298736	0.00360217	0.04727938
Correlation Coefficient	0.99210958	0.9963144	0.96394025

Although the same molding compound was used for Package II and Package III, the same effect and tendency could not be observed for every package in this study. Because of this reason, the influence of the design parameters on the package life must be explained for each package separately.

For the first package (Package I), as the thermal expansion coefficient increases, the fatigue life of the electronic package will increase. As the elasticity modulus increases, the fatigue life will slightly increase. Although increasing the thermal expansion coefficient improves and extends the fatigue life, the thermal expansion

coefficient has more influence on the fatigue life than the elasticity modulus. It is also observed the same tendency for each three package. The thermal expansion coefficient has the largest effect on the fatigue life of the first electronic package and the elasticity modulus has less influence than this. The higher elasticity modulus makes the electronic package stiffer, so more stress will be transmitted to the solder joints and this will result in a higher fatigue life. A lower the thermal expansion coefficient will increase both the local and global mismatch, which increases the strain applied to the joints. Since both the solder and printed circuit board have a higher the thermal expansion coefficient than the molding compound, reducing the molding compound's thermal expansion coefficient further only makes the situation worse and reduces the fatigue life.

For the second package (Package II), as the elasticity modulus rises, the fatigue life of the electronic package will increase. It cannot be said that the fatigue life will increase as the thermal expansion coefficient increases. It increases up to the certain fatigue life value and then it starts to decrease.

For the third package (Package III), increasing the thermal expansion coefficient and the elasticity modulus does not extend the fatigue life and there is not certain tendency to increase or decrease for the fatigue life. A curve surface is available. Therefore, a maximum point at around the middle of the curve can be determined for the fatigue life.

Taking into account the changeable effects of the molding compounds, optimum results should be received from the diagrams, which is given in this study and these diagrams should be absolutely taken into considerations before choosing the mold compound's material.

Additional results are also achieved supporting the researchers worked in the past decade. The most critical solder ball determined by using the macro, which was created in this study and using the strain energy density method; it is consistent with data on PBGA where the most critical one was generally under the corner of the silicon chip. Constituted quadratic functions can be used to predict the fatigue life for the electronic packages, which were taken through the industry in this study.

As there is increasing need for package design tools that enable integrated package design decisions in the electrical, thermal, and mechanical domains, the influence of the design parameters on solder joint reliability in electronic packages should be kept examining in different respects. The sensitivity of the design variables must be

investigated without doing any finite element analyses. Sensitivity analysis deals with the calculation of derivatives of a systems response with respect to the problem parameters. In structural design, the task of computing the gradients of the structural responses with respect to the design variables is called the behavior sensitivity analysis. Behavior sensitivity analysis is a fundamental part of structural optimization. It is used both to couple the structural analysis capabilities with the mathematical programming methods and also to determine the search direction in the numerical optimization problem. Also commonly encountered in structural design optimization is the optimum sensitivity analysis, which deals with methods for estimating the effect of changes in design variables on the optimum design, without actually, solving the optimization problem over again.

There are two different approaches, the first approach is the sensitivity analysis to discretized system and the second is the sensitivity analysis to distributed parameter systems followed by discretization. The first approach requires discretization of the structure into finite elements and then differentiating a set of equilibrium equations to obtain the necessary derivatives. On the other hand, the second approach is based on variational calculus where the governing equations of the structure are differentiated before discretization. This method also requires access to the element stiffness and mass matrices and load vectors, whereas the latter approach can be implemented external to the structural analysis programs. This subject of sensitivity analysis has matured to the extent that it is implemented in major commercial finite element codes.

Finite difference method for sensitivity analysis or eigenvalue and eigenvector sensitivity analyses can be used to compute the derivative of a response with respect to system parameters. Using the optimum sensitivity analysis, effect of changes in design variables on the optimum design can be estimated without performing any optimization problem over again.

REFERENCES

[1] **Martin P.L.,** 1999, Electronic Failure Analysis Handbook, McGraw-Hill Inc., New York.

[2] **Lee Y.C. and Chen W.T.,** 1998, Manufacturing Challenges in Electronic Packaging, Chapman & Hall, New York.

[3] **Ginsberg G.L.,** 1991, Electronic Equipment Packaging Technology, Van Nostrand Reinhold, New York.

[4] **Lau, J. H.,** 1996, Flip Chip Technologies, MC Graw-Hill, New York.

[5] **Darveaux, R., Banerji, K., Mawer, A., and Dody, G.,** 1995, Reliability of Plastic Ball Grid Array Assembly, *Ball Grid Array Technology* (Lau, J. H., Editor), pp. 379-442, MC Graw-Hill, New York.

[6] **Lau, J.H.,** 1991, Solder Joint Reliability, Theory, and Applications, Van Nostrand Reinhold, New York.

[7] **Darveaux, R.,** 1997, Solder Joint Fatigue Life Model, Design, and Reliability of Solder, and Solder Interconnections, Proceedings of TMS, Orlando, Florida, February.

[8] **Darveaux, R.,** 2000, Effect of Simulation Methodology on Solder Joint Crack Growth Correlation, 50th Electronic Components and Technology Conference, Las Vegas, Nevada.

[9] **Anderson, T., Guven, I., Madenci, E., and Gustafsson, G.,** 1999, The Necessity of Reexamining Previous Life Prediction Analyses of Solder Joints in Electronic Packages, *49th Electronic Components and Technology Conference*, San Diego, California, pp. 1010-1014.

[10] **Darveaux, R., Heckman, J., and Mawer, A.,** 1998, Effect of Test Board Design on the 2nd Level Reliability of A Fine Pitch BGA Package, Proc. SMI, pp. 105-110.

[11] **Miles, B., Fusaro, J., Panczak, T., and Darveaux, R.,** 1998, Fine Pitch BGA Package Assembly, Proc. SMI, pp. 29-33.

[12] **Syed, A., Panczak, T., Darveaux, R., Lee, S.G., Lee, C.H., and Partridge, J.,** 1999, Solder Joint Reliability of Chip Array BGA™, Proc. SMTA, pp. 90-97.

[13] **Fijelstad, J., DiStefano, T., and Perry, M.,** 1996, Compliancy Modeling of An Area Array Chip Scale Package, Proc. SMI, pp. 236-243.

[14] **Ejim, T., Holliday, A., Bader, F.E., and Gahr, S.,** 1995, Designed Experiment To Determine Attachment Reliability Drivers for PBGA Packages, Proc. SMI, pp. 385-392.

[15] **El-Gore, M.K., Peterson, M. Pavuluri, K., Settles, J., Hundt, P., Berry, J., and Takeda, H.,** 1999, Evaluation of 64 Pin Micro Star BGA™ Package, Proc. Pan Pacific Microelectronics Symposium, pp. 98-105.

[16] **Sato, T., Tanaka, K., Sumikawa, M., Yoshioka, C., Yamamura, K., and Nukii, T.,** 1998, Reliability and Fatigue Life Prediction of Mounted CSP, Proc. ISHM International Symposium on Microelectronics, pp. 531-536.

[17] **Schueller, R.D. and Geissinger, J.,** 1997, New Chip Scale Package With CTE Matching To The Board, Proc. IRE6 1st Electronics Packaging Technology Conference, EPTC, pp. 219-227.

[18] **Schueller, R.D., Harrey, P., Heidick, R., and Kinningham, A.,** 1997, Electrical Performance and Reliability of TBGA with Grounded Stiffener, Proc. SMI, pp. 16-27.

[19] **Atterwala, A.I., and Stierman R.,** 1994, Failure Mode Analysis of A 540 Pin Plastic Ball Grid Array, Proc. SMI, pp. 252, 257.

[20] **Masumoto, K.,** 1997, Development of Fine-Pitch Micro Star BGA™, Proc. Semicon West.

[21] **Juso, H., Yamaji, Y., Kimura, T., Fujita, K., and Kada, M.,** 1998, Board Level Reliability of CSP, Proc. ECTC, pp. 525-531.

[22] **Darveaux, R., and Mawer, A.,** 1995, Thermal and Power Cycling Limits of Plastic Ball Grid Array (PBGA) Assemblies, Proc. SMI, pp. 315-326.

[23] **Darveaux, R.,** 1995, Optimizing The Reliability of Thin Small Outline Package (TSOP) Solder Joints, Advances in Electronic Packaging, Proc. ASME Interpack' 95, pp.675-685.

[24] **Mawer, A., Cho, D., and Darveaux, R.,** 1996, The Effect of PBGA Solder Pad Geometry On Solder Joint Reliability, Proc. SMI, pp. 127-135.

[25] **Mawer, A. Simmons, K., Burnett, T., and Oyler, B.,** 1998, Assembly and Interconnect Reliability of BGA Assembled On To Blind Micro and Through-Hole Drilled Via In Pad, Proc. SMI, pp. 21-28.

[26] **Darveaux, R., Heckman, J., Syed, A., and Mawer, A.,** 2000, Solder Joint Fatigue Life of Fine Pitch BGAs – Impact of Design and Material Choices, Microelectronics Reliability 40, Pergamon, pp. 1117-1127.

[27] **Gill, P.E., Murrey, W., and Wright, M.H.,** 1981, *Practical Optimization,* Academic Press, New York, NY.

[28] **Haug, E.J. and Arora, J.S.,** 1979, *Applied Optimal Design,* John Wiley&Sons, New York, NY.

[29] **Haftka, R.T. and Gurdal, Z.,** 1992, *Elements of Structural Optimization,* Kluwer Academic Publishers Group, Boston, MA.

[30] **Gill, P.E., Murrey, W., Saunders, M.A., and Wright, M.H.,** 1986, Users's Guide for NPSOL, Version 4.0, *Technical Report Sol 86-2,* Department of Operation Research, Stanford University, Stanford, CA.

[31] **Schittkowski, K.,** 1985, NLPQL: A Fortran Sobroutine Solving Constrained Nonlinear Programming Problems, *Annals of Operation Research 5 (1985/6),* pp. 485-500.

[32] **Sarihan, V.,** 1993, A Robust Design Optimization Methodology for Life Enhancement of Electronic Packages, *Advances in Electronic Packaging,* Engel, P.A. and Chen, W.T. eds., EEP, Vol 4-1, pp. 397-403.

[33] **Subbarayan, G.,** 1995a, A Procedure for Automated Profile and Life Prediction in Flip-Chip and BGA Solder Joints Part I: Mathematical Model, ASME Paper No. 95-WA/EEP-17.

[34] **Subbarayan, G.,** 1995b, A Procedure for Automated Profile and Life Prediction in Flip-Chip and BGA Solder Joints Part II: Numerical Solution, ASME Paper No. 95-WA/EEP-25.

[35] **Subbarayan, G.,** 1996a, A Procedure for Automated Profile and Life Prediction in Flip-Chip and BGA Solder Joints, ASME Journal of Electronic Packaging, Vol. 118, No. 3, pp. 127-133.

[36] **Deshpande, A.M., Subbarayan, G. and Mahajan, R.L.,** 1997, Maximizing Solder Joint Reliabilty Through Optimal Design, ASME Journal of Electronic Packaging, Vol. 119, No. 4, pp. 149-155.

[37] **Mertol, A.,** 2000, Application of the Taguchi Method To Chip Scale Package (CSP) Design, IEEE Transactions on Advanced Packaging, 23: (2) pp. 266-276, May.

[38] **ANSYS, Inc.,** 2000, ANSYS Manual, Southpointe 275 Technology Drive Canonsburg, PA.

[39] **Garfola, F.,** 1965, Fundamentals of Creep and Creep Rupture in Metals, The MacMillan Company, New York, N.Y.

[40] **Murty, K.L. and Turlik, I.,** 1992, Deformation Mechanisms in Lead-Tin Alloys, Application to the Solder Reliability in Electronic Packages, Proceedings 1st Joint Conference on Electronic Packaging, ASME/JSME, pp.309-318.

[41] **Frost, H.J. and Ashby, M.F.,** 1982, Deformation Mechanism Maps, Pergamon Press, Chap. 2.

[42] **Murty, K.L., Clevinger, G.S., and Papazoglu, T.P.,** 1977, Thermal Creep of Zircaloy-4 Cladding, Proceedings 4st International Conference on Structural Mechanics in Reactor Technology, C ¾.

[43] **Meyers, M.A. and Chawla, K.K.,** 1984, Mechanical Metallurgy, Principles and Applications, Prentice-Hall.

[44] **Darveaux, R.,** 1993, Mechanical Evaluation of Indium for Die Attachment in A Multichip Package, Ph.D. Dissertation, North Carolina State University.

[45] **Manson, S.S.,** 1966, Thermal Stress and Low Cycle Fatigue, McGraw-Hill, New York.

[46] **Ianuzelli, R.J., Pitarresi, J.M., and Prakash, V.,** 1996, Solder Joint Reliability Prediction by The Integrated Matrix Creep Method, Journal of Electronic Packaging, Vol. 118, pp. 55-61.

[47] **Akay, H.U., Paydar, N.H., and Bilgic, A.,** 1997, Fatigue Life Predictions for Thermally Loaded Solder Joints Using a Volume- Weighted Averaging Technique, Journal of Electronic Packaging, Vol. 119, pp. 228-235.

[48] **Ozmat, B.,** 1990, A Nonlinear Thermal Stress Analysis of Surface Mount Solder Joints, Proc. 40th IEEE ECTC, Vol. II, pp. 959-972.

[49] **Wild, R.N.,** 1988, Some Factors Affecting Leadless Chip Carrier Solder Joint Fatigue Life II, Circuit World, Vol. 14, no. 4, pp. 29-36, 41.

[50] **Wolverton, W.M.,** 1987, The Mechanisms and Kinetics of Solder Joint Degradation, Brazing&Soldering, No. 13, pp. 33-38.

[51] **Wong, B. and Helling, D.E.,** 1990, A Mechanistic Model for Solder Joint Failure Prediction Under Thermal Cycling, Journal of Electronic Packaging, Vol. 112, pp. 104-109.

[52] **Smeby, J.M.,** 1985, Solder joint Behavior in HWC/PWB Interconnections, IEEE Trans. CHMT, Vol. CHMT-8, No. 3, pp. 391-396.

[53] **Brierley, C.J. and Pedder, D.J.,** 1984, Surface Mounted IC Packages-Their Attachment and Reliability on PWBs, Circuit World, Vol. 10, No. 2, pp. 28-31.

[54] **Satoh, R., Arakawa, K., Harada, M., and Matsui, K.,** 1991, Thermal Fatigue Life of Pb-Sn Alloy Interconnections, IEEE Trans. CHMT, Vol. 14, No. 1, pp. 224-232.

[55] **McShane, M., Lin, P., Dody, G., and Bigler, J.,** 1990, Lead Configuration and Performance for Fine Pitch SMT Reliability, Proc. NEPCON West, pp. 238-257.

[56] **Norris, K.C. and Landzberg, A.H.,** 1969, Reliability of Controlled Collapse Interconnections, IBM Journal of Research and Development, pp. 266-271.

[57] **Agarwala, B.N.,** 1985, Thermal Fatigue Damage in Pb-In Solder Interconnections, Proceedings International Reliability Physics Symposium, pp. 198-205.

[58] **Solomon, H.D.,** 1985, Low Cycle Fatigue of 60/40 Solder-plastic Strain Limited vs. Displacement Limited Testing, Proc. ASM 2nd Electronic Packaging Conference, pp. 29-47.

[59] **Solomon, H.D.,** 1989, Low Cycle Fatigue of Surface Mounted Chip Carrier/Printed Wiring Board Joints, Proc. IEEE 39th ECC, pp. 227-292.

[60] **Subrahmanyan, R.,** 1990, A Damage Integral Approach for Low-Cycle Isothermal and Thermal Fatigue, Ph.D. thesis, Cornell University.

[61] **Attarwala, A.I., Tien, J.K., Masada, G.Y., and Dody, G.,** 1992, Confirmation of Creep and Fatigue Damage in Pb-In Solder Joints, Journal of Electronic Packaging, Vol. 114, pp. 109-111.

[62] **Cletch, J.P., Noctor, D.M., Manock, J.C., Lynoot, G.W., and Bader, F.E.,** 1994, Surface Mount Assembly Failure Statistics and Failure Free Time, Proc. 44th IEEE ECTC.

[63] **Nicewarner, E.,** 1993, Historical Failure Distribution and Significant Factors Affecting Surface Mount Solder Joint Fatigue Life, Proc. IEPS, pp. 553-563.

[64] **Darveaux, R.,** 1992, Crack Initiation and Growth in Surface Mount Solder Joints, Proc. ISHM International Symposium on Microelectronic Packaging, Vol. 114, pp. 109-111.

[65] **Uegai, Y., Tani, S., Inoue, A., Yoshioka, S., and Tamura, K.,** 1993, A Method of Fatigue Life Prediction for Surface-Mount Solder Joints of Electronic Devices by Mechanical Fatigue Test, Proc. ASME International Electronic Packaging Conference, Vol. 1, pp. 493-498.

[66] **Cletch, J.P. and Augis, J.A.,** 1987, Engineering Analysis of Thermal Cycling Accelerated Tests for Surface-Mount Attachment Reliability Evaluation, Proc. 7th IEPS, pp. 385-410.

[67] **Subrahmanyan, R., Stone, D., and Li, C.Y.,** 1988, Deformation Behavior of Leadless 60Sn40Pb Solder Joints, Proceedings MRS Symposium, Vol 108, pp. 381-384.

[68] **Sauber, J. and Seyyedi, J.,** 1992, Predicting Thermal Fatigue Lifetimes for SMT Solder Joints, Trans. ASME Journal of Electronic Packaging, Vol. 114, pp. 473-476.

[69] **Darveaux, R. and Banerji, K.,** 1991, Fatigue Analysis of Flip Chip Assemblies Using Thermal Stress Simulations and a Coffin-Manson Relation, Proc. 41st IEEE ECTC, pp. 797-805.

[70] **Shine, M.C. and Fox, L.R.,** 1988, Fatigue of Solder Joints in Surface Mount Devices, Low Fatigue Cycle, ASTM STP 942, H. D. Solomon, G. R. Halford, L. R. Kaisand, and B. N. Leis, eds., American Society for Testing and Materials, Philadelphia, Pa.

[71] **Ianuzzelli, R.,** 1993, Predicting Solder Joint Reliability-Model Validation, Proc. IEEE 43rd ECTC, pp. 839-851.

[72] **Engelmaier, W.,** 1984, Functional Cycles and Surface Mounting Attachment Reliability, ISHM Technical Monograph Series 6984-002, International Society for Hybrid Microelectronics, Silver Springs, MD, pp. 87-114.

[73] **Cletch, J.P., Manock, J.C., Noctor, D.M., Bader, F.E., and Augis, J.A.,** 1993, A Comprehensive Surface Mount Reliability (SCMP) Model Covering Several Generations of Assembly Technology, Proc. IEEE 43rd ECTC, pp. 62-70.

[74] **Sarihan, V.,** 1993, Energy-Based Methodology for Damage and Life Prediction of Solder Joints under Thermal Cycling, Proc. IEEE 43rd ECTC.

[75] **Lau, J.H.,** 1993, Fatigue Life Prediction of Flip Chip Solder Joints by Fracture Mechanics, pp. 643-654.

[76] **Darveaux, R.,** 1997, Solder Joint Fatigue Life Model, Proc. TMS, Design & Reliability of Solders and Solders Interconnections, Orlando, Florida, February 10-13.

[77] **Gustaffson, G., Guven. I., Kradinov, V., and Madenci, E.,** 2000, Finite Element Modeling of BGA Packages for Life Prediction, 50th Electronic Components and Technology Conference, Las Vegas, Nevada.

[78] **L. Anand,** 1985, Constituve Equations for Hot-Working of Metals, International Journal of Plasticity, Vol. 1, pp. 213-231.

[79] **S.B. Brown, K.H. Kim, and L. Anand,** 1989, An Internal Variable Constituve Model for Hot-Working of Metals, International Journal of Plasticity, Vol. 5, pp. 95-130.

[80] **Nigro, N.J., Elkouth, A.F., Heinrich, S.M., Chang, P., and Lee, P.S.,** 1991, Computer Aided Design of Solder Joints, *Surface Mount Technology*, Vol. 5, No. 4, pp. 59-61.

[81] **Montgomery, D.C.,** 1991, *Introduction to Statistical Quality Control,* 2nd Edition, John Wiley and Sons, Inc., New York.

[82] **Peace, G.S.,** 1993, *Taguchi Methods: A Hands-On Approach,* Addison-Wesley, Reading, MA.

APPENDIX A

Table A.1 Package I.

Solder Ball Volume=0.080065`49 Solder Ball Upper Radius=0.136 Standoff Height=0.45905314 Solder Ball Radius=0.270554 Package Life=848.234114 Plastic Work=45.6229446	-%20 Radius Size %0 Volume	Solder Ball Volume=0.08008264 Solder Ball Upper Radius=0.17 Standoff Height=0.43426121 Solder Ball Radius=0.269981 Package Life=1034.54774 Plastic Work =45.2066199	+%20 Radius Size %0 Volume	Solder Ball Volume=0.08006552 Solder Ball Upper Radius=0.204 Standoff Height=0.40375943 Solder Ball Radius=0.2708760 Package Life=1260.87473 Plastic Work =43.6353243
%0 Radius Size +%20 Volume	-%20 Radius Size +%20 Volume	%0 Radius Size +%20 Volume	+%20 Radius Size +%20 Volume	%0 Radius Size +%20 Volume
Solder Ball Volume=0.06672080 Solder Ball Upper Radius=0.136 Standoff Height=0.42299521 Solder Ball Radius=0.255444 Package Life=848.4959 Plastic Work=45.6106819	-%20 Radius Size +%0 Volume	Solder Ball Volume=0.06672098 Solder Ball Upper Radius=0.17 Standoff Height=0.39628168 Solder Ball Radius=0.255 Package Life=1038.85492 Plastic Work=45.0409374	+%20 Radius Size %0 Volume	Solder Ball Volume=0.06672113 Solder Ball Upper Radius=0.204 Standoff Height=0.36358386 Solder Ball Radius=0.25651 Package Life=1270.24459 Plastic Work=43.3480542
%0 Radius Size -%20 Volume	-%20 Radius Size -%20 Volume	%0 Radius Size -%20 Volume	+%20 Radius Size -%20 Volume	%0 Radius Size -%20 Volume
Solder Ball Volume=0.05337673 Solder Ball Upper Radius=0.136 Standoff Height=0.3811032 Solder Ball Radius=0.238402 Package Life=851.881632 Plastic Work=45.4527333	-%20 Radius Size %0 Volume	Solder Ball Volume=0.05337688 Solder Ball Upper Radius=0.17 Standoff Height=0.35192473 Solder Ball Radius=0.238213 Package Life=1044.26702 Plastic Work=44.834607	+%20 Radius Size %0 Volume	Solder Ball Volume=0.05337705 Solder Ball Upper Radius=0.204 Standoff Height=0.3163579 Solder Ball Radius=0.240814 Package Life=1282.82824 Plastic Work=42.9685937

Table A.2 Package II.

Solder Ball Volume=0.01702309 Solder Ball Upper Radius=0.108 Standoff Height=0.24978609 Solder Ball Radius=0.179705 Package Life=406.533503 Plastic Work=73.3253319	-%20 Radius Size %0 Volume	Solder Ball Volume=0.017023 Solder Ball Upper Radius=0.135 Standoff Height=0.23298377 older Ball Radius=0.18229 Package Life=584.548206 Plastic Work=62.882691	+%20 Radius Size %0 Volume	Solder Ball Volume=0.0170228 Solder Ball Upper Radius=0.162 Standoff Height=0.21376031 older Ball Radius=0.18763 Package Life=819.795949 Plastic Work=53.5430755
%0 Radius Size +%20 Volume	-%20 Radius Size +%20 Volume	%0 Radius Size +%20 Volume	+%20 Radius Size +%20 Volume	%0 Radius Size +%20 Volume
Solder Ball Volume=0.01418582 Solder Ball Upper Radius=0.108 Standoff Height=0.22976428 Solder Ball Radius=0.173082 Package Life=392.280203 Plastic Work=75.6489668	-%20 Radius Size +%0 Volume	Solder Ball Volume=0.01418582 Solder Ball Upper Radius=0.135 Standoff Height=0.212675025 Solder Ball Radius=0.176 Package Life=568.127584 Plastic Work=64.4827833	+%20 Radius Size %0 Volume	Solder Ball Volume=0.01418583 Solder Ball Upper Radius=0.162 Standoff Height=0.19341032 Solder Ball Radius=0.182122 Package Life=804.659141 Plastic Work=54.4351905
%0 Radius Size -%20 Volume	-%20 Radius Size -%20 Volume	%0 Radius Size -%20 Volume	+%20 Radius Size -%20 Volume	%0 Radius Size -%20 Volume
Solder Ball Volume=0.01134877 Solder Ball Upper Radius=0.108 Standoff Height=0.207326 Solder Ball Radius=0.166133 Package Life=375.247599 Plastic Work=78.6462166	-%20 Radius Size %0 Volume	Solder Ball Volume=0.01134865 Solder Ball Upper Radius=0.135 Standoff Height=0.19005233 Solder Ball Radius=0.16943 Package Life=549.495818 Plastic Work=66.4090143	+%20 Radius Size %0 Volume	Solder Ball Volume=0.01134872 Solder Ball Upper Radius=0.162 Standoff Height=0.17097496 Solder Ball Radius=0.176566 Package Life=790.51759 Plastic Work=55.2982125

Table A.3 Package III.

Solder Ball Volume=0.02745525 Solder Ball Upper Radius=0.1168 Standoff Height=0.29137501 Solder Ball Radius=0.198814 Package Life=1679.9327 Plastic Work=23.0052247	-%20 Radius Size %0 Volume	Solder Ball Volume=0.02745529 Solder Ball Upper Radius=0.146 Standoff Height=0.2653638 Solder Ball Radius=0.19879 Package Life=2174.42346 Plastic Work=21.3342446	+%20 Radius Size %0 Volume	Solder Ball Volume=0.02745549 Solder Ball Upper Radius=0.1752 Standoff Height=0.23411127 Solder Ball Radius=0.201509 Package Life=2436.09911 Plastic Work=21.8859255
%0 Radius Size +%20 Volume	-%20 Radius Size +%20 Volume	%0 Radius Size +%20 Volume	+%20 Radius Size +%20 Volume	%0 Radius Size +%20 Volume
Solder Ball Volume=0.022879299 Solder Ball Upper Radius=0.1168 Standoff Height=0.26577654 Solder Ball Radius=0.189758 Package Life=1636.33469 Plastic Work=23.5152457	-%20 Radius Size +%0 Volume	Solder Ball Volume=0.02287948 Solder Ball Upper Radius=0.146 Standoff Height=0.23820851 Solder Ball Radius=0.19 Package Life=2120.76217 Plastic Work=21.7907577	+%20 Radius Size %0 Volume	Solder Ball Volume=0.022879717 Solder Ball Upper Radius=0.1752 Standoff Height=0.205429126 Solder Ball Radius=0.193767 Package Life=2384.56408 Plastic Work=22.292524
%0 Radius Size -%20 Volume	-%20 Radius Size -%20 Volume	%0 Radius Size -%20 Volume	+%20 Radius Size -%20 Volume	%0 Radius Size -%20 Volume
Solder Ball Volume=0.01830375 Solder Ball Upper Radius=0.1168 Standoff Height=0.23643273 Solder Ball Radius=0.179992 Package Life=1576.19886 Plastic Work=24.262116	-%20 Radius Size %0 Volume	Solder Ball Volume=0.0183034 Solder Ball Upper Radius=0.146 Standoff Height=0.20703699 Solder Ball Radius=0.180644 Package Life=1984.73104 Plastic Work=23.0521817	+%20 Radius Size %0 Volume	Solder Ball Volume=0.01830333 Solder Ball Upper Radius=0.1752 Standoff Height=0.1727054 Solder Ball Radius=0.186057 Package Life=2322.72218 Plastic Work=22.8030276

APPENDIX B

Table B.1 Package I.

Elasticity Modulus=20000 Thermal Expansion Coefficient=$15x10^{-6}$ Package Life=1041.05658 Plastic Work=44.956754	-% E	Elasticity Modulus=26000 Thermal Expansion Coefficient=$15x10^{-6}$ Package Life=1058.32885 Plastic Work=44.3079657	+% E	Elasticity Modulus=30000 Thermal Expansion Coefficient=$15x10^{-6}$ Package Life=1068.23244 Plastic Work=43.9450265
+% α	-% E +% α	+% α	+% E +% α	+% α
Elasticity Modulus=20000 Thermal Expansion Coefficient=$10.5x10^{-6}$ Package Life=1023.61106 Plastic Work=45.633136	-% E	Elasticity Modulus=26000 Thermal Expansion Coefficient=$10.5x10^{-6}$ Package Life=1038.85492 Plastic Work=45.0409374	+% E	Elasticity Modulus=30000 Thermal Expansion Coefficient=$10.5x10^{-6}$ Package Life=1047.56274 Plastic Work=44.7099624
-% α	-% E -% α	-% α	+% E -% α	-% α
Elasticity Modulus=20000 Thermal Expansion Coefficient=$5x10^{-6}$ Package Life=988.175903 Plastic Work=47.0778673	-% E	Elasticity Modulus=26000 Thermal Expansion Coefficient=$5x10^{-6}$ Package Life=996.982003 Plastic Work=46.7096958	+% E	Elasticity Modulus=30000 Thermal Expansion Coefficient=$5x10^{-6}$ Package Life=1002.02609 Plastic Work=46.5016017

Table B.2 Package II.

Elasticity Modulus=5000 Thermal Expansion Coefficient=25x10^{-6} Package Life=545.376041 Plastic Work=66.8519296	-% E	Elasticity Modulus=13800 Thermal Expansion Coefficient=25x10^{-6} Package Life=557.285446 Plastic Work=65.5886929	+% E	Elasticity Modulus=20000 Thermal Expansion Coefficient=25x10^{-6} Package Life=581.64021 Plastic Work=63.1597577
+% α	-% E +% α	+% α	+% E +% α	+% α
Elasticity Modulus=5000 Thermal Expansion Coefficient=17x10^{-6} Package Life=530.723968 Plastic Work=68.4804615	-% E	Elasticity Modulus=13800 Thermal Expansion Coefficient=17x10^{-6} Package Life=568.127584 Plastic Work=64.4827833	+% E	Elasticity Modulus=20000 Thermal Expansion Coefficient=17x10^{-6} Package Life=602.473715 Plastic Work=61.2313408
-% α	-% E -% α	-% α	+% E -% α	-% α
Elasticity Modulus=5000 Thermal Expansion Coefficient=10x10^{-6} Package Life=514.101176 Plastic Work=70.4355198	-% E	Elasticity Modulus=13800 Thermal Expansion Coefficient=10x10^{-6} Package Life=563.789666 Plastic Work=64.920379	+% E	Elasticity Modulus=20000 Thermal Expansion Coefficient=10x10^{-6} Package Life=600.688593 Plastic Work=61.3915635

Table B.3 Package III.

Elasticity Modulus=5000 Thermal Expansion Coefficient=0,30x10^{-4} Package Life=1951.09058 Plastic Work=23.3897214	-% E	Elasticity Modulus=13800 Thermal Expansion Coefficient=0,30x10^{-4} Package Life=2226.207920 Plastic Work=23.3897214	+% E	Elasticity Modulus=25000 Thermal Expansion Coefficient=0,30x10^{-4} Package Life=1548.07908 Plastic Work=28.5031978
+% α	-% E +% α	+% α	+% E +% α	+% α
Elasticity Modulus=5000 Thermal Expansion Coefficient=0,17x10^{-4} Package Life=1440.03921 Plastic Work=30.3320471	-% E	Elasticity Modulus=13800 Thermal Expansion Coefficient=0,17x10^{-4} Package Life=2120.732170 Plastic Work=21.7907577	+% E	Elasticity Modulus=25000 Thermal Expansion Coefficient=0,17x10^{-4} Package Life=2143.60850 Plastic Work=21.593759
-% α	-% E -% α	-% α	+% E -% α	-% α
Elasticity Modulus=5000 Thermal Expansion Coefficient=0,10x10^{-4} Package Life=1216.23618 Plastic Work=35.0951634	-% E	Elasticity Modulus=13800 Thermal Expansion Coefficient=0,10x10^{-4} Package Life=1700.739120 Plastic Work=26.2963515	+% E	Elasticity Modulus=25000 Thermal Expansion Coefficient=0,10x10^{-4} Package Life=1971.80392 Plastic Work=23.1806009

AUTOBIOGRAPHY

Aylin YENİLMEZ was born in Emirdağ in 1971. She graduated from Bursa Girl High School in 1987. She obtained her B.Sc. degree in Mechanical Engineering from Istanbul Technical University in 1991. She continued her graduate studies at the same university and received her M.Sc. degree in 1994 and then attended Ph.D. program offered in I.T.U. She has been studying as a research assistant at Machine Design Department in Istanbul Technical University.